

ACTA GEOTECHNICA SLOVENICA

VOL. 19
2022/2

The resilient modulus of hybrid construction and demolition wastes reinforced by a geogrid

Geotechnical characterization of zeolite-sand and bentonite-sand mixtures

SPT-based soil-liquefaction models using nonlinear regression analysis and artificial intelligence techniques



Ustanovitelji Founders

Univerza v Mariboru, Fakulteta za gradbeništvo, prometno inženirstvo in arhitekturo
University of Maribor, Faculty of Civil Engineering, Transportation Engineering and Architecture

Univerza v Ljubljani, Fakulteta za gradbeništvo in geodezijo
University of Ljubljana, Faculty of Civil and Geodetic Engineering

Univerza v Ljubljani, Naravoslovnotehniška fakulteta
University of Ljubljana, Faculty of Natural Sciences and Engineering

Slovensko geotehniško društvo
Slovenian Geotechnical Society

Društvo za podzemne in geotehniške konstrukcije
Society for Underground and Geotechnical Constructions

Izdajatelj Publisher

Univerza v Mariboru, Fakulteta za gradbeništvo, prometno inženirstvo in arhitekturo
Faculty of Civil Engineering, Transportation Engineering and Architecture

Odgovorni urednik Editor-in-Chief

Borut Macuh University of Maribor

Tehnična urednica Technical Editor

Tamara Bračko University of Maribor

Uredniki Co-Editors

Jakob Likar	Geoportal d.o.o.
Janko Logar	University of Ljubljana
Primož Jelušič	University of Maribor
Stanislav Škrabl	University of Maribor
Goran Vižintin	University of Ljubljana
Bojan Žlender	University of Maribor

Posvetovalni uredniki Advisory Editors

Heinz Brandl	Vienna University of Technology
Chandrakant. S. Desai	University of Arizona
Bojan Majes	University of Ljubljana
Pedro Seco e Pinto	National Laboratory of Civil Eng.

Lektor Proof-Reader

Paul McGuinness

Naklada Circulation

-

Cena Price

25 EUR/letnik - 25 EUR/vol.; (50 EUR for institutions/za institucije)

Tisk Print

-

Revija redno izhaja dvakrat letno. Članki v reviji so recenzirani s strani priznanih mednarodnih strokovnjakov. Baze podatkov v katerih je revija indeksirana: SCIE - Science Citation Index Expanded, JCR - Journal Citation Reports / Science Edition, ICONDA - The international Construction database, GeoRef. Izid publikacije je finančno podprla Javna agencija za raziskovalno dejavnost Republike Slovenije iz naslova razpisa za sofinanciranje domačih periodičnih publikacij.

Uredniški odbor Editorial Board

Marx Ferdinand Ahlinhan	National University in Abomey
Amin Barari	Aalborg University
Theodoros Hatzigogos	Aristotle University of Thessaloniki
Vojkan Jovičič	IRGO-Ljubljana
Rolf Katzenbach	Technical University Darmstadt
Nasser Khalili	The University of New South Wales, Sydney
Svetlana Melentijevic	Complutense University of Madrid
Seyed Hamed Mirmoradi	Federal University of Rio de Janeiro
Ana Petkovšek	University of Ljubljana
Borut Petkovšek	Slovenian National Building and Civil Engineering Institute
Mihael Ribičič	University of Ljubljana
César Sagasetta	University of Cantabria
Patrick Selvadurai	McGill University
Stephan Semprich	University of Technology Graz
Devendra Narain Singh	Indian Institute of Technology, Bombay
Abdul-Hamid Soubra	University of Nantes
Kiichi Suzuki	Saitama University
Antun Szavits-Nossan	University of Zagreb
Kosta Urumović	Croatian geological survey
Ivan Vaniček	Czech Technical University in Prague

Založnik Published by

Univerzitetna založba Univerze v Mariboru	University of Maribor Press
Slomškov trg 15, 2000 Maribor, Slovenija	Slomškov trg 15, 2000 Maribor, Slovenia
e-pošta: zalozba@um.si, http://press.um.si/, http://journals.um.si/	e-mail: zalozba@um.si, http://press.um.si/, http://journals.um.si/

Naslov uredništva Address

ACTA GEOTECHNICA SLOVENICA
Univerza v Mariboru, Fakulteta za gradbeništvo, prometno inženirstvo in arhitekturo
Smetanova ulica 17, 2000 Maribor, Slovenija
Telefon / Telephone: +386 (0)2 22 94 300
Faks / Fax: +386 (0)2 25 24 179
E-pošta / E-mail: ags@um.si

Spletni naslov web Address

<http://www.fg.uni-mb.si/journal-ags/>

The journal is published twice a year. Papers are peer reviewed by renowned international experts. Indexation data bases of the journal: SCIE - Science Citation Index Expanded, JCR - Journal Citation Reports / Science Edition, ICONDA- The international Construction database, GeoRef. The publication was financially supported by Slovenian Research Agency according to the Tender for co-financing of domestic periodicals.

<i>T. Sarici in drugi</i> Modul prožnosti hibridnih gradbenih odpadkov in odpadkov pri rušenju, ojačen z geomrežo	<i>T. Sarici et al.</i> The resilient modulus of hybrid construction and demolition wastes reinforced by a geogrid	2
<i>Ö. Yildiz in Ç. Ceylan</i> Geotehnična karakterizacija mešanic zeolita in peska ter bentonita in peska	<i>Ö. Yildiz and Ç. Ceylan</i> Geotechnical characterization of zeolite-sand and bentonite-sand mixtures	15
<i>M. Cemal Acar in T. Hakan</i> Modeli utekočinjenja zemljin na osnovi SPT z uporabo regresijske analize in tehnik umetne inteligence	<i>M. Cemal Acar and T. Hakan</i> SPT-based soil-liquefaction models using nonlinear regression analysis and artificial intelligence techniques	33
Navodila avtorjem	Instructions for authors	46

THE RESILIENT MODULUS OF HYBRID CONSTRUCTION AND DEMOLITION WASTES REINFORCED BY A GEOGRID

MODUL PROŽNOSTI HIBRIDNIH GRADBENIH ODPADKOV IN ODPADKOV PRI RUŠENJU, OJAČAN Z GEOMREŽO

Talha Sarici (corresponding author)

Inonu University,
Department of Civil Engineering
Malatya, Turkey
E-mail: talha.sarici@inonu.edu.tr

Bahadır Ok

Adana Alparslan Turkes Science and Technology University,
Department of Civil Engineering
Adana, Turkey
E-mail: bahadirok@atu.edu.tr

Aykan Mert

General Directorate of Highways,
Research and Development Department
Ankara, Turkey
E-mail: amert@kgm.gov.tr

Senol Comez

General Directorate of Highways,
Research and Development Department
Ankara, Turkey
E-mail: scomez@kgm.gov.tr

DOI <https://doi.org/10.18690/actageotechslov.19.2.2-14.2022>

Keywords

construction and demolition waste, Geogrid, geotechnical engineering, sustainability, resilient modulus, waste management

Ključne besede

gradbeni odpadki in odpadki pri rušenju objektov, geomreže, geotehnični inženiring, trajnost, modul prožnosti, ravnanje z odpadki

Abstract

The use of construction and demolition wastes (C&D) in engineering applications is an important development for better sustainability. The main objective of this study, therefore, was to increase the use of C&D by improving their engineering behaviour. For this purpose, two methods were employed in this study: first, adding the virgin aggregates (VA) to the C&D, called hybrid C&D (C&D-VA), and second, reinforcing the C&D with a geogrid material. Test samples were prepared in six groups. The first three test groups were prepared with C&D, VA and C&D-VA. The other three test groups were formed with geogrid-reinforced C&D, VA and C&D-VA. Firstly, for the strength characteristics of the samples, the unconfined compressive strength and the California bearing ratio values were obtained with large-scale experiments. Subsequently, for the resilient behaviour of the samples, the resilient modulus values were determined using a large-scale triaxial test device. Consequently, some significant improvements

Izvleček

Uporaba gradbenih odpadkov in odpadkov pri rušenju (C&D) v inženirskih objektih je pomemben pri razvoju za večjo trajnost. Glavni cilj pričujoče študije je torej povečati uporabo C&D z izboljšanjem njihovega inženirskega obnašanja. V ta namen sta bili v tej študiji uporabljeni dve metodi, in sicer prva dodajanje neobdelanih agregatov (VA) v C&D, imenovano hibridni C&D (C&D-VA), in druga, ojačitev z geomrežami C&D. Preizkušanci so bili pripravljani v šestih skupinah. Prve tri preizkusne skupine so bile pripravljene s C&D, VA in C&D-VA. Druge tri preizkusne skupine so bile pripravljene tako, da so zgornjim trem skupinam bile dodane geomreže, torej ojačane C&D, VA in C&D-VA. Najprej so bile z izvajanjem obsežnih preizkusov enoosne tlačne trdnosti in kalifornijskega faktorja nosilnosti pridobljene vrednosti trdnostnih karakteristik preizkušancev. Nato so bile za deformacijsko obnašanje vzorcev določene vrednosti modula prožnosti z uporabo velike triosne preskusne naprave. Posledično

were achieved via the methods employed in this study. In addition, it was observed that the best reinforcement effect for the C&D occurred when the geogrid was used and the VA was added to the C&D.

1 INTRODUCTION

Construction and demolition wastes (C&D) occur in construction, repair, maintenance, environmental disasters and demolition activities [1]. The C&D can consist of different types of materials, depending on the construction or demolition activities. These materials can be concrete, brick, tile, ceramic, wood, glass, plastic, bituminous mixtures, coal, petroleum products, metals, soil pieces, insulating materials, building materials containing asbestos, gypsum-based construction materials, etc. [2]. On the other hand, C&D is some of the heaviest and most voluminous waste and constitutes between 30 % and 40 % of the total solid waste [3]. Therefore, this solid waste can cause negative impacts on the environment when it is stored in a landfill. In addition, this storage is not economic. However, if the C&D is reused in some construction applications by recycling, the storage costs of the solid waste produced by the construction industry can be reduced, the need for the area of the landfill can be diminished, the use of natural resources for construction can be decreased, energy waste and greenhouse-gas emissions can be reduced, and sustainability can be increased [4-6].

Many undeveloped and developing countries store C&D without recycling in landfills. Although some developed countries recycle a part of the C&D, the level of recycling is insufficient [3]. Overall, the recycling of C&D in developed or developing countries should be increased, since recycling, recovery and sustainability are indispensable for our world at this time. Therefore, many researchers have recommended increased studies on the subject to expand the areas of use for C&D [5-11].

Generally, it is predicted that the C&D in some geotechnical applications such as fillings for various aims and base/subbase layer in an unbound pavement can be reused instead of virgin aggregate. Accordingly, several studies were conducted involving conventional laboratory tests such as proctor, unconfined compressive strength, and California bearing ratio tests. In these studies, it was mentioned that the C&D could be a good alternative to virgin aggregates in fillings. However, in many studies, it is stated that the quality of the C&D in terms of several geotechnical and physical parameters is less than that of virgin aggregates [2, 8]. In these studies, it is suggested that the engineering behaviours of

je bilo z metodami, uporabljenimi v tej študiji, doseženih nekaj pomembnih izboljšav. Poleg tega je bilo ugotovljeno, da je najboljši učinek ojačitve za C&D dosežen, ko je bila nameščena geomreža in dodana VA v C&D.

the C&D should be improved. Therefore, some studies have used geosynthetics [12, 13] or additives [9, 14, 15] to improve the engineering properties of the C&D. Moreover, for the same purpose, the C&D was mixed with virgin aggregates in a few studies, and subsequently some tests were carried out with mixture aggregates [16-18]. However, because the studies usually involve small-scale conventional laboratory tests, more comprehensive research is needed to increase the reuse of C&D.

In some geotechnical applications, such as fillings and unbound pavement layers, granular soils are generally used as the filling material. Geogrids, which are a type of geosynthetics and used for reinforcement purposes, can be more suitable for an improvement of the C&D since they have an interlocking mechanism with particles if the C&D is to be transformed into a granular material and reused. Although in the literature there are many studies on the advantages of the interaction mechanism between geogrids and virgin granular soils [19-28], there are only a few studies related to C&D reinforced by geogrids [12, 13]. In addition, in studies on C&D reinforced by a geogrid, it was emphasized that the subject should be examined in more detail. On the other hand, the granular fill layers should be capable of resisting static and repeated stresses [29, 30]. Generally, the C&D consists of a wide variety of waste materials that would further complicate the behaviour under repeated stresses. When the use of C&D instead of virgin aggregates is investigated, the complex behaviour under repeated stresses of the C&D needs to be determined. The resilient modulus tests, which are performed by applying the cycling stresses in different stress combinations in a repeated load triaxial test device, can help us to understand this complex behaviour. For this reason, a few researchers have conducted resilient modulus tests on C&D. In those studies, it was stated that the C&D needs reinforcement in terms of resilient behaviour [31-34]. Recently, Chen et al. [29] in their study stated that the resilient behaviour of low-quality virgin aggregate can be improved with a geogrid. Accordingly, the resilient behaviour of the C&D can be improved with a geogrid, for example, low-quality aggregates. In this regard, Rahman et al. [35] in their study reported that the inclusion of a geogrid had effects on the resilient modulus and permanent deformation behaviour of the C&D. However, in this study, it was mentioned that studies that are related to C&D reinforced with geogrids

are limited and the reinforcement effects of the geogrids under repeated stresses are still unknown.

In summary, it is necessary to improve some properties such as the resilient behaviour and the compressive strength of the C&D to increase the reuse of C&D in fillings. However, according to the literature, further investigations need to be conducted for that. In this study, two different improvement methods were investigated to improve the C&D. The first was to mix the C&D with virgin aggregates (VA). In other words, to produce a type of hybrid C&D (C&D-VA), which is an easy improvement method. The second was reinforcing the C&D with a geogrid, which is a widely used method to improve granular soils. In addition, in the case of using both methods together, the improvement of the C&D was investigated as well. The effects of improvements were evaluated for both monotonically increased stresses and cycling stresses. Accordingly, tests were carried out on large-scale test samples. It is believed that this study will make a great contribution to the literature as it investigates the effects of different improvement types and evaluates these effects in terms of monotonically increased stresses and cycling stresses. It is also estimated that the suggestions to be presented to the designer at the end of the study will increase the reuse rate of the C&D. Besides, this study offers alternatives related to reusing even low-strength C&Ds by means of some improvements. The focus of this study is to investigate the reusability by improving the C&D obtained from low-strength, classically reinforced concrete structures, of which the mean compressive strength of the concrete core samples was 14.5 MPa. The C&D was obtained by carrying out several recycling processes. For the improvement of the C&D, two methods were used for the mixing with the VA of the C&D, (C&D-VA), and the reinforcing with the geogrid. In addition, those methods were also used together. Reinforced and unreinforced C&D and the VA test samples were prepared. The resilient modulus for the resilient behaviour and the unconfined compressive strength for the compressive strength of the samples were determined using large-scale samples. The results are presented in the form of a comparison.

2. MATERIALS

2.1. Recycled, virgin and hybrid aggregates

Three different types of filling materials (granular materials) such as recycled aggregates, virgin aggregates and hybrid aggregates were used. These materials are construction and demolition waste aggregates (C&D) obtained from debris as recycled aggregates, virgin aggregates (VA) taken from a quarry and hybrid aggre-



Figure 1. C&D, VA and C&D-VA.

gates (C&D-VA) derived by mixing the C&D with the VA in equal amounts (Figure 1).

The debris was taken from the group of low-strength RC structures, where the concrete compressive strengths of the core samples were varied between 7.5 MPa and 20 MPa, and the C&D was obtained by carrying out several recycling processes on this debris. Firstly, the debris was transferred to a crushing machine to produce proper-sized granular materials. Subsequently, steel bars and iron pieces in the debris were removed by passing them through a magnet system. After this process, the debris was crushed and the C&D materials, which have three different grain-size ranges, i.e., 0–5, 5–12, and 12–25 mm [36], were obtained. Subsequently, based on the particle size of those C&D materials, a mixture calculation was made to obtain a gradation that is suitable for use in highway base and sub-base courses [37]. Finally, the C&D materials obtained in different gradations were mixed and the C&D used as a test sample was obtained. On the other hand, for a comparison with the C&D, the VA with limestone particles was obtained from a quarry in Turkey. The gradation of the VA was made suitable to

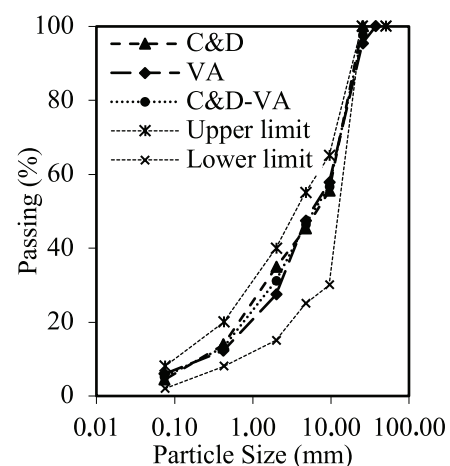


Figure 2. Gradations of the C&D, VA and C&D-VA with limit values recommended by ASTM [37].

use in highway base and sub-base courses [37], similar to the C&D [38]. Furthermore, the C&D with the VA, which has similar gradations, was mixed in equal amounts and the C&D-VA mixtures were obtained. The gradations of the C&D, the VA and the C&D-VA are shown in Figure 2.

When the C&D was examined in detail, it was clear that the C&D includes different recycled wastes, such as concrete, aggregate, brick, glass and some other materials. According to the tests carried out considering BS EN 933-11 [39], the C&D in this study consists of 36.33 % concrete (R_c), 52.65 % aggregate (R_u), 10.53 % brick (R_b), 0.11 % glass (R_g) and 0.38 % other materials (metals, non-floating wood plastic, rubber, plaster) (X). It also contains 0.7 kN/m^3 of floating particles (FL) [8].

Some physical and geotechnical properties of the C&D, the VA and the C&D-VA were obtained with laboratory tests, such as a sieve analysis, flatness index, Los Angeles abrasion, water absorption, pycnometer tests and modified compaction tests [36, 40-44]. The results obtained from these tests are shown in Table 1. In addition, compaction curves obtained from modified compaction

tests are shown in Figure 3. Detailed characteristics of the C&D and the VA were reported by Ok et al. [8].

2.2 Geogrid

In this research, a triaxial geogrid, which is obtained from a manufacturer, was used to improve the resilient modulus and the unconfined compressive strength of the C&D and the C&D-VA. This triaxial geogrid was manufactured from punched polypropylene sheets and has an equilateral direction to form its triangular apertures. The texture of the geogrid is shown in Figure 4, and the physical and mechanical properties of the geogrid, as provided by the manufacturer, are presented in Table 2.

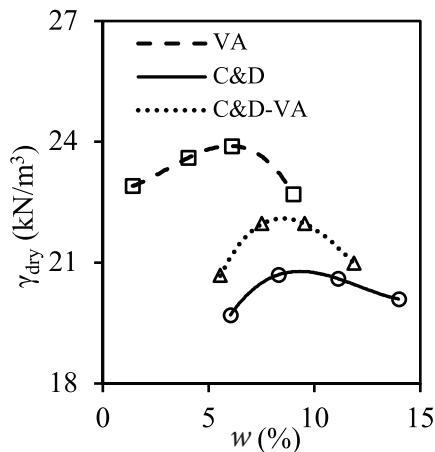


Figure 3. Compaction curves of the granular materials.

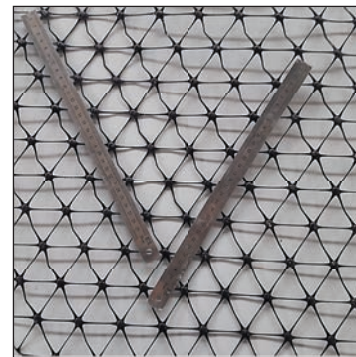


Figure 4. Geogrid.

Table 2. Properties of geogrid.

Properties	Unit	Description or value
Raw Material	-	Polypropylene
Aperture Type	-	Triangle
Aperture Dimensions	mm	40×40×40
Thickness	mm	1.1
Tensile Strength at 5 % strain, md/cmd*	kN/m	300

*: machine direction/cross machine direction

Table 1. Physical and geotechnical properties of C&D, VA and C&D-VA mixture.

Properties	Unit	C&D	VA	C&D-VA
Coefficient of uniformity (C_u)	-	41.87	35.88	39.97
Coefficient of curvature (C_c)	-	1.06	1.89	1.35
Flakiness index	%	11.68	12.66	12.11
Los Angeles abrasion loss	%	33.58	23.40	29.89
Particle Density (γ_s)	kN/m^3	$26.30^f, 26.10^c$	$26.90^f, 27.10^c$	$26.55^f, 26.50^c$
Water absorption	%	$6.82^f, 4.06^c$	$0.40^f, 0.36^c$	$3.88^f, 2.51^c$
Maximum dry unit weight (γ_{drymax})	kN/m^3	20.77	23.90	21.10
Optimum water content, (w_{opt})	%	9.7	6.0	8.5

^f: Fine particle, ^c: Coarse particle

3 TESTING METHODS

3.1 California bearing ratio (CBR)

The CBR test is commonly used to compare the strength of filling materials. The test is performed by penetrating a cylindrical steel piston of 50 mm diameter into the sample, which is placed in a mold (152.4 mm diameter), at a rate of 1.27 mm/min [45]. The result of the test can be presented both in terms of load–displacement curves and percent relative (CBR value) to the reference value in the ASTM D1883–99 [45]. For the CBR tests, the filling materials with optimum water content were placed in a mold, which is used in modified compaction tests, by compacting to provide their maximum dry unit weight. Then, the prepared samples were tested according to ASTM D1883–99 [45] and their CBR values were obtained.

3.2 Large-scale unconfined compressive strength (UCS)

The UCS test is one of the most popular tests used as a key design index parameter for estimating the stiffness of soils. The UCS test includes the application of an axial vertical load through loading platens, using strain-control conditions, to a cylindrical soil sample that is unconfined. The maximum unit stress obtained from the result of the UCS test is defined as the UCS [46]. Large-scale UCS tests on geogrid-reinforced and unreinforced C&D, VA and C&D-VA were performed in this study. In the preparation of test samples, since the maximum aggregate size of the filling materials is 20 mm, a large-scale split mold, in which the effective internal height is 300 mm and the effective internal diameter is 150 mm, was used. For large-scale UCS tests, the filling materials with optimum water content were placed in a large-scale split mold and compacted to achieve the maximum dry

unit weight. According to ASTM D2166 [46], the UCS tests were conducted by applying an axial strain rate of 0.5 % per minute to the samples.

3.3 Resilient modulus (M_R)

The fillings beneath oil storage tanks, silos or machine foundations and embankments such as road base/sub-base are subjected to repeated loads. In these cases, and many similar situations, the resilient behaviour of the fillings is significant in addition to the unconfined compressive strength. However, the resilient behaviour of granular materials depends on some agents. For example, granular materials can have different resilient deformation values according to the stress levels applied to them. Hence, the resilient behaviour can usually be characterized by the resilient modulus (M_R), which has different values for different stress levels. Accordingly, M_R was used by several researchers to characterize the resilient behaviour of the base/sub-base course material and the subgrade soil [47]. M_R is defined as the ratio of the deviator stress to the vertical elastic deformation [48]. In this study, M_R tests were performed using a large-scale cyclic triaxial test device to determine the resilient behaviour of the geogrid-reinforced and unreinforced C&D, VA and C&D-VA [49]. The M_R test samples with optimum water content were placed in the split mold with a diameter of 150 mm and a height of 300 mm, by providing the maximum dry unit weight. M_R tests were performed with 1000 cycles in the initial stage and then 100 cycles in each stage, for a total of 2500 load cycles. Since permanent deformation values are almost constant in the last cycles of the stress stages, the resilient modulus value of any stress stage is determined by considering the last five cycles. The stress stages for aggregate materials are shown in Table 3. According to AASHTO T-307 [49], the load pulses applied in M_R tests had a haversine-shaped loading of 0.1 seconds and rest periods of 0.9 seconds.

Table 3. Stress stages and values according to AASHTO [49].

Stress stages	Confining stress (kPa)	Deviator stress (kPa)	Bulk stress (kPa)	Stress stages	Confining stress (kPa)	Deviator stress (kPa)	Bulk stress (kPa)
0	103.4	103.4	413.7	8	68.9	137.9	344.7
1	20.7	20.7	82.7	9	68.9	206.8	413.7
2	20.7	41.4	103.4	10	103.4	68.9	379.2
3	20.7	62.1	124.1	11	103.4	103.4	413.7
4	34.5	34.5	137.9	12	103.4	206.8	517.1
5	34.5	68.9	172.4	13	137.9	103.4	517.1
6	34.5	103.4	206.8	14	137.9	137.9	551.6
7	68.9	68.9	275.8	15	137.9	275.8	689.5

3.4 Geogrid reinforcement

Geogrid reinforcement (RF) has been used to improve the resilient behaviour and compressive strength of filling materials (C&D and C&D-VA) obtained from recycled aggregates in this study. Furthermore, to compare the effect of geogrid reinforcement, samples of the geogrid-reinforced VA were also prepared and tested. For this purpose, the M_R and the UCS tests were carried out on geogrid-reinforced and unreinforced C&D, VA and C&D-VA. Abu-Farsakh et al. [25] conducted resilient modulus tests on virgin aggregates by placing the geogrid at different locations on the test specimen. Consequently, they stated that when the geogrid is placed in the upper or middle of the test specimen, more improvement than other locations was obtained. In this study, considering some studies in the literature [25, 35, 50], the geogrid reinforcement was placed at the mid-height of the test samples. The placement and layout of the geogrid reinforcement are shown in Figure 5.

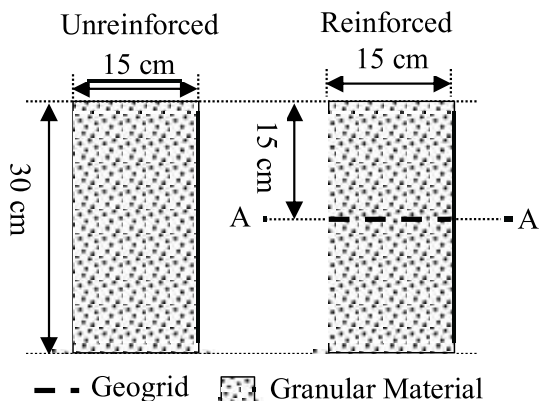


Figure 5. Placement and layout of the geogrid reinforcement.

4 DISCUSSION OF RESULTS

4.1 Evaluation of the CBR values of filling aggregates

The CBR tests were carried out on the C&D, the VA and the C&D-VA samples. The CBR values and load-displacement curves of the samples were determined according to the results of those tests. The CBR values of the C&D, the VA and the C&D-VA samples were 98.99 %, 125.16 % and 105.51 %, respectively. The load-displacement (N - s) curves of those aggregates are shown in Figure 6.

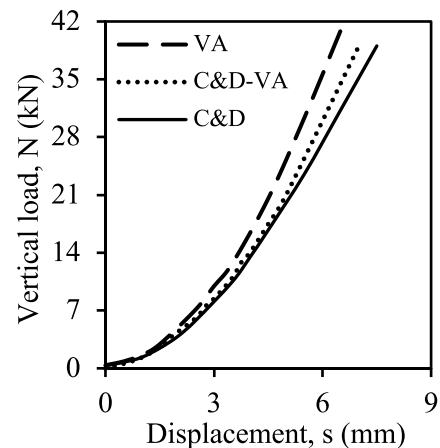


Figure 6. Load-displacement curves of the filling aggregates in CBR tests.

Considering the CBR test results, the behaviour of the load-displacement curves for all the samples were similar for displacements of less than 2 cm. However, as with the displacement increases, the situation changed in favour of the VA. This result is attributed to the fact that the VA particles are stronger than the C&D particles, as seen in the Los Angeles abrasion tests [8]. However, the CBR values indicate that the C&D and the C&D-VA samples are appropriate for use as a filling material according to some technical specifications [51, 52].

4.2 Comparison C&D with VA

Firstly, the M_R and the UCS tests were performed to determine the resilient behaviour and compressive strength of the C&D. Subsequently, for comparison, those tests were conducted on the VA. The results of those tests are shown by comparing each in Figure 7.

Figure 7 shows that the C&D is less than that of the VA in terms of both M_R and UCS. The UCS value of the VA is 30.7 % higher than that of the C&D. Moreover,

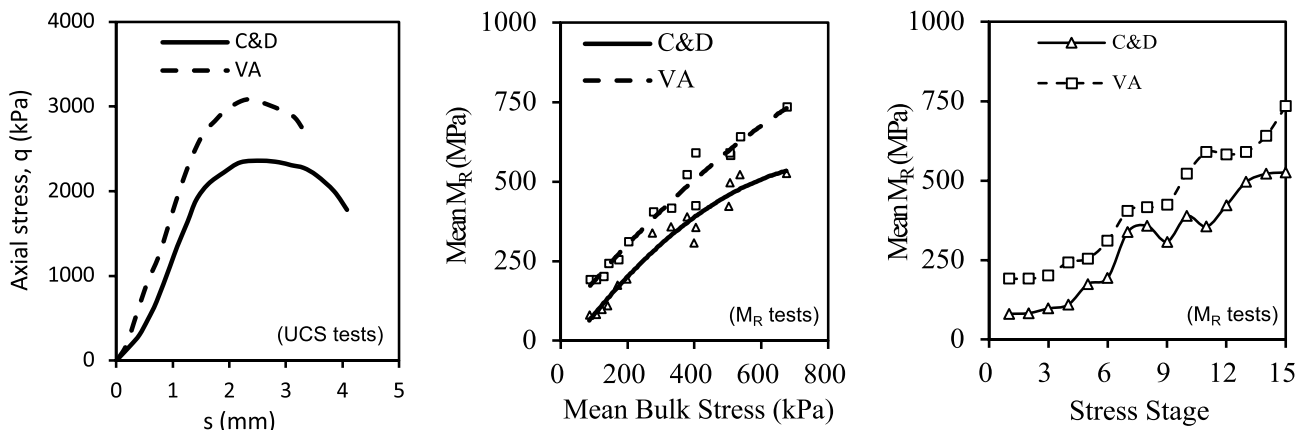


Figure 7. Stress-displacement curves and the M_R values of the C&D and the VA.

for all the stress stages, the M_R values of the C&D are lower than those of the VA. Although it has been stated in various studies that C&D can be used in some fillings, even with this performance, it has been mentioned in those studies that various improvements are needed to increase the performance of the C&D [6, 8, 16, 35, 53, 54]. Therefore, in this study, the performance of the C&D was increased by mixing the C&D with VA or using the geogrid reinforcement.

4.3 Evaluation of the C&D-VA mixture

A new aggregate mixture, namely the hybrid C&D (C&D-VA), was obtained by mixing the C&D with VA in the same proportions to increase the M_R and the UCS of the C&D. The results of the UCS and the M_R tests of the C&D-VA are shown by comparing with that of the C&D and the VA in Figure 8.

Mixing the C&D with the VA increased the UCS by approximately 11 %. Also, in all stress stages, the M_R values of the C&D-VA are more than those of the C&D. However, the improvement of both the M_R and the UCS are very limited, and the M_R and the UCS values of the VA are greater than the C&D-VA. Even if according to those results, also the C&D-VA like the C&D may be an alternative to the VA to use as a filling material, it is thought that it might need an improvement such as geogrid reinforcement [6, 8, 35].

4.4 Effects of geogrid reinforcement

Geogrid reinforcement (RF) was used to increase the M_R and the UCS of the C&D and C&D-VA. Furthermore, to compare the effect of geogrid reinforcement, the M_R and the UCS tests were also carried out on the VA reinforced by the geogrid. Accordingly, the effects of geogrid on

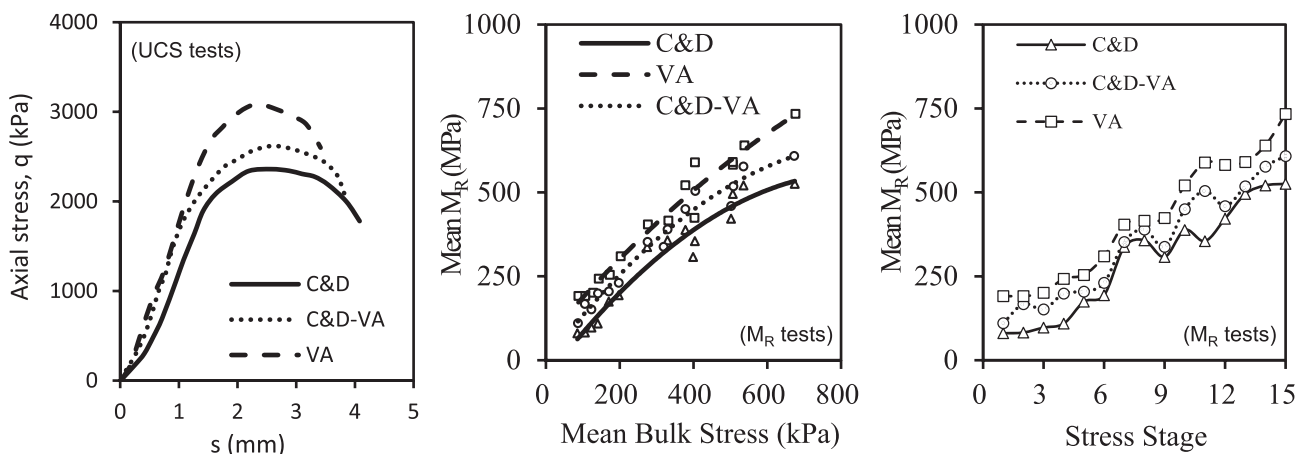


Figure 8. Stress-displacement curve and M_R values of the C&D-VA in comparison to C&D and VA.

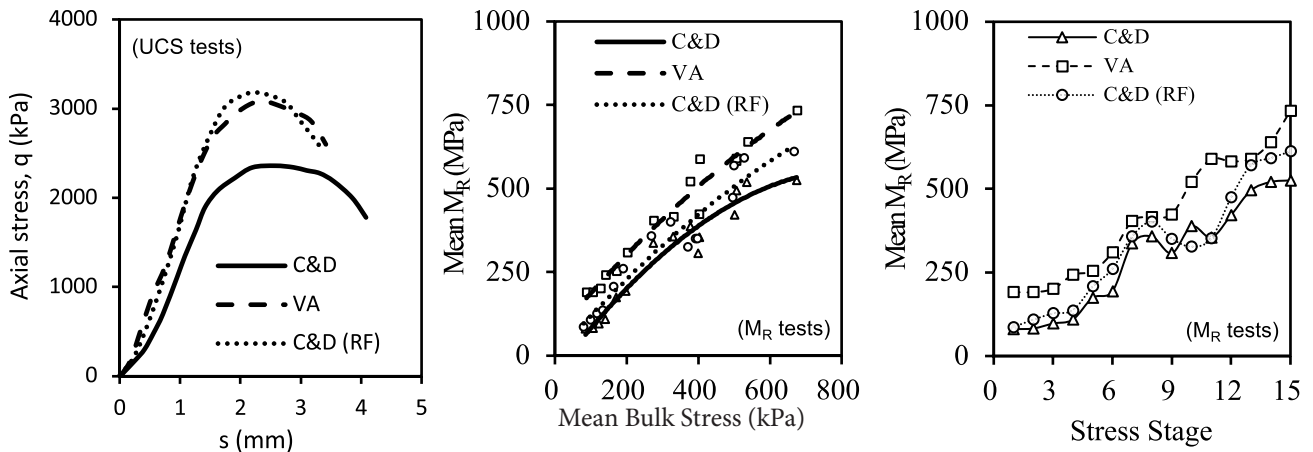


Figure 9. Stress-displacement curve and the M_R values of the C&D (RF) in comparison with the C&D and the VA.

those parameters were discussed in terms of the C&D and the VA according to the results of the tests on both reinforced C&D and reinforced VA. The results of the UCS and the M_R tests of the geogrid reinforced C&D, namely, C&D (RF), are shown by comparing with that of the C&D and the VA in Figure 9.

According to the results of tests performed on the C&D (RF), the UCS value of the C&D (RF) was approximately 35 % higher than that of the C&D. In other words when the C&D is reinforced by a geogrid, the UCS value exceeded that of the VA. However, in all the stress stages, although the M_R values of the C&D (RF) are more than those of the C&D, they are less than those of the VA. Therefore, there is a significant improvement in monotonic stress for the geogrid-reinforced C&D, while the improvement is limited in cycling stress. Consequently, for fillings exposed to static loads, the geogrid-reinforced C&D can achieve the performance of natural aggregates,

but it may be necessary to develop different solutions to obtain the performance of natural aggregates in fillings exposed to repeated stress such as cycling stress. For this, reinforcement of the C&D-VA sample with a geogrid was considered. Accordingly, the UCS and the M_R tests on the C&D-VA reinforced by the geogrid, namely C&D-VA (RF), were performed. The results of those tests are shown by comparing with that of the C&D and the VA in Figure 10.

According to the results of the tests performed on the C&D-VA (RF), the UCS value of the C&D-VA (RF) was obtained as approximately 44 % and 10 % higher than that of the C&D and that of the VA, respectively. On the other hand, for all the stress stages, the M_R values of the C&D-VA (RF) are more than those of the C&D. Moreover, in the low-stress stages, although the M_R values of the C&D-VA (RF) are slightly less than those of the VA, in high-stress stages, the M_R values of the C&D-VA (RF)

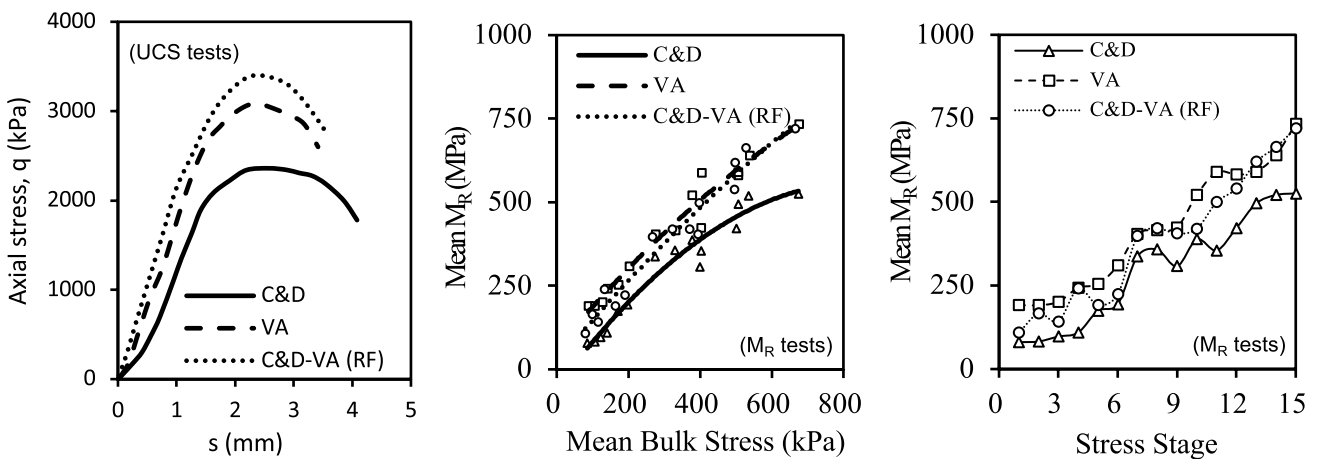


Figure 10. Stress-displacement curve and the M_R values of the C&D-VA (RF) in comparison with the C&D and the VA.

are close to those of the VA. This result is thought to be obtained due to the geogrid's reinforcement mechanisms. Geogrids have main reinforcement functions, such as lateral confinement and a membrane effect. [55]. The lateral confinement function, one of the geogrid reinforcement mechanisms, is due to the soil particles interlocking within the geogrid aperture. While soil particles cannot resist the tensile stress, the geogrid material can resist a higher tensile stress than soil particles. As the soil particles begin to deform laterally, they fall into the geogrid apertures. This situation caused the interlocking mechanism. Thus, the tensile stresses occurring in the soil particles transmit to the geogrid. Since the geogrid can resist much more tensile stress, the strength of the soil layer increases [48]. The membrane effect, another of the geogrid-reinforcement mechanisms, occurs as a result of the deformation of the soil. When any stress is applied to the soil layers, the soil layers can move down from its current position. As a result of this situation, the geogrid is deformed and tensioned. The vertical deformation creates a concave shape in the geogrid. Due to tensile stiffness of the geogrid, the concave shape performs an upward force to support the applied load and reduce the vertical stress on the soil layers. However, to achieve this effect, there must be a significant deformation [56]. When Figure 10 is examined, the deformation and stress increase, the improvement of the sample increases due to the reinforcement mechanisms, such as the membrane effect and the lateral confinement of the geogrid. Similarly, the same reinforcement mechanism was observed in geogrid-reinforced (i.e., the VA (RF)) and unreinforced VA.

The results of the M_R and the UCS tests of the VA (RF) and VA are shown Figure 11. As the deformation and stress increase, the improvement of the sample increases. For virgin aggregates, this event is in line with previous

studies in the literature. In this study, in the geogrid-reinforced C&D, a reinforcement mechanism similar to the geogrid-reinforced VA was observed. Therefore, it was considered that C&D is a convenient material to reinforce with a geogrid. However, it should be considered that the reinforcement with a geogrid is more effective in high deformation and stress.

4.5 UCSR and M_{RR}

Two coefficients, the UCSR and the M_{RR} , have been defined as dimensionless parameters obtained from the results of tests. The UCSR was defined as the ratio of the UCS value obtained in the result of a test, which will be compared to the UCS value of the C&D. Similarly, M_{RR} was defined as the ratio of the M_R value obtained in the result of a test, which will be compared to the M_R value of the C&D, which has the same stress stages. A calculation of those coefficients is shown in Equation 1 and 2. The UCSR and M_{RR} values calculated from the test results are shown in Figure 12 and Figure 13, respectively.

$$UCSR = \frac{UCS}{UCS_{C\&D}} \quad (1)$$

$$M_{RR} = \frac{Mean M_R}{Mean M_{R(C\&D)}} \quad (2)$$

As seen in the UCSR values obtained from the results of the tests, for monotonically increased stresses, the performance of the C&D can increase sufficiently to obtain that of the VA when it is reinforced by a geogrid only. However, as seen in the MRR values, in repeated stresses, the reinforcing with the geogrid of the C&D might not be enough to obtain the performance of the VA. In this case, i.e., under repeated stresses, if the C&D is mixed with the VA and then the mixture is reinforced

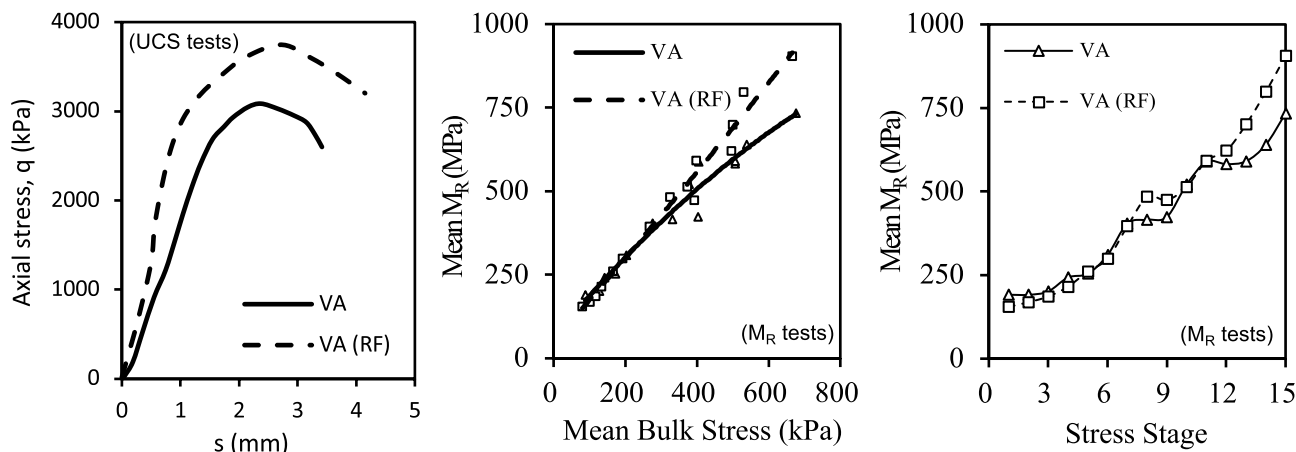


Figure 11. Stress-displacement curves and the M_R values of the reinforced and unreinforced VA.

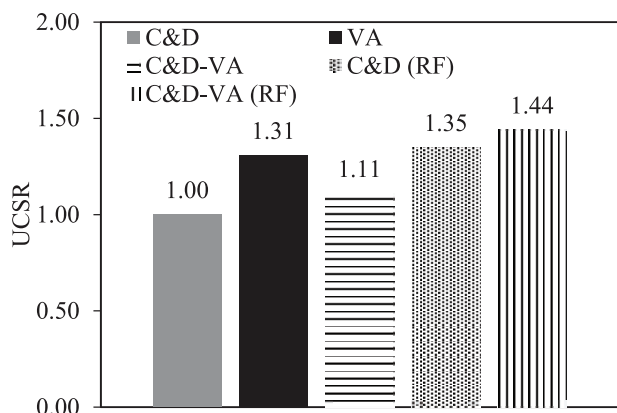


Figure 12. UCSR values.

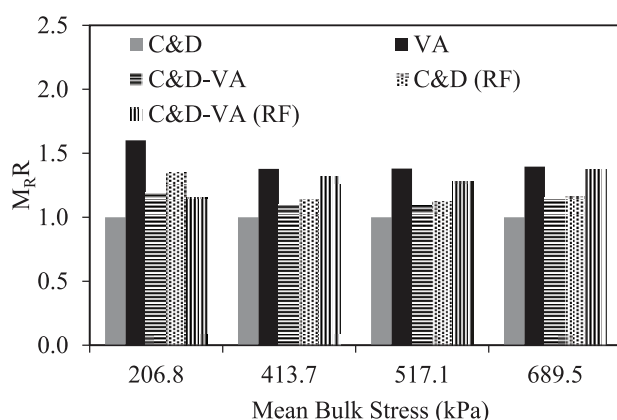


Figure 13. M_R values according to mean bulk stress.

by the geogrid, it is clear that the performance of the VA can be achieved. It was considered that the reason for this was that the effect of cyclic loads on brittle soil grains could be greater.

5 CONCLUSIONS

In this study, laboratory tests such as resilient modulus tests and unconfined compressive tests, including large-scale tests, to improve the resilient behaviour and compressive strength of the C&D were performed. For this purpose, the effectiveness of some improvement methods, such as both the mixing with the VA of the C&D (in other words producing a type of hybrid C&D) and reinforcing the C&D with geogrid was evaluated. On the basis of the results of these tests, the following conclusions can be drawn:

- The UCS value of the C&D was obtained as 30.7 % less than that of the VA. Moreover, it was seen that the M_R values in all the stress stages of the C&D are

less than those of the VA. These results, similar to those from Los Angeles abrasion tests, are assumed to be due to the VA particles being stronger than the C&D particles. The CBR test results confirm this result. So, the test results show that there is a quality difference between the C&D and the VA in terms of both monotonically increasing and repeated stresses.

- According to the results of tests on the hybrid aggregate (C&D-VA), the M_R values in all the stresses stages and the UCS value of the C&D-VA were more than those of the C&D. In the case of adding the VA to the C&D, the UCS value was increased by 11 %. However, the improvement is limited and the values of C&D-VA do not reach those of the VA.
- C&D (RF)'s UCS was approximately 35 % higher than that of C&D, thus exceeding that of the VA. However, it was found that although the M_R values of the C&D (RF) are more than those of the C&D, they are less than those of the VA for all stress stages. Therefore, it was a significant improvement in monotonically increased stresses, while the improvement was limited in the cycling stresses because the C&D is reinforced by a geogrid. If C&D is to be used in the construction of a fill, these consequences should be considered for a filling material that could be subjected to repeated stresses.
- According to the results of tests on the hybrid aggregate reinforced by a geogrid, the UCS value of the C&D-VA (RF) is approximately 44 % higher than that of the C&D, and the M_R values of the C&D-VA (RF) are more than those of the C&D.
- The UCS value of the C&D-VA (RF) was approximately 10 % higher than that of the VA. Also, the M_R values of the C&D-VA (RF) are close to those of the VA in high-stress stages, although in the low-stress stages they are slightly less. This result is thought to be due to reinforcement mechanisms, such as lateral confinement and the membrane effect of the geogrid.
- The reinforcement mechanisms of all the test samples reinforced with the geogrid were similar. Therefore, the C&D could be a suitable material to reinforce with a geogrid.
- In the case of both mixing with the VA and reinforcing with the geogrid, for the C&D it can be considered that the best improvement was achieved on both the monotonically increased and the repeated stresses. With these improvements it can be possible to have durable fillings even when using low-strength C&D, and this can increase the reuse of the C&D. Nevertheless, it should be considered that reinforcement with a geogrid is more effective for high deformation and stress in designs.
- Due to the energy-absorption feature of the geogrid, there are important advantages in dynamic cases. So,

it is recommended to conducted studies that include earthquake analysis such as Edinçliler and Yildiz [57] and Yildiz [58] for a better understanding of the behaviour of geogrid-reinforced C&D and C&D-VA.

REFERENCES

- [1] Shen, L.Y., Tam, V.W., Tam, C.M., Drew, D. 2004. Mapping approach for examining waste management on construction sites. *Journal of construction engineering and management* 130(4): 472-481, [https://doi.org/10.1061/\(ASCE\)0733-9364\(2004\)130:4\(472\)](https://doi.org/10.1061/(ASCE)0733-9364(2004)130:4(472)).
- [2] Vieira, C.S., Pereira, P.M. 2015. Use of recycled construction and demolition materials in geotechnical applications: A review. *Resources, Conservation and Recycling* 103: 192–204. <http://dx.doi.org/10.1016/j.resconrec.2015.07.023>.
- [3] European Commission (DG ENV) 2011. Service contract on management of construction and demolition waste prepared by Bio Intelligent Service, Available online: http://ec.europa.eu/environment/waste/pdf/2011_CDW_Report.pdf.
- [4] Arulrajah, A., Piratheepan, J., Aatheesan, T., Bo, M.W. 2011. Geotechnical properties of recycled crushed brick in pavement applications. *Journal of Materials in Civil Engineering* 23(10):1444–52, [https://doi.org/10.1061/\(ASCE\)MT.1943-5533.0000319](https://doi.org/10.1061/(ASCE)MT.1943-5533.0000319).
- [5] Jimenez, J.R., Ayuso, J., Agrela, F., López, M., Galvín, A.P. 2012. Utilisation of unbound recycled aggregates from selected CDW in unpaved rural roads. *Resources, Conservation and Recycling* 58: 88–97, <https://doi.org/10.1016/j.resconrec.2011.10.012>.
- [6] Jallu, M., Arulrajah, A., Saride, S., Evans, R. 2020. Flexural fatigue behavior of fly ash geopolymer stabilized-geogrid reinforced RAP bases. *Construction and Building Materials* 254-119263: 1-9, <https://doi.org/10.1016/j.conbuildmat.2020.119263>.
- [7] Evangelista, L., de Brito, J. 2014. Concrete with fine recycled aggregates: a review, *European Journal of Environmental and Civil Engineering*, 18(2), 129-172, <https://doi.org/10.1080/19648189.2013.851038>
- [8] Ok, B., Sarici, T., Talaslioglu, T., Yildiz, A. 2020. Geotechnical properties of recycled construction and demolition materials for filling applications. *Transportation Geotechnics* 24-100380: 1-9, <https://doi.org/10.1016/j.trgeo.2020.100380>.
- [9] Mohammadinia, A., Arulrajah, A., Horpibulsuk, S., Shourijeh, P.T. 2019. Impact of potassium cations on the light chemical stabilization of construction and demolition wastes. *Construction and Building Materials* 203: 69-74, <https://doi.org/10.1016/j.conbuildmat.2019.01.083>.
- [10] Asprone, D., Bilotta, E., Capasso, I., Caputo, D., Flora, A., Liguori, B., Lirer, S. 2015. Re-use of construction and demolition waste for geotechnical applications. *Geotechnical Engineering for Infrastructure and Development* 1(1): 2589–2594.
- [11] Aldemir, A., Akduman, S., Kocaer, O., Aktepe, R., Sahmaran, M., Yildirim, G., ... Ashour, A. 2022. Shear behaviour of reinforced construction and demolition waste-based geopolymer concrete beams. *Journal of Building Engineering*, 47, 103861. <https://doi.org/10.1016/j.jobe.2021.103861>
- [12] Vieira, C.S., Pereira, P.M. 2015. Damage induced by recycled construction and demolition wastes on the short-term tensile behaviour of two geosynthetics. *Transportation Geotechnics* 4: 64-75, <http://dx.doi.org/10.1016/j.trgeo.2015.07.002>.
- [13] Arulrajah, A., Rahman, M.A., Piratheepan, J., Bo, M.W., Imteaz, M.A. 2013. Interface shear strength testing of geogrid-reinforced construction and demolition materials. *Advances in Civil Engineering Materials* 2(1): 189–200, <https://doi.org/10.1520/ACEM20120055>.
- [14] Arulrajah, A., Mohammadinia, A., Phummiphan, I., Horpibulsuk, S., Samingthong, W. 2016. Stabilization of recycled demolition aggregates by geopolymers comprising calcium carbide residue, fly ash and slag precursors. *Construction and Building Materials* 114: 864-873, <https://doi.org/10.1016/j.conbuildmat.2016.03.150>.
- [15] Li, L., Zhang, H., Xiao, H., Pei, Y., Wang, J. 2020. Mechanical and microscopic properties of alkali-activated fly-ash-stabilised construction and demolition waste. *European Journal of Environmental and Civil Engineering*, 1-17, <https://doi.org/10.1080/19648189.2020.1792351>
- [16] Bennert, T., Papp, Jr. W.J., Maher, A., Gucunski, N. 2000. Utilization of construction and demolition debris under traffic-type loading in base and subbase applications. *Transportation research record* 1714(1): 33-39, <https://doi.org/10.3141/1714-05>.
- [17] Ayan, V., Limbachiya, M.C., Omer, JR., Azadani, S.M.N. 2014. Compaction assessment of recycled aggregates for use in unbound subbase application. *Journal of Civil Engineering and Management* 20(2): 169-174, <https://doi.org/10.3846/13923730.2013.801882>.
- [18] Li, L., Qin, L., Xiao, H., Hu, Z., Xu, G., Ma, Q. 2020. The triaxial test of construction and demolition (C&D) materials with different particle sizes and sand contents. *European Journal of Environmental*

- and Civil Engineering, 1-22, <https://doi.org/10.1080/19648189.2020.1820908>.
- [19] Haas, R., Walls, J., Carroll, R.G. 1988. Geogrid reinforcement of granular bases in flexible pavements. *Transportation research record* 1188(1): 19–27.
- [20] Al-Qadi, IL., Brandon, T.L., Valentine, R.J., Lacina, B.A., Smith, T.E. 1994. Laboratory evaluation of geosynthetic reinforced pavement sections. *Transportation Research Record*. 1439: 25–31.
- [21] Perkins, S.W. 2002. Evaluation of geosynthetic reinforced flexible pavement systems using two pavement test facilities. Department of Transportation, Federal Highway Administration, Washington, D.C. FHWA/MT-02–008/20040, pp. 1-120, Available online: <https://rosap.nrl.bts.gov/view/dot/42085>
- [22] Berg, R.R., Christopher, B.R., Perkins, S.W. 2000. Geosynthetic reinforcement of the aggregate base course of flexible pavement structures. GMA White Paper II, Geosynthetic Materials Association, Roseville, MN, USA, pp. 1-176, Available online: https://geosynthetics.ifai.com/wp-content/uploads/sites/10/2016/06/geosynthetic_reinforcement_gma_white_paper_ii.pdf
- [23] Cancelli, A., Montanelli, F. 1999. In-ground test for geosynthetic reinforced flexible paved roads. In *Twelfth European Conference on Soil Mechanics and Geotechnical Engineering*. Roseville, MN, vol. 2, pp. 863–878.
- [24] Nazzal, M., Abu-Farsakh, M., Mohammad, L. 2007. Laboratory characterization of reinforced crushed limestone under monotonic and cyclic loading. *Journal of Materials in Civil Engineering* 19(9): 772-783, [https://doi.org/10.1061/\(ASCE\)0899-1561\(2007\)19:9\(772\)](https://doi.org/10.1061/(ASCE)0899-1561(2007)19:9(772)).
- [25] Abu-Farsakh, M., Souci, G., Voyiadjis, G.Z., Chen, Q. 2012. Evaluation of factors affecting the performance of geogrid-reinforced granular base material using repeated load triaxial tests. *Journal of Materials in Civil Engineering* 24(1): 72-83, [https://doi.org/10.1061/\(ASCE\)MT.1943-5533.0000349](https://doi.org/10.1061/(ASCE)MT.1943-5533.0000349).
- [26] Tutumluer, E., Huang, H., Bian, X. 2012. Geogrid-aggregate interlock mechanism investigated through aggregate imaging-based discrete element modeling approach. *International Journal of Geomechanics* 12(4): 391-398, [https://doi.org/10.1061/\(ASCE\)GM.1943-5622.0000113](https://doi.org/10.1061/(ASCE)GM.1943-5622.0000113).
- [27] Kamalzare, M., Ziaie-Moayed, R. 2011. Influence of geosynthetic reinforcement on the shear strength characteristics of two-layer sub-grade. *Acta Geotechnica Slovenica*, 8(1), 39-49.
- [28] Haimin, W., Yiming, S., Linjun, D., Zhaoming, T., 2015. Implementation and verification of a geosynthetic-soil interface constitutive model in the Geogrid element of FLAC3D. *Acta geotechnica Slovenica*, 12(1), 27-35.
- [29] Chen, Q., Abu-Farsakh, M., Voyiadjis, G.Z., Souci, G. 2013. Shakedown analysis of geogrid-reinforced granular base material. *Journal of materials in civil engineering* 25(3): 337-346, [https://doi.org/10.1061/\(ASCE\)MT.1943-5533.0000601](https://doi.org/10.1061/(ASCE)MT.1943-5533.0000601).
- [30] Chen, W.B., Feng, W.Q. Yin, J.H. 2020. Effects of water content on resilient modulus of a granular material with high fines content. *Construction and Building Materials* 236-117542: 1-14, <https://doi.org/10.1016/j.conbuildmat.2019.117542>.
- [31] Gabr, A.R., Cameron, D.A. 2012. Properties of recycled concrete aggregate for unbound pavement construction. *Journal of Materials in Civil Engineering* 24(6): 754-764, [https://doi.org/10.1061/\(ASCE\)MT.1943-5533.0000447](https://doi.org/10.1061/(ASCE)MT.1943-5533.0000447).
- [32] Dong, Q., Huang, B. 2014. Laboratory evaluation on resilient modulus and rate dependencies of RAP used as unbound base material. *Journal of Materials in Civil Engineering* 26(2): 379-383, [https://doi.org/10.1061/\(ASCE\)MT.1943-5533.0000820](https://doi.org/10.1061/(ASCE)MT.1943-5533.0000820).
- [33] da Conceição Leite, F., dos Santos Motta, R., Vasconcelos, K.L., Bernucci, L. 2011. Laboratory evaluation of recycled construction and demolition waste for pavements. *Construction and Building Materials* 25(6): 2972-2979, <https://doi.org/10.1016/j.conbuildmat.2010.11.105>.
- [34] Arulrajah, A., Piratheepan, J., Disfani, M.M., Bo, M.W. 2013. Resilient moduli response of recycled construction and demolition materials in pavement subbase applications. *Journal of materials in civil engineering* 25(12): 1920-1928, [https://doi.org/10.1061/\(ASCE\)MT.1943-5533.0000766](https://doi.org/10.1061/(ASCE)MT.1943-5533.0000766).
- [35] Rahman, M.A., Arulrajah, A., Piratheepan, J., Bo, M.W., Imteaz, M.A. 2014. Resilient modulus and permanent deformation responses of geogrid-reinforced construction and demolition materials. *Journal of Materials in Civil Engineering* 26(3): 512-519, [https://doi.org/10.1061/\(ASCE\)MT.1943-5533.0000824](https://doi.org/10.1061/(ASCE)MT.1943-5533.0000824).
- [36] ASTM D422-63. 2009. Standard test method for particle-size analysis of soils. American Society for Testing and Materials, West Conshohocken, USA.
- [37] ASTM D1241-07. 2007. Standard Specification for materials for soil-aggregate subbase, base, and surface courses. American Society for Testing and Materials, West Conshohocken, USA.
- [38] Ok, B. 2018. Investigation of the behaviour under static and cyclic loading of construction and demolition waste embankment reinforced with geosynthetics. PhD thesis, Cukurova University Institute of Natural and Applied Sciences, Adana, Turkey, pp. 1-414.

- [39] BS EN 933-11. 2009. Tests for geometrical properties of aggregates part 11: classification test for the constituents of coarse recycled aggregate. British Standards Institution, London, United Kingdom.
- [40] ASTM C131-03. 2003. Standard test method for resistance to degradation of small-size coarse aggregate by abrasion and impact in the los angeles machine. American Society for Testing and Materials, West Conshohocken, USA.
- [41] ASTM C127-01. 2001. Standard test method for density, relative density (specific gravity), and absorption of coarse aggregate. American Society for Testing and Materials, West Conshohocken, USA.
- [42] ASTM C128-01. 2001. Standard test method for density, relative density (specific gravity), and absorption of fine aggregate. American Society for Testing and Materials, West Conshohocken, USA.
- [43] ASTM D4791-10. 2010. Standard test method for flat particles, elongated particles, or flat and elongated particles in coarse aggregate. American Society for Testing and Materials, West Conshohocken, USA.
- [44] ASTM D1557. 2012. Standard test methods for laboratory compaction characteristics of soil using modified effort. American Society for Testing and Materials, West Conshohocken, USA.
- [45] ASTM D1883-99. 1999. Standard test method for CBR (California bearing ratio) of laboratory-compacted soils. American Society for Testing and Materials, West Conshohocken, USA.
- [46] ASTM D2166. 2006. Standard test method for unconfined compressive strength of cohesive soil. American Society for Testing and Materials, West Conshohocken, USA.
- [47] Moghaddas-Nejad, F., Small, J.C. 2003. Resilient and permanent characteristics of reinforced granular materials by repeated load triaxial tests. *Geotechnical Testing Journal* 26(2): 152-166, <https://doi.org/10.1520/GTJ11324J>.
- [48] Souci, G. 2009. Laboratory characterization of geogrid-reinforced unbound granular material for use in flexible pavement structures. MSc Thesis Baton Rouge, USA: Louisiana State University, Available online: https://digitalcommons.lsu.edu/cgi/viewcontent.cgi?referer=https://scholar.google.com.tr/&httpsredir=1&article=1702&context=gradschool_theses.
- [49] AASHTO T 307-99. 2000. Determining the resilient modulus of soil aggregate materials. Standard Specifications for Transportation Materials and Methods of Sampling and Testing. The American Association of State Highway and Transportation Officials, Washington D.C., USA.
- [50] Han, B., Ling, J., Shu, X. et al. 2019. Quantifying the effects of geogrid reinforcement in unbound granular base. *Geotextiles and Geomembranes* 47(3): 369-376, <https://doi.org/10.1016/j.geotexmem.2019.01.009>.
- [51] Hubner, D., Vuong, B., Jameson, G., Sharp, K., Fielding, B. 2008. Guide to pavement technology part 4a: Granular base and subbase materials, Austroads Ltd., Sydney, Australia.
- [52] TSH. 2013. Technical Specifications for Highways. General Directorate of Highways, Ankara, Turkey.
- [53] Arulrajah, A., Rahman, M.A., Piratheepan, J., Bo, M.W., Imteaz, M.A. 2014. Evaluation of interface shear strength properties of geogrid-reinforced construction and demolition materials using a modified large-scale direct shear testing apparatus. *Journal of Materials in Civil Engineering* 26(5): 974-982, [https://doi.org/10.1061/\(ASCE\)MT.1943-5533.0000897](https://doi.org/10.1061/(ASCE)MT.1943-5533.0000897).
- [54] Mehrjardi, G.T., Azizi, A., Haji-Aziz, A., Asdolafardi, G. 2020. Evaluating and improving the construction and demolition waste technical properties to use in road construction. *Transportation Geotechnics* 23-100349: 1-13, <https://doi.org/10.1016/j.trgeo.2020.100349>.
- [55] Holtz, R.D., Christopher, B.R., Berg, R.R. 1998. Geosynthetic design and construction guidelines. Federal Highway Administration, Washington, DC, FHWA-HI-98-038, pp. 1-460, Available online: <https://ntlrepository.blob.core.windows.net/lib/21000/21600/21668/PB99130841.pdf>.
- [56] Zornberg, J.G., Prozzi, J.P., Gupta, R. et al. 2008. Validating mechanisms in geosynthetic reinforced pavements. Federal Highway Administration, Texas, USA, FHWA/TX-08/0-4829-1 pp. 1-268, Available online: http://www.utexas.edu/research/ctr/pdf_reports/0_4829_1.pdf.
- [57] Edinçliler, A., Yildiz, O. 2018. Seismic behavior of tire waste-sand mixtures for transportation infrastructure in cold regions. *Sciences in Cold and Arid Regions*, 7(5), 626-631. <https://doi.org/10.3724/SP.J.1226.2015.00626>.
- [58] Yildiz, Ö. 2021. Numerical Analysis of Geotechnical Seismic Isolation System for High-Rise Buildings. *Naturengs*, 2(1), 34-43. <https://doi.org/10.46572/naturengs.872231>

GEOTECHNICAL CHARACTERIZATION OF ZEOLITE-SAND AND BENTONITE-SAND MIXTURES

GEOTEHNIČNA KARAKTERIZACIJA MEŠANIC ZEOLITA IN PESKA TER BENTONITA IN PESKA

Özgür Yıldız (corresponding author)

Malatya Turgut Ozal University,
Faculty of Engineering and Natural Sciences
Civil Engineering Department
Malatya, Turkey
E-mail: ozgur.yildiz@ozal.edu.tr

Çiğdem Ceylan

Malatya Turgut Ozal University,
Faculty of Engineering and Natural Sciences
Civil Engineering Department
Malatya, Turkey

DOI <https://doi.org/10.18690/actageotechslov.19.2.15-32.2022>

Keywords

zeolite, bentonite, shear strength, correlation, neural networks, prediction

Ključne besede

zeolit, bentonit, strižna trdnost, korelacija, nevronske mreže, napovedovanje

Abstract

This paper presents the characterization of pure bentonite- and zeolite-type clays and of various contents mixed with sand. The engineering properties of zeolites, bentonites and sand, which are commonly found in Malatya, Turkey, were evaluated in terms of their suitability for geotechnical applications. The crystallinity and structure of solid specimens of bentonite and zeolite were analysed with X-ray diffraction. Then both soils were mixed with sand in various proportions and the enhancement of the engineering properties was investigated. The properties of the mixtures, such as specific gravity, optimum water content, and dry unit weight mixtures, were initially determined. A set of direct shear tests was carried out to determine the shear-strength parameters of the specimens. As a result of extensive laboratory tests, linear correlations were observed between the water content and the consistency limits with the bentonite and zeolite contents in the sand mixtures. The highest for among each sample tested was achieved with the addition of 50 % bentonite and zeolite (i.e., BS50 and ZS50) as 44 and 38 kPa, respectively. A literature survey was carried out to reveal the test results of similar studies. In addition, using the test results from these literature studies and the current study, an NN-based prediction model was developed. The forecast models developed separately for cohesion and internal friction angle had high correlation coefficients: R^2 equal to 0.84 for cohesion and R^2 equal to 0.78 for the friction angle.

Izvleček

V prispevku je predstavljena karakterizacija čistih bentonitnih in zeolitnih glin z različnimi vsebnostmi mešanic s peskom. Ocenjene so bile inženirske lastnosti zeolitov, bentonitov in peska, ki jih običajno najdemo v Malatyi v Turčiji, glede na njihovo primernost za uporabo v geotehniko. Z rentgensko difrakcijo sta bili analizirani kristaliničnost in struktura trdnih vzorcev bentonita in zeolita. Nato sta bili obe zemljini zmešani s peskom v različnih razmerjih in raziskano izboljšanje inženirskih lastnosti. Na začetku so bile določene lastnosti mešanic, kot so specifična gravitacija, optimalna vlažnost in suhe prostorninske teže mešanic. Za določitev parametrov strižne trdnosti preizkušancev je bil izveden niz direktnih strižnih preizkusov. Kot rezultat obsežnih laboratorijskih preizkusov so bile opažene linearne korelacije med vlažnostjo in mejami konsistence z vsebnostjo bentonita in zeolita v peščenih mešanicah. Najvišji kohezijski del strižne trdnosti med posameznimi preizkušanci je bil dosežen z dodatkom 50 % bentonita in zeolita (tj. BS50 in ZS50), in sicer 44 oziroma 38 kPa. Poleg tega je bil z uporabo rezultatov preizkusov študij iz literature in trenutne študije razvit napovedni model osnovan na nevronskih mrežah. Modela napovedi, razvita ločeno za kohezijo in kot notranjega trenja, imata visoke korelacijske koeficiente, in sicer: R^2 enak 0,83 za kohezijo in R^2 enak 0,78 za kot notranjega trenja.

1 INTRODUCTION

Soils that can be found freely in nature in different forms can provide remarkable improvements in terms of engineering and strength properties when combined with different types of soils or materials. Zeolites are natural and synthetic inorganic aluminosilicates that belong to a large family of open-framework materials consisting of aluminosilicate minerals. One of the most important features of zeolites, which contain a large number of channels and voids, is that they lose the water in these channels at high temperatures without destroying their structure. There are silicon, aluminum, and oxygen in their skeletal structures, and water molecules, alkaline and alkaline-earth cations allow ion exchange in their pores [1]. There are varieties of natural and synthetic zeolites such as clinoptilolite, chabazite, phillipsite and mordenite, which basically have similar molecular structures [2, 3]. Bentonites, on the other hand, are soft, porous and easily shaped, open rock, predominantly having a colloidal silica structure and consisting of clay minerals (mainly montmorillonite) with very small crystals formed by chemical weathering or the degradation of volcanic ash, tuff and lava rich in aluminum and magnesium. These two soil types, which stand out with their different structural and mechanical properties, are widely used in engineering applications and are still the subject of detailed experimental studies by researchers.

Zeolite, because of its abundance in nature and eco-friendliness, as well as its high potential to increase soil strength, can be a good alternative to a binding material. Due to its high cation-exchange capacity, zeolite can also be used as an adsorbent for the removal of pollutants in wastewater [4]. Besides, it is widely used as a soil-stabilization additive [5, 6, 7, 8, 9]. Yilmaz et al. [10] investigated the effects of zeolite on the mechanical properties of soil under the freeze-thaw effect. Mola-abasi and Shooshpasha [6] performed experiments and numerical modeling studies on the enhancement of the unconfined compressive strength of sand with the inclusion of zeolite. Yukselen and Aksoy [11] proposed zeolite-soil mixtures to be used as embankment- and landfill-liner material. Vogiatzis et al. [12] used Hellenic natural zeolite in mixtures with sand and portland cement. Natural zeolites used instead of sand in mortar mixes decreased the P-wave velocity of sand per unit weight. Mola-abasi et al. [13] investigated the effect of zeolite and cement on the strength of cemented sand specimens. Villalobos et al. [14] stated that zeolites improve the shear strength of the mixtures to which they are added, dependent on their grain size.

Bentonites, on the other hand, are defined as clays containing predominantly montmorillonite and have formed as a result of the chemical decomposition of volcanic ash, tuff, and lava rich in aluminum and magnesium. Its high swelling capacity is the most important feature that distinguishes bentonites from other clay minerals. Bentonite's properties, such as swelling with water, color, grain size, and moisture absorption ratio, mainly determine its usage areas. They are often used as an additive material and their physical properties are made use of rather than their chemical properties. Composed of high-swelling montmorillonite, bentonite has been used in various applications such as nuclear-waste dumps, drilling mud, and shear walls due to its water-holding capacity and permeability [15, 16]. To enhance the geotechnical properties of the host material, bentonites are jointly used with fly ash, graphite, basalt, or crushed rock as an additive [17, 18, 19]. The hydraulic conductivity of pure bentonite and bentonite-sand mixtures was investigated by considering the difference between the size of both materials [20]. Proia et al. [21] performed experiments with sand-bentonite mixtures of various contents. The inclusion of bentonite even at smaller amounts (i.e., $\leq 5\%$) reduces the hydraulic conductivity and with the inclusion of higher amounts of bentonites, the mixture becomes more compressible. The hydraulic conductivity of sand-bentonite mixtures decreases by four orders of magnitude with the inclusion of 5 % bentonite [22]. Muntohar [23] stated that the existence of bentonite in the soil mixtures influences the swelling behavior, through a hyperbolic curve model. Alkaya and Esener [24], using various contents of cement and bentonite, revealed that the mixture with 10 % bentonite has the best performance in terms of hydraulic conductivity. Durukan et al. [25] investigated the suction behavior of zeolite-bentonite and sand-bentonite mixtures. In experimental studies where zeolite is used in different physical forms, it has been observed that as the grain size increases, the suction capacity increases, and zeolite-bentonite mixtures exhibit higher matric suction values than sand-bentonite mixtures.

The above-mentioned studies demonstrate that both bentonite and zeolite materials have been used in a wide range of applications and investigated in accordance with different purposes. In many of the studies, zeolite and bentonite were mixed with sand for different purposes and a summary of the literature survey is given in Table 1. In this study, experimental investigations will be carried out, particularly on zeolite and bentonites, which are two common soil types in the investigation area of the city of Malatya. In the first place, engineering properties (i.e., grain size, specific gravity, optimum water content, maximum dry unit

weight, consistency limits and shear strength) were determined. The results obtained for both pure and mixed materials were examined to assess the materials' suitability for geotechnical applications. A literature survey was carried out and the results of similar tests were compiled. Using both literature and current test results, a prediction model was developed. The shear parameters of the specimens were estimated using the prediction model. The feasibility of NN-based prediction models in estimating the shear-strength parameters of multi-component composite materials such as the used soil pairs was demonstrated.

2 GENERAL GEOLOGY

The city of Malatya is located in eastern Turkey. It has an area of 12,313 km² (Figure 1). The Malatya plain was formed after the Alpine folding by the fractures and folds during the tectonic movements that emerged at the end of the third geological time and the beginning of the fourth period. It is one of the densest settlements in eastern Anatolia. The base rock unit in Malatya and

its environs is metamorphites consisting of permo-carboniferous schists and crystallized limestones cropping out. In the south of Yeşilyurt and Gündüzbey, there is a conglomerate consisting of red-colored terrestrial conglomerate, sandstone, and mudstone from bottom to top. Inekpinari limestone consists of shallow marine carbonates, the Kapullu formation consists of conglomerate, sandstone, limestone, and shale alternation, and Haçova formation consisting of tuff and andesites exists at the top. On the other hand, in the surrounding Yeşilyurt and Gündüzbey areas, the Yeşilyurt group consists of Zorban pebblestone, red-colored conglomerate, and sandstones in the form of alluvials from bottom to top, and Yıldız limestone, which consists of reefal limestones. Overlying the Yıldız limestone, the upper Banazi formation with conglomerate, sandstone, and shale alternations emerge. This formation is also harmoniously overlain by Banaz limestones, the Malkuyu formation consisting of marls, and the Gedik formation consisting of reefal limestones. At the bottom of the Lower-Middle Miocene aged terrestrial formations outcropping in the near west, north, and east of Malatya, there is the Akyar formation, which consists of Lower

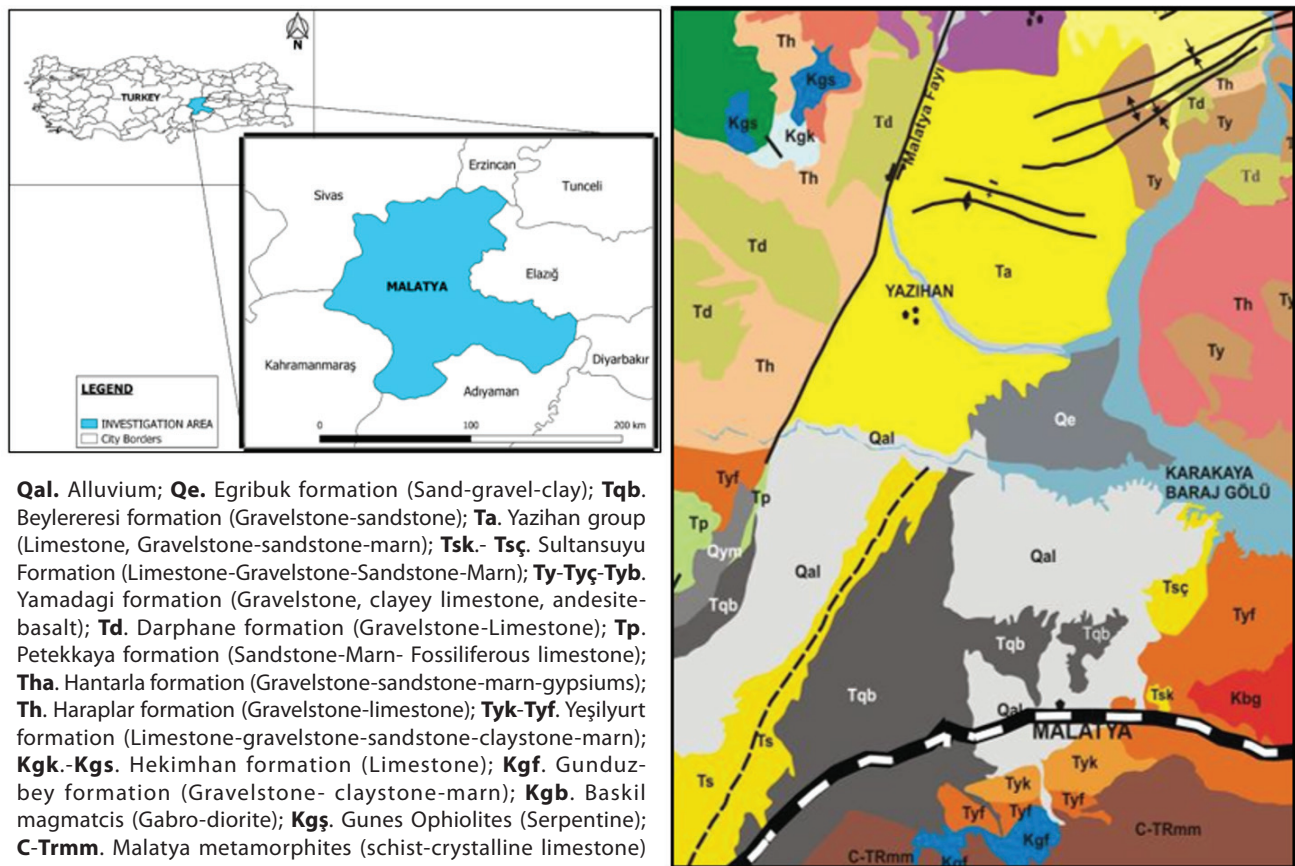


Figure 1. Site location and the general geological map of Malatya [26].

Miocene aged reef limestone and marls. The Kuseyin formation, which consists of red conglomerate, sandstone, mudstone, and gypsum conformably overlies the Akyar formation. This Lower Miocene-aged succession is conformably overlain by the Middle Miocene-aged Kilayık, Parçikan, Şeyhler, Sultansuyu, and Beylereresi formations. The general geological map created by the local government officers is given in Figure 1.

The zeolites located in the vicinity of Hekimhan, a district of Malatya, are of marine origin and spread over an area of approximately 90 km². The Upper Cretaceous unit is separated into two different units: the lower zeolite and the upper zeolite unit. The lower zeolite unit consists of zeolite with mafic minerals and layers with massive zeolite minerals. Its thickness is at most 15 m and a lateral continuation of 5 km is observed. The upper zeolite unit consists of zeolite minerals with sandstone interlayers. Its thickness is at most 38 m and a lateral continuity of 24 km is observed. The total geological reserve of the lower and upper zeolite levels is 190 million tons [27]. In addition, it is predicted that there are bentonite reserves at the rate of 50 thousand tons/year in Malatya province Battalgazi, Arapgir, Taskiran and Karahüyük districts and localities. It is stated that when the research is expanded to include the surrounding provinces, important reserve areas suitable for the use of different industries can also be determined. The directorates of mineral research and exploration, affiliated with the central government, are actively operating in the region.

3 EXPERIMENTAL STUDY

3.1 Materials and Methods

In the experimental studies carried out within the scope of this paper, three different soils were used, i.e., sand, zeolite and bentonite. The selected sand type is widely used in Malatya, especially in the construction industry, and was obtained from the Hekimhan district of Malatya. Zeolite material is freely available in the district of Hekimhan in Malatya. Bentonite is also found freely in nature in the Battalgazi district of Malatya. Both of the materials were supplied in block form; they were grinded and were suitable for our experiments. The grain-size-distribution curves of sand, bentonite and zeolite are shown in Figure 2. According to the USCS (Unified Soil Classification System), sand is classified as SW. The bentonite and zeolite are categorized as MH and CH, respectively. Each of the tested materials and mixtures with varies proportions were demonstrated in Figures 3–5. A series of geotechnical laboratory tests were carried out to determine the engineering parameters of the sand, bentonite, and zeolite, as well as their mixtures with specified contents. In addition to clean specimens, bentonite and zeolite were mixed in five different contents with sand: 10 %, 20 %, 30 %, 40 %, and 50 %. The specimens were abbreviated as B, S, Z, BS10, ZS50, etc. The letters represent the initials of the components of the mixture. The numeral represents the percentage of the additive in the mixture. For instance, BS20 is the abbreviation for the mixture of sand with

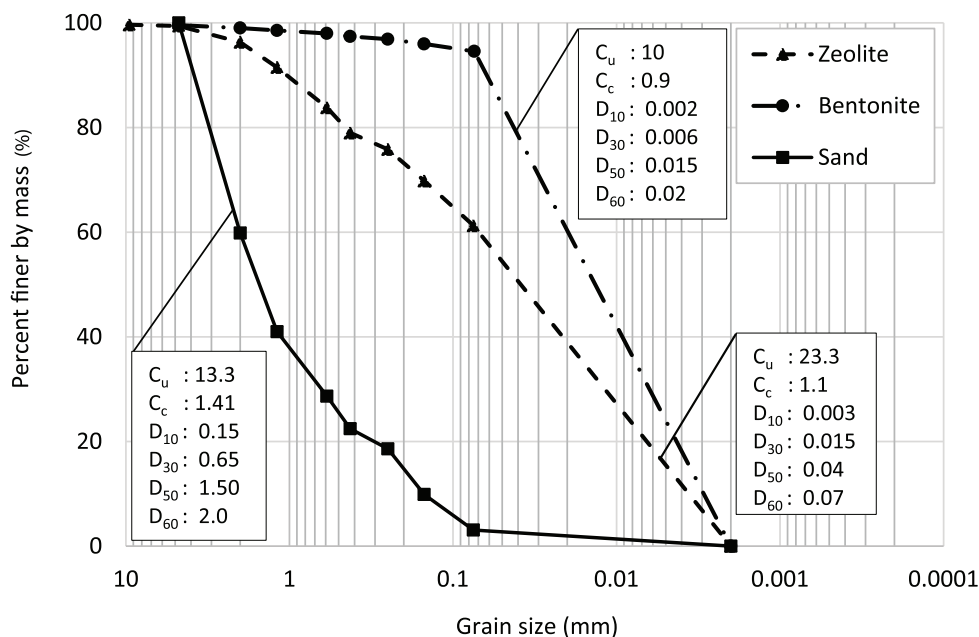


Figure 2. Grain size distribution of the soils.

Table 1. The summary of the recent studies on use of zeolite and bentonite.

Case	Soil*	Content (%)	PI (%)	w_{opt} (%)	γ (kN/m ³)	C (kPa)	φ (°)	Reference
1	B/S	10/90	13.7			3	28.7	[33]
	B/S	20/80	59.3			10	19.6	
	B/S	30/70	98.9			6	8.7	
	B/S	40/60	157.6			7	5.6	
	B/S	50/50	201.7			5	3.8	
	B/S	70/30	312.4			6	3.8	
2	B/S	10/90		18.6	16.1			[34]
	B/S	20/80		19	15.63			
3	Z/S	25/75		10.14	19.33			[35]
	Z/S	50/50		18.26	15.93			
	Z/S	75/25		27.03	13.89			
4	B/S	50/50		22.5	15.35			[36]
	B/S	60/40		19	15.96			
	B/S	70/30		16	16.3			
	B/S	80/20		15.1	16.77			
	B/S	90/10		14.5	16.39			
	B/S	50/50		22.5	15.54			
	B/S	60/40		20.5	15.64			
	B/S	70/30		18	16.23			
	B/S	80/20		18.4	16.68			
	B/S	90/10		17.2	16.08			
5	B/S	15/85	52	17	16.6			[37]
	B/S	25/75	70	15	17,2			
6	B/S	3/97		10	19.35	6.43	47	[22]
	B/S	5/95		10.5	19.1	21.47	37	
	B/S	7/93		11.2	18.68	24.11	35	
	B/S	9/91		12	18.56	24.9	33	
7	B/S	20/80		15.28	1727	16.4	24.9	[38]
8	B/S	15/85	115	15	17.3			[39]
	B/S	25/75	231	15.8	17.2			
	B/S	50/50	333	20	15.2			
9	B/S	70/30	59	27	15.1			[40]
	B/S	60/40	46	22	15.9			
	B/S	50/50	30	18	16.6			
10	B/S	5/95		19.4	15.79			[41]
	B/S	10/90		17.6	16.08			
	B/S	20/80		17	16.47			
	B/S	30/70		14.6	16.87			
	B/S	50/50		17.5	16.28			
11	Z/S	25/75		16.5	17.5	30.6	37.3	[42]
	Z/S	50/50		20	16.8	32.5	35.8	
	Z/S	75/25		22.5	15.7	31.2	31.7	
12	Z/S	5/95	3.85	9	20.08		31.23	[43]
	Z/S	10/90	3.848	10.2	19.5		31.48	
	Z/S	15/85	3.328	11.5	18.7		32.55	
	Z/S	20/80	3.08	12.3	18.3		33.34	
	Z/S	25/75	2.92	13	18		33.18	
	Z/S	30/70	3.84	13.8	17.93		33.27	
	Z/S	35/65	4.16	15.3	17.25		33.29	

* Z, B and S denote the zeolite, bentonite and sand, respectively.

20 % bentonite. Grain-size-distribution analyses, compaction tests, consistency limit tests, permeability tests, and direct shear tests were performed in accordance with ASTM D422-63, ASTM D698, ASTM D4318, ASTM D2434-94, and ASTM D3080-98, respectively [28, 29, 30, 31, 32]. The clean sand specimen used in the experiments was left to dry at room temperature in a laboratory environment. The dried specimens were sieved with # 4 (4.75 mm) and # 200 (0.075 mm) sieves, and the material remaining between the number # 4 and # 200 sieves were used in the experiments. Bentonite and zeolite specimens were taken from a depth of 1.5 to 2 m from the surface and left to dry at room temperature.

The dried specimens were grinded in a ball mill and sieved through sieve # 200. In the experiments, materials finer than 0.075 mm were used. The materials were prepared by dry mixing the bentonite and zeolite with sand separately at the specified mixing ratios (i.e., 10 %, 20 %, 30 %, 40 %, and 50 %). While the samples for the consistency limit test were kept in a desiccator overnight, the samples soaked in the standard proctor test were subjected to the test by keeping them in sealed bags for at least 3 hours. The specimens that were moistured and compressed at an optimum water content were used in direct shear tests. Pure water was used for wetting specimens by spraying to form a homogeneous mixture.



Figure 3. Pure materials used in the experimental study.

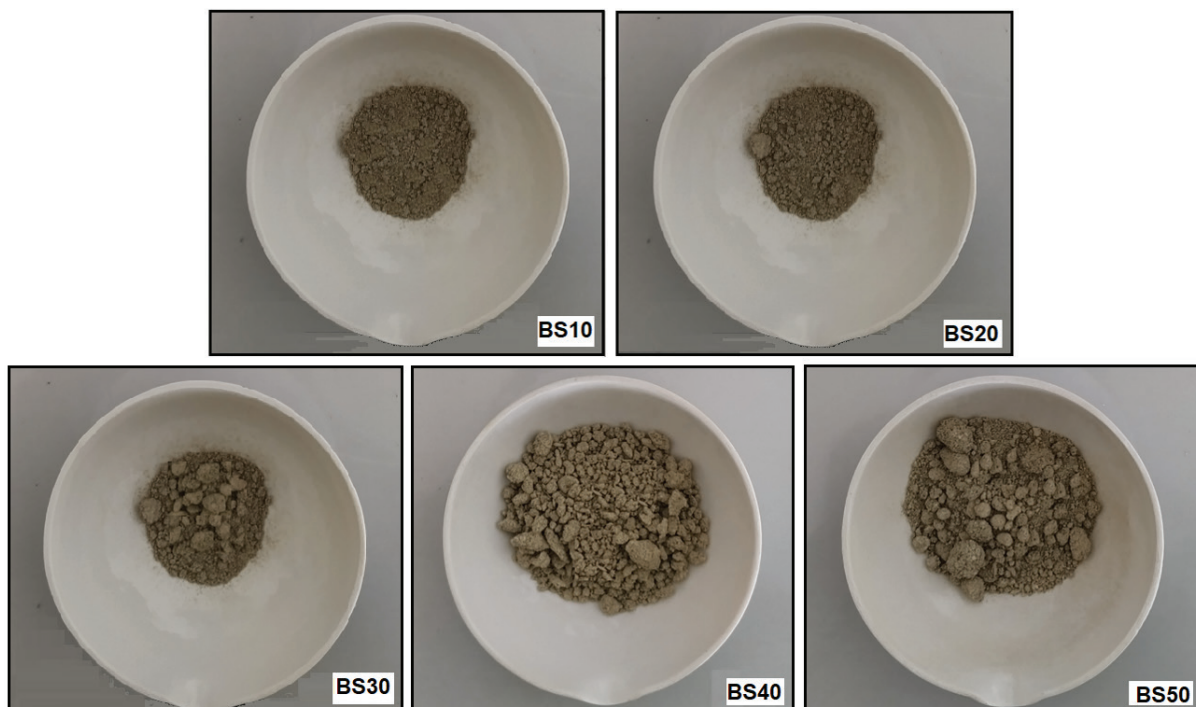


Figure 4. BS specimens with various bentonite contents.

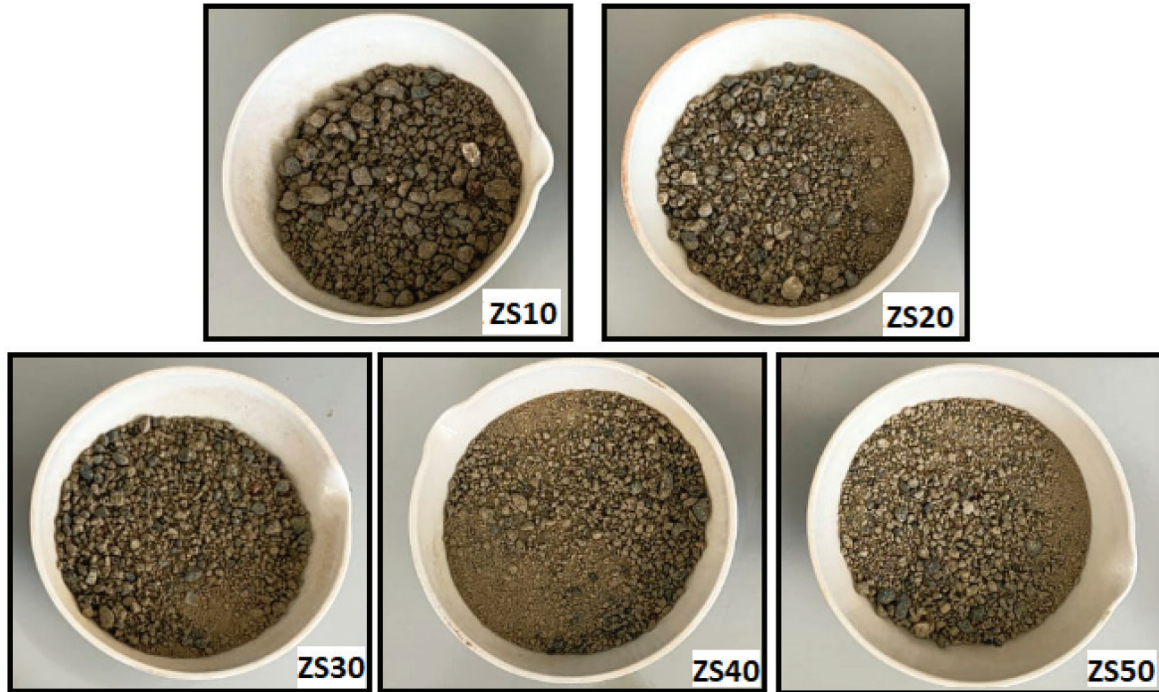


Figure 5. ZS specimens with various zeolite contents.

4 DISCUSSION AND RESULTS

4.1 Laboratory tests

Prior to the geotechnical laboratory tests, mineralogy and microscopic analyses of the zeolite were carried out. The identification of the zeolites using X-ray techniques is difficult because of the different cell dimensions and the differences in the relative intensities of the bands [11]. As can be seen in the XRD pattern in Figure 6, the zeolite has a high concentration of quartz

and lower calcite and clinoptilolite content. controlled XRD analyzes were performed in İnönü University laboratories (IBTAM). The basis of the work was to detect different crystal structures or the parameters in crystalline materials based on the reflection (refraction) of the x-ray. The beam is reflected (i.e. or refracted) on the sample and the beam detected with the help of a detector is transferred to the graph with the 2θ value corresponding to the reflection intensity using software. To determine the mineralogical compositions of the raw materials used the materials were prepared by passing

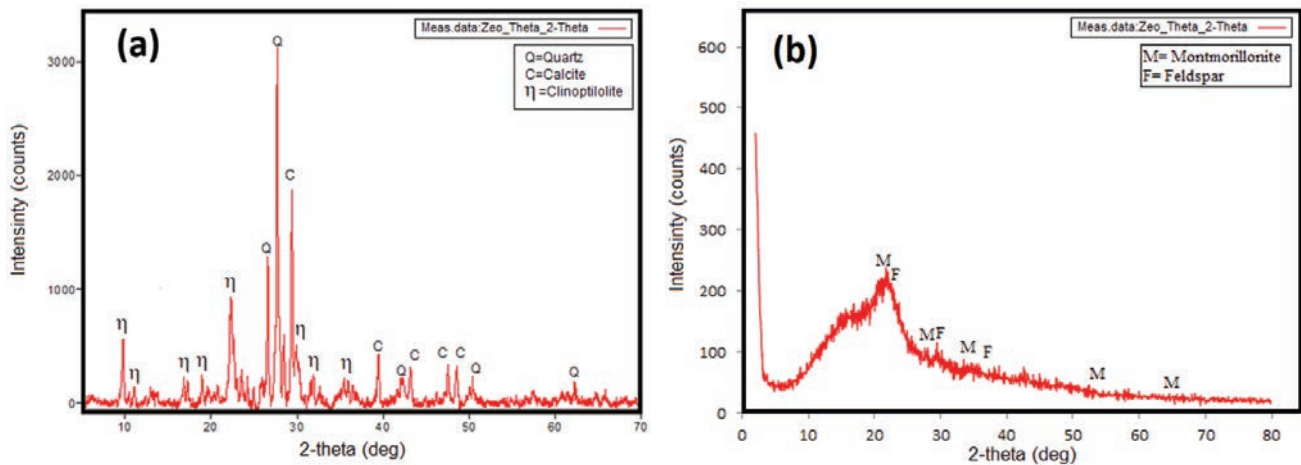


Figure 6. X-ray diffraction spectra of the (a) zeolite, (b) bentonite.

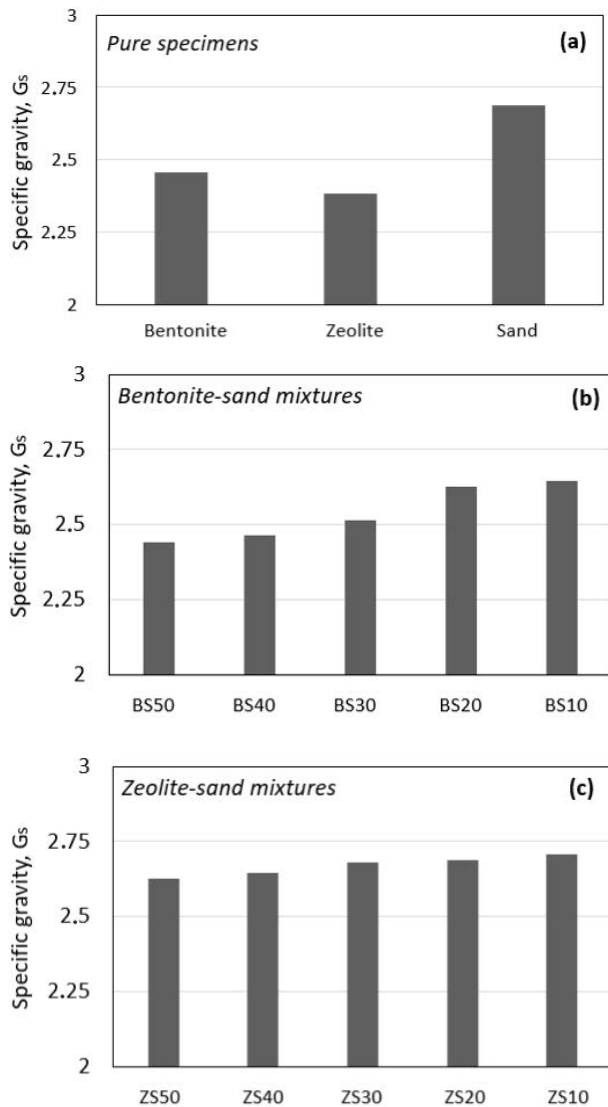


Figure 7. Specific gravity of pure specimens and mixtures.

through a 150- μ m sieve. The X-rays were detected with a RigakuRadB-DMAX II computer-controlled X-ray diffractometer using Cu-K α radiation. Measurements were scanned between $2\theta = 3^\circ$ to 80° degrees and at a constant speed of $3^\circ/\text{min}$. The analyses were performed according to the ASTM D5758 standard [44]. The diffractogram of natural zeolite shows the intensity at a 2θ angle of 26° with a peak of 3100 counts corresponding to the presence of quartz (SiO_2), which is a very common and important mineral. The bentonite, on the other hand, includes montmorillonite at a 2θ angle of 22° with a peak of 235 counts. The second-most intense mineral was found to be feldspar in bentonite. The specific gravities of the sand, bentonite and zeolite were calculated as 2.69, 2.46 and 2.38, respectively. Accordingly, the increasing content of both bentonite and zeolite leads to a decrease in the specific gravity of the

mixtures (Figure 7). As a host material, when the sand is mixed with bentonite or zeolite, a soil mass is formed in which sand particles make up the skeleton structure and additive particles occupy the voids in the matrix [41]. The size, distribution and compressibility of these voids are mainly dependent on the size, shape and proportions of sand particles in the mixture [36, 45]. Also, the mineralogy, content, compaction energy applied and moisture content are the influencing parameters for the mechanical characteristics of the compacted specimens [36, 41, 46, 47, 48, 49]. A set of modified proctor compaction tests was carried out and the optimum water content for the maximum compaction and unit weight was obtained for the specimens. As can be seen, the amount of water required to obtain the maximum unit weight is increasing with the increasing bentonite and zeolite content. The maximum unit weight of the BS10 specimen is 2.1 g/cm^3 for 12.3 % of water inclusion. The BS50 specimen including 50 % of bentonite in the mixture reaches the maximum unit weight as 1.67 g/cm^3 with 21 % of water content (Figure 8). In bentonite-sand mixtures, the values reached regarding the optimum water content are higher than that of the zeolite-sand mixtures (Figure 9). This is most likely because the included bentonite specimens have a relatively large surface area that causes a higher amount of water absorption than the included zeolite specimens. Since the bentonite particles are finer than the zeolite particles, the pores between the sand grains are reduced more easily in the BS specimens. Therefore, the optimum moisture content of the bentonite sand mixtures is higher than that of the zeolite-sand mixtures for the same additive content. The highest unit weight can be achieved with less water content for the ZS specimens. For example, the unit weight of the BS50 specimen is observed to be 14 % lower than that of ZS50 (i.e., 1.90 to 1.67 g/cm^3). The amount of water for the BS50 and ZS50 specimens is 21 % and 15 %, respectively. Even the compressibility of the clay-coarse-soil mixture is assumed to be dependent on the complex physicochemical interactions of the clay particles and the contribution of the mechanical properties of coarse soil (Bolt, 1956), a very clear pattern observed by the compaction curves [46].

Figure 10a shows the variation of the optimum water content needed to achieve the maximum unit weight for each content of bentonite and zeolite in the sand. The variations in the optimum water content due to bentonite and zeolite addition to the sand can be clearly observed. As the amount of inclusion increases, the optimum water content increases. Both the compaction curves of the BS and ZS specimens were following a definite pattern. As can be seen from the regression curves, the optimum water content for the maximum

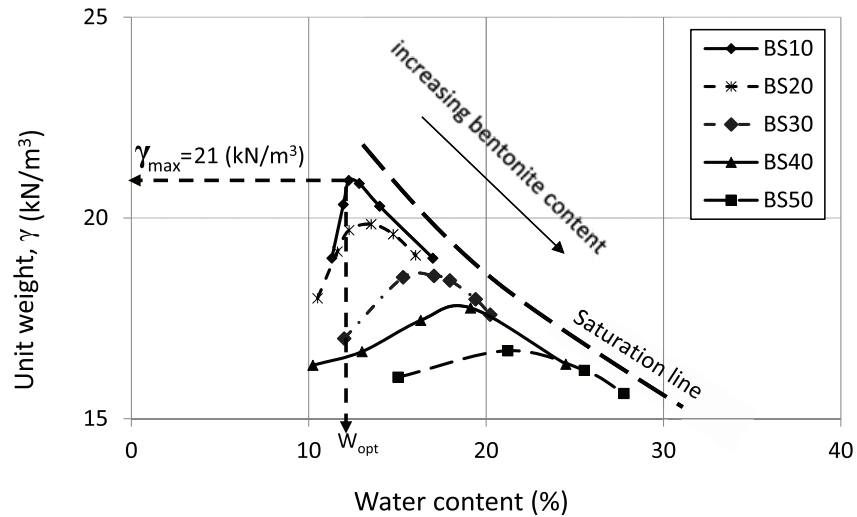


Figure 8. Compaction curves of the bentonite-sand mixtures.

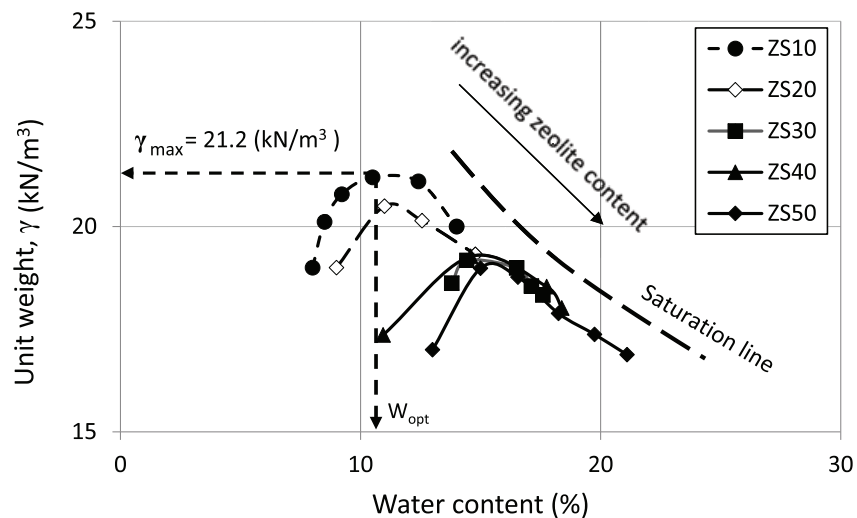


Figure 9. Compaction curves of the zeolite-sand mixtures.

compacted unit weight in correlation with bentonite/zeolite content in the mixtures. The amount of water required to bring the mixtures to the maximum unit weight is much less for the ZS specimens than for the BS specimens (Figure 10b). This is necessarily related to the difference between the gradational parameters and the compactional characteristics of both materials. It was observed that the water-holding capacity of bentonite is higher than zeolite for the same mixing ratios. In other words, the water-adsorption capacity of bentonite is higher than that of zeolite. The maximum unit weight of specimens decreases with the increasing water content. It should also be remembered that bentonite is used in engineering applications as a dispersive material. The high correlation coefficients between the content of both bentonite and zeolite in

the mixture and the optimum water content clearly show how much the compaction behavior is suppressed by the additive content in the mixture. Depending on the types of soil used, linear relationships between the optimum water content, the maximum unit weight and the applied compaction energy were also developed with similar studies [24, 34, 50, 51, 52].

The plasticity characteristic of the mixtures depends on the content and type of mineral in the additive [53]. In some studies, it has been suggested that at low clay contents, the mixture exhibits predominantly granular properties, while higher ratios a gradual transition to mechanical behavior of the plastic clay occurs [21]. However, Bowles [54] stated that the addition of 2 % clay to sand is the initial value for transforming the

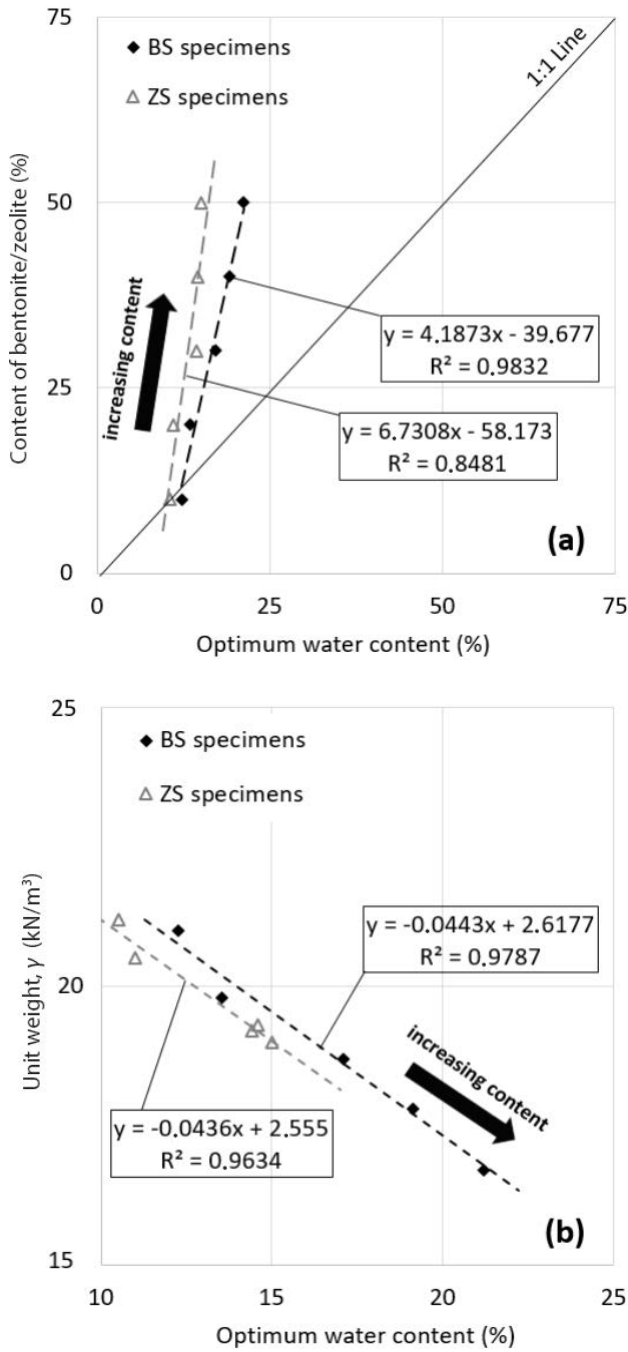
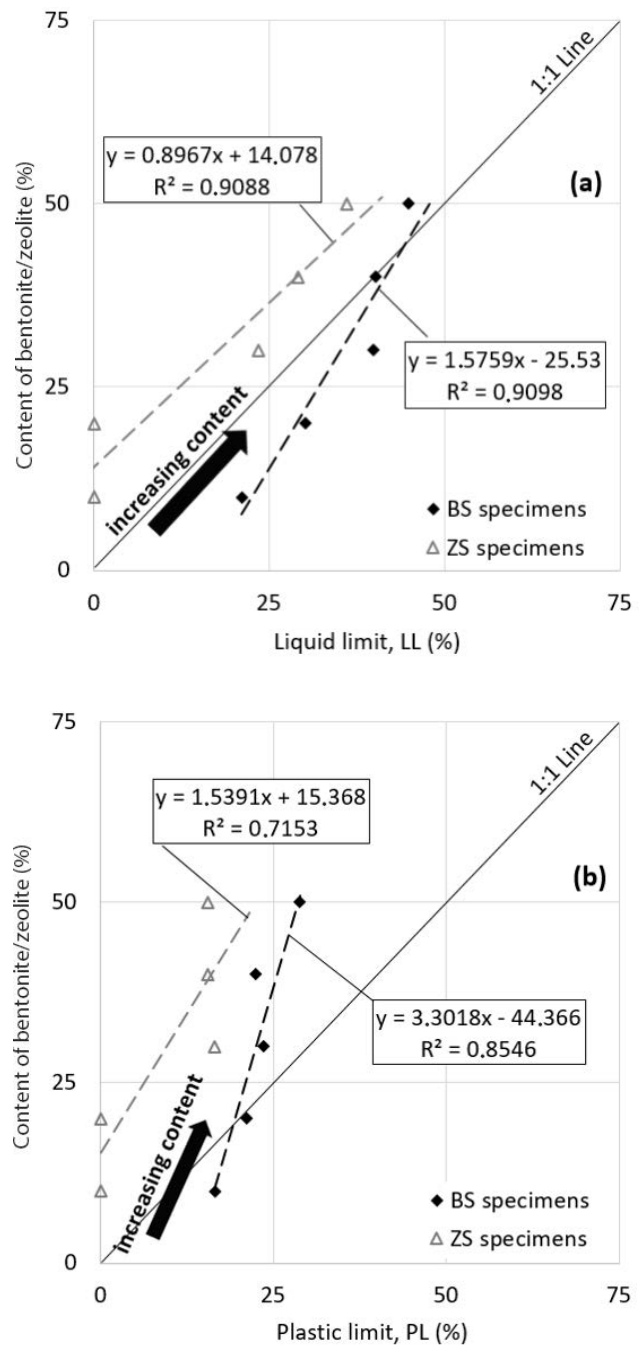


Figure 10. Variation of (a) additive content and (b) unit weight of specimens with optimum water content.

mixture from a sandy state to a clayey state. It is, therefore, the amount of zeolite and bentonite in the mixture was set at higher contents in this study. The variation of the consistency limits with additive content is presented in Figure 11. The consistency parameters of the mixtures increase with increasing both bentonite and zeolite content. The zeolite at a higher content of 20 % displayed an increase in the plasticity of the

mixtures. The ineffectiveness of the zeolite addition at less than 6–10 % on the plasticity is attributed to chemical properties such as the sodium absorption ratio (SAR) and exchangeable sodium percentages (ESP) [55]. The bentonite, on the other hand, even with smaller contents, has led to an increase in plasticity. The montmorillonite included in the bentonite has a key role in its plastic behavior. As can be seen from the high correlation coefficient, the variation between the content and the liquid limit is almost linear



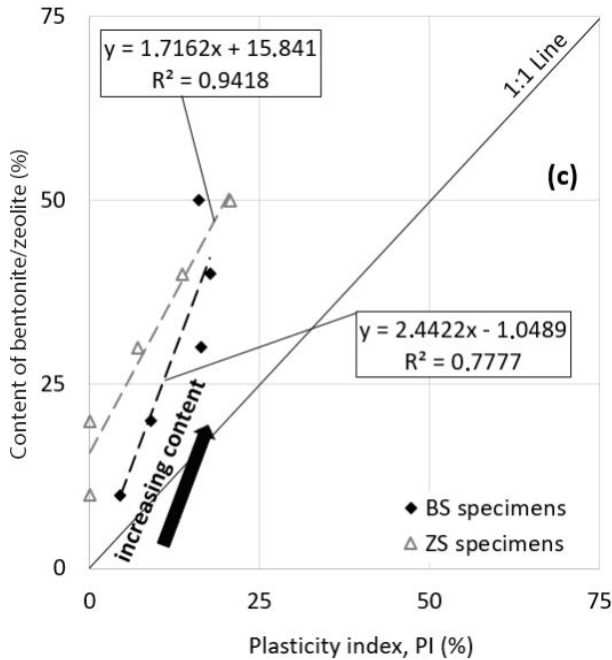


Figure 11. Variation of the consistency limits with additive content.

(Figure 11a). The regression lines show that the inclusion of additives has a lower effect on the plastic limit than on the liquid limit (Figure 11b). Bowles [54] also stated that the increasing bentonite inclusion into sand leads to a linear increase in the liquid limit, but has a limited effect on the plastic limit. It is clear that zeolite is more effective than bentonite on the plasticity index at mixing ratios greater than 20 % (Figure 11c). The plasticity characteristics of the sand-bentonite mixtures

are dependent on the clay content and the clay-mineral type [56]. The granulometry and mechanical characteristics are also found to be factors influencing the plasticity [57]. It is assumed that the plasticity effect induced by the addition of zeolite and bentonite, even with the same content, is not at the same level. The Casagrande plasticity chart built with the consistency limits of the specimens is shown in Figure 12.

The specimens were obtained by artificially mixing soils with different physical and mechanical properties. Thus, the advantages of both materials can be combined by trying combinations with different contents [21]. It is important to examine the shear strength of the BS and ZS specimens formed by mixing at different ratios. The shear-strength parameters of the specimens are significant, especially for a stability analysis. In the case of their use as liners or backfill materials, the shear strength of the zeolites and bentonites was investigated for both the drained and undrained cases. In this study the cohesion and internal friction angle of the specimens were determined through undrained direct shear tests. The compacted BS and ZS specimens were sheared immediately after compaction. The normal stresses applied as 28, 56 and 111 kPa. A strain rate of 0.5 mm/min was used for all tests and the time required for shearing the specimens to failure was about 10 to 15 min. For each content of zeolite and bentonite, the test results demonstrated that increasing the applied normal stress leads to an increase in the shear stress. It was also observed that the measured maximum shear stress decreases with increasing additive content. The mixture with a 50 % inclusion of bentonite and zeolite (i.e., BS50 and ZS50) had the best performance as 92 and 87 kPa

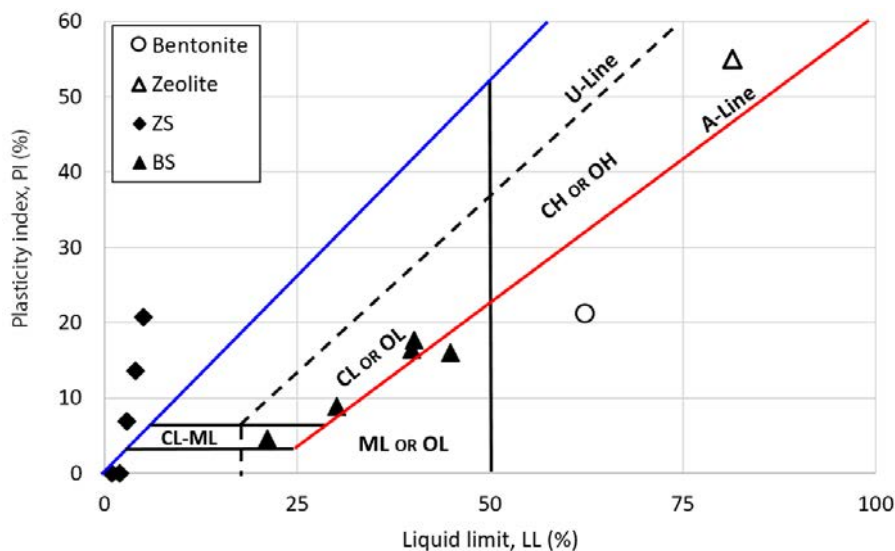


Figure 12. Casagrande plasticity chart of tested specimens.

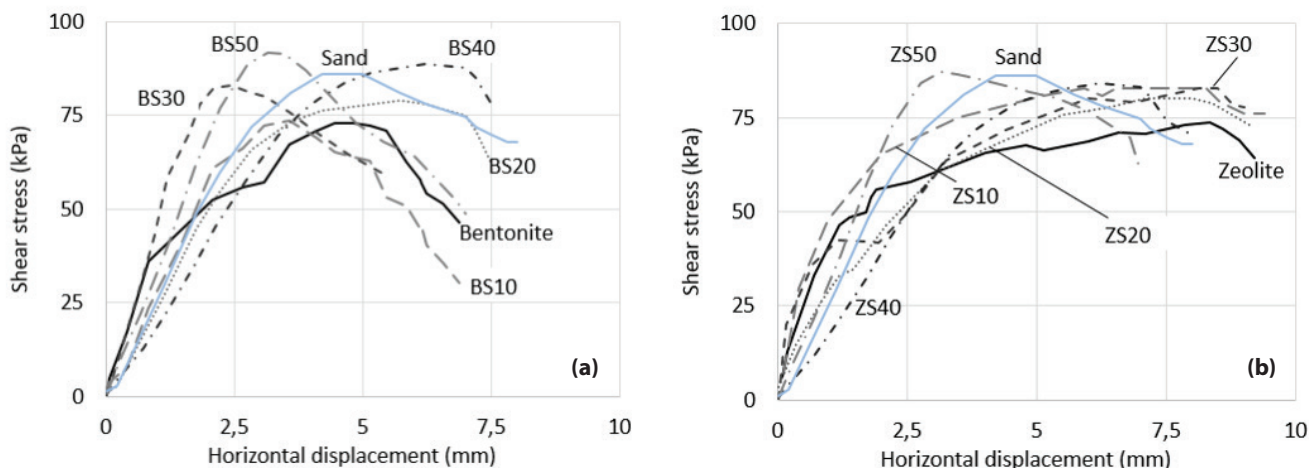


Figure 13. Direct shear test results of the specimens; (a) Bentonite and BS specimens, (b) Zeolite and ZS specimens.

under 111 kPa normal stress, respectively (Figure 13). The specimens having smaller contents of additives display a hardening behavior during shearing, which is more visible for the ZS specimens. The variation of the maximum shear stress with the normal stress is shown in Figure 14. Specimens containing both bentonite and zeolite under lower normal stresses show a higher shearing response than the clean sand. However, when the applied normal stress increases from 28 kPa to 111 kPa, the response of the clean sand and the mixtures to shearing becomes closer. Under higher normal stresses, only specimens with a greater content of bentonite and zeolite (i.e., BS40, BS50 and ZS50) have higher shear stresses than clean sand. This shows that the shear behavior of the mixtures is sensitive to the applied normal stress, so it makes sense to interpret the shear behavior in two parts. In contrast to some literature studies, the specimens appear to exhibit sand-like behavior at high bentonite and zeolite mixing ratios in terms of shear behavior.

The variation of the engineering properties of the specimens with multi-component soils is directly affected by the proportional distribution of the soil types in the mixture. As previously mentioned, one of the main motivations of this study is to combine different soil types and to take advantage of the better engineering properties of each of the components. Therefore, triple graphical representations of direct shear test results are given in Figure 15. While the shear stress was measured under 111 kPa normal stress with clean sand and pure bentonite was 86 and 73 kPa, respectively, this value increased to 92 kPa with the BS50 specimen. This situation occurred similarly to the ZS50 sample (i.e., 87 kPa) (Figure 15b). The shear strength of the specimens consists of two components: the cohesion and the internal friction angle. When bentonite and zeolite as cohesive materials were combined with sand, a decrease in the cohesion values was measured, as expected. Cohesion values of 67 and 69 kPa, measured for pure bentonite and pure zeolite, were decreased to 44 kPa and

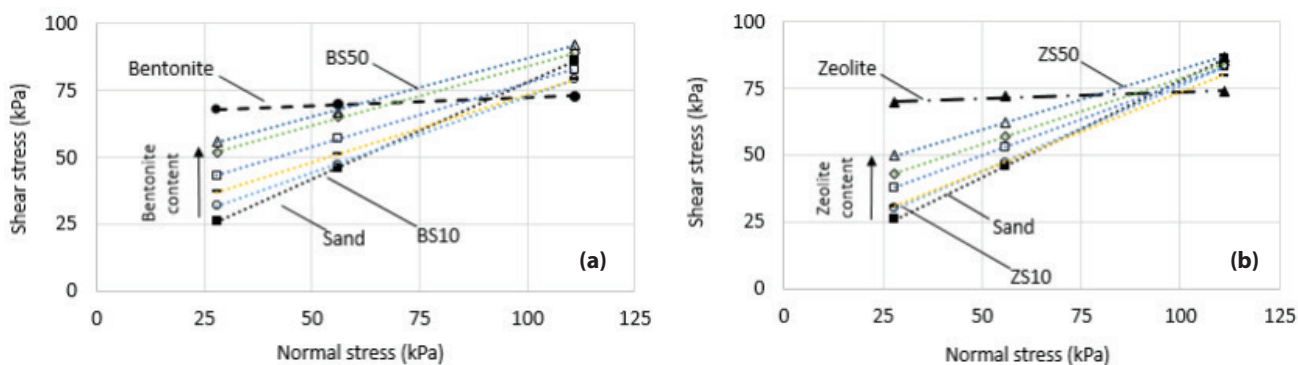


Figure 14. Shear resistance of the specimens tested under various normal stress; (a) Bentonite and BS specimens, (b) Zeolite and ZS specimens.

38 kPa for the BS50 and ZS50 specimens, respectively (Figure 15c-d). However, the internal friction angles of the pure specimens, which were 3° and 2°, increased to 23° and 33°, respectively. When bentonite is mixed with sand, due to its very small particle size it occupies the pore space present between the individual sand grains which is also valid for zeolite [53]. The optimum amount of material replacement by zeolite or bentonite for the highest improvement in the shear-strength parameters was also investigated by different researchers [4, 58, 59, 60]. It is essential to determine the optimum content of the materials, which will meet the design

target, with both strength values and other engineering properties. The basic engineering properties, compaction, consistency limits and direct shear test results of all specimens are collectively given in Table 3.

5 PREDICTION MODEL

Soft-computing methods, which are used in the analysis of multivariate and multi-parameter numerical problems that are difficult to interpret with analytical models, are widely used in almost every field. These methods have

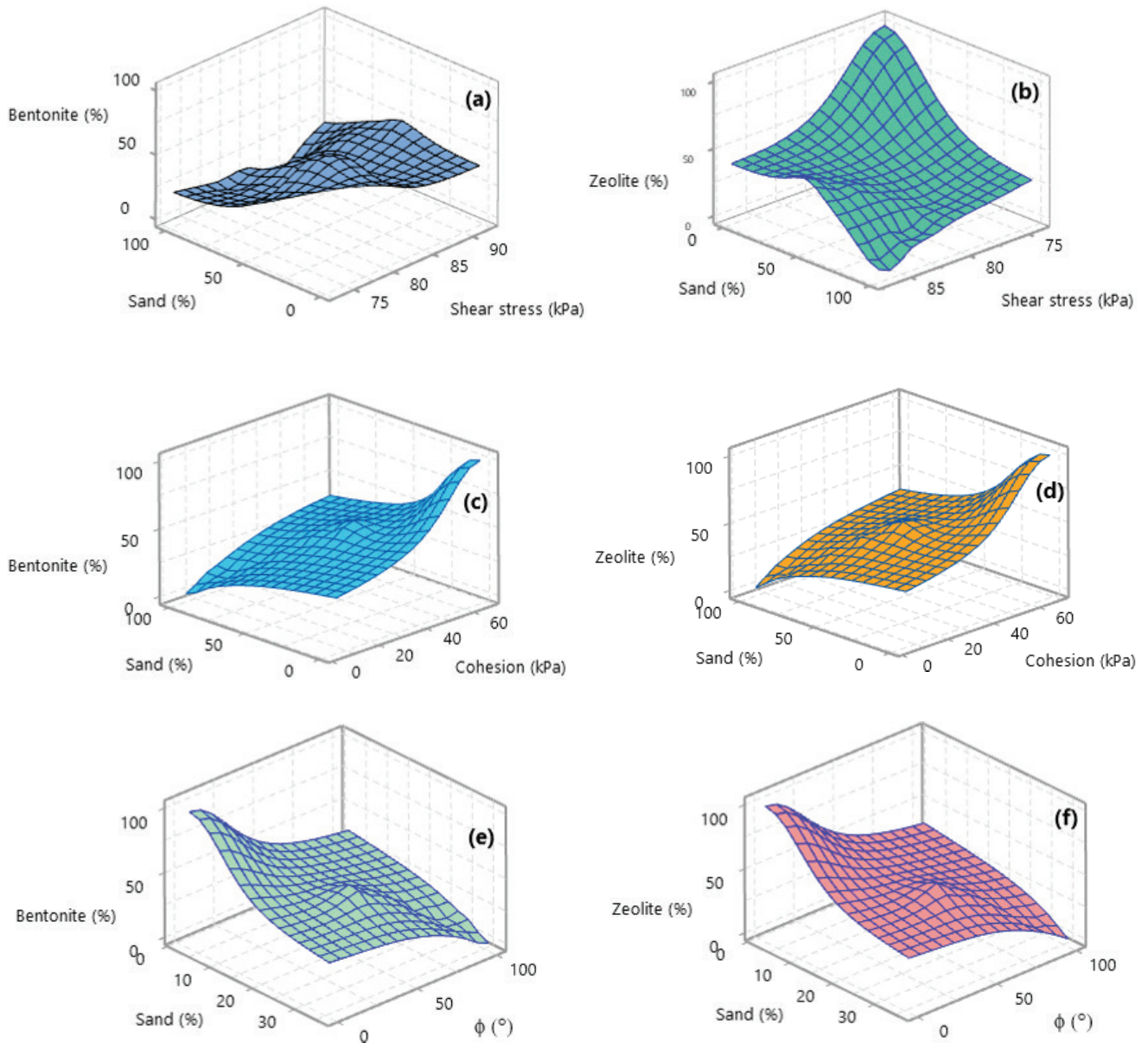


Figure 15. Variation of direct shear test results (a) bentonite, (b) zeolite content

Table 2. Summary of the geotechnical experiment results.

Specimen	G_s	LL (%)	PL (%)	PI (%)	w_{opt} (kPa)	ρ_{dmax} (g/cm ³)	C (kPa)	φ (°)	USCS
S	2.69	NP	NP	NP	-	1.34	6	36	SW
Z	2.38	81.5	26.5	55.0	20.4	1.49	69	2	CH
B	2.46	62.3	41.0	21.3	32	1.22	67	3	MH
BS10	2.65	21.1	16.5	4.5	12.3	2.10	16	30	ML
BS20	2.63	30.1	21.2	8.9	13.5	1.98	24	26	CL
BS30	2.51	39.9	23.6	16.3	17.1	1.87	30	25	CL
BS40	2.46	40.2	22.5	17.7	19.1	1.78	39	24	CL
BS50	2.44	44.9	28.8	16.1	21.2	1.67	44	23	ML
ZS10	2.69	NP	NP	NP	10.5	2.12	12	33	NP
ZS20	2.69	NP	NP	NP	11	2.05	15	30	NP
ZS30	2.68	23.5	16.5	7.0	14.4	1.92	23	28	CL
ZS40	2.65	29.1	15.5	13.6	14.6	1.93	29	26	CL
ZS50	2.63	36.1	15.5	20.6	15.0	1.90	38	24	CL

also been widely used by researchers in geotechnical engineering [61, 62, 63, 64, 65, 66]. Also, a comprehensive literature survey was carried out on the use of neural networks in geotechnics [67]. Prediction models were developed with the experimental results obtained from the literature review and this study. These models consist of an input layer with 6 parameters, a hidden layer and an output layer with target parameters. The input parameters are the soil types and their ratios in the mixture, the plasticity index, the optimum water content and the unit weight. The target parameters are set as the shear-strength parameters: the cohesion and the internal friction angle. The flowchart of the developed model is presented in Figure 16. Two sets of predictions were made separately with the prediction model developed for both the cohesion and the internal friction angle. As a result of a trial-and-error process, 10 neurons were identified in the hidden layer. A feed-forward error back propagation model is developed using the Levenberg Marquardt algorithm. The architecture of the model is given in Figure 17.

Laboratory test results are displayed as target values on the x-axis, and numerical analysis results are displayed on the y-axis. A performance evaluation of the model was made using MSE and square of correlation coefficient (R^2). The linear output indicates the success of the predictive model. In fact, the prediction models work separately on each data set randomly divided for training, validation and testing, and the correlation coefficients and MSE are calculated individually for each stage. However, the overall performance is represented by combining each of the three cases in one graph. The

regression curves of the predictions for both target parameters, i.e., cohesion and frictional angle, were presented separately in Figure 18. Correlation coefficients for the measured and estimated cohesion and friction angle were obtained as 0.84 and 0.78, respectively. These success performances, which were developed with a limited number of data sets, showed a reasonable estimation of success. Although it was obtained from differ-

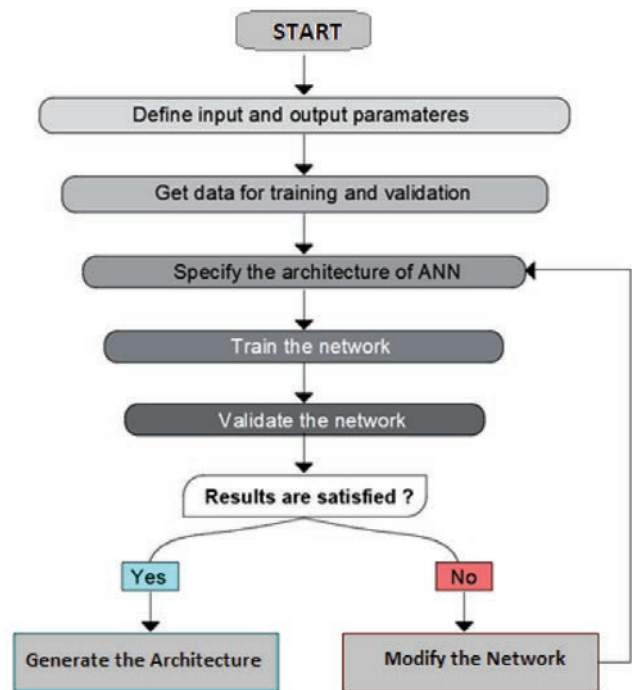


Figure 16. Flowchart of the neural network model.

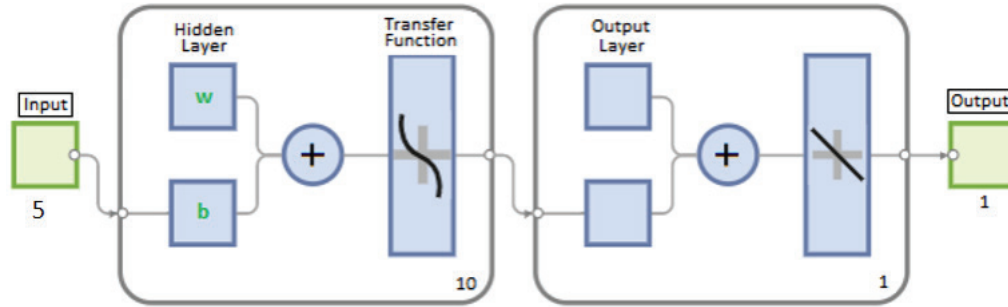


Figure 17. Architecture of the prediction model.

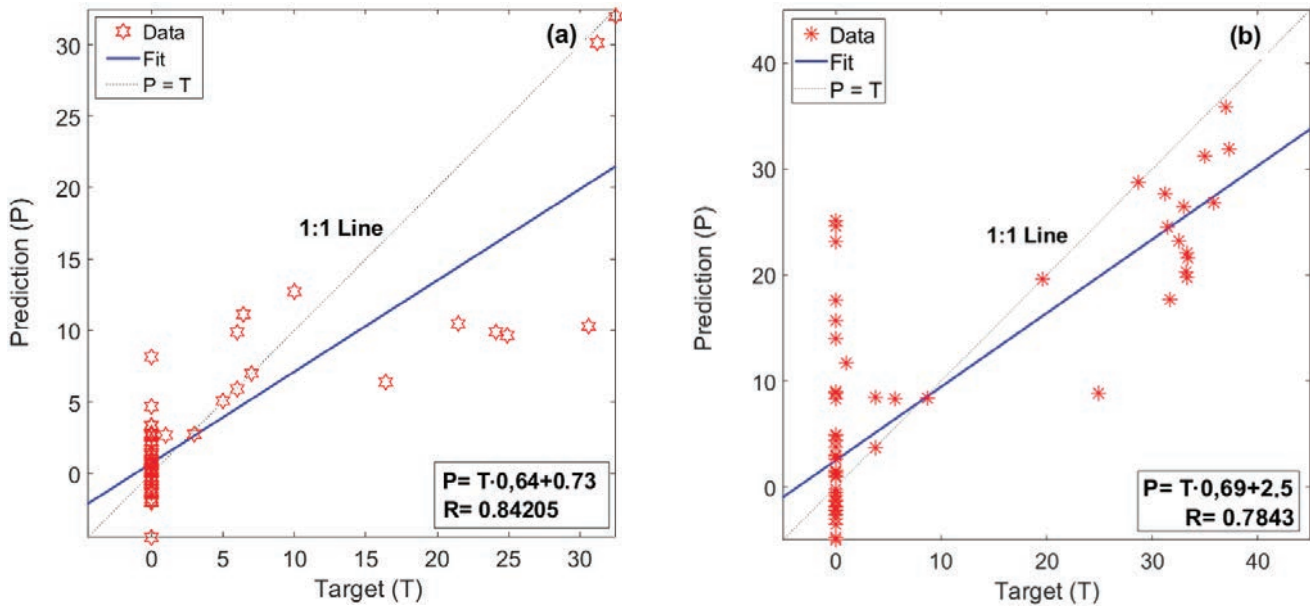


Figure 18. Scatter plots of the predicted versus target values of (a) cohesion and (b) frictional angle.

ent studies and consisted for a limited number of data, an acceptable success performance was obtained with the studied dataset. It is convenient in that it shows that the strength parameters can be estimated practically by soft-computing methods using the principle engineering properties. The statistical data of the predictions were summarised in Table 3.

Table 3. Statistical data of the predicted parameters.

	Cohesion		Angle of friction	
	MSE	R	MSE	R
Training phase	10.8881	0.9050	77.4662	0.8303
Validation phase	48.7666	0.7643	33.7122	0.8802
Test phase	45.0875	0.7929	18.0818	0.2991

6 CONCLUSION

This study was carried out to determine the geotechnical properties of pure zeolite and bentonite and their mixtures with sand, which are two common local soil types in the investigated area. In this context, the geotechnical properties and mineralogical properties of the materials were determined. In order to examine the improvements in the shear-strength parameters, direct shear tests were carried out on the combination of locally supplied sand with different contents. A NN-based model has been developed for the prediction of the shear-strength parameters of mixtures with existing geotechnical properties, with both results of literature studies and the current study. The main results are drawn in this study as follows:

- A significant increase was observed in the shear-strength parameters of the sand specimens with a mixture of zeolite and bentonite. The shear-strength parameters of the mixtures increase proportionally with increasing zeolite and bentonite content.
- The improvement in the shear-strength parameters with the addition of zeolite and bentonite is much more pronounced under low normal stresses. As the applied normal stress increases, the shear strength of both mixtures and the pure sand draw closer to each other.
- The maximum cohesion and friction angle measured for the BS50 and BS10 specimens were 44 kPa and 30°, respectively. Those parameters were measured by ZS50 and ZS10 specimens as 38 kPa and 24°, which indicates a remarkable difference in favor of the BS specimens in terms of the shear-strength parameters.
- Among the tested specimens it was observed that the BS40, BS50 and ZS50 specimens exhibited the highest strength values. These specimens significantly increased the plasticity properties of the clean sand in mixtures.
- With the compiled database, an acceptable accuracy was obtained regarding the estimation of the cohesion and the friction angle. The correlation coefficient $R^2 = 0.84$ was obtained for cohesion and $R^2 = 0.78$ was obtained for the internal friction angle, which shows the efficiency of the prediction models developed for multi-component soil specimens.

REFERENCES

- [1] Breck, D.W. (1974). *Zeolite Molecular Sieves, Structure, Chemistry and Use*, John Wiley & Sons, New York.
- [2] Ören, A. H., & Özdamar, T. (2013). Hydraulic conductivity of compacted zeolites. *Waste Manag. Res.* 31(6):634-40. DOI: 10.1177/0734242X13479434.
- [3] Dyer, A. (1988). *An introduction to zeolite molecular sieves*. Chichester; New York: J. Wiley.
- [4] Norouznejad, G., Shooshpasha, I., Mirhosseini, S. M., Afzalirad, M., & Afzalirad, M. (2021). Influence of Zeolite on the Compaction Characteristics and Shear Strength Parameters of Cemented Sand. *Sains Malaysiana*, 50(11), 3181–3191. <https://doi.org/10.17576/jsm-2021-5011-03>
- [5] Savas, H. (2016). Consolidation and swell characteristics of dispersive soils stabilized with lime and natural zeolite. *Sci Eng Compos Mater* 26:589–598. <https://doi.org/10.1515/secm-2014-0202>.
- [6] Mola-Abasi, H., & Shooshpasha, I. (2017). Polynomial models controlling strength of zeolite-cement-sand mixtures. *Scientia Iranica*, 24(2), 526–536.
- [7] Eyo, E. U., Ng'ambi, S., & Abbey, S. J. (2020). Performance of clay stabilized by cementitious materials and inclusion of zeolite/alkaline metals-based additive. *Transportation Geotechnics*, 23(February), 100330. <https://doi.org/10.1016/j.trgeo.2020.100330>
- [8] Shahriarkian, M., Kabiri, S., & Bayat, M. (2021). Utilization of zeolite to improve the behavior of cement-stabilized soil. *Int J Geosynth Ground Eng* 7(2). <https://doi.org/10.1007/s40891-021-00284-9>
- [9] Chenarboni, H.A., Lajevardi, S. H., MolaAbasi, H., & Zeighami, E. (2021). The effect of zeolite and cement stabilization on the mechanical behavior of expansive soils. *Constr Build Mater* 272:121630. <https://doi.org/10.1016/j.conbuildmat.2020.121630>
- [10] Yilmaz, F., Sadoğlu, E., & Kamiloğlu, H. A. (2022). Evaluation of the effect of waste zeolite on the strength and micro-macrostructure of a high plasticity clayey soil stabilized with lime-waste zeolite mixtures subjected to freezing–thawing cycles. *Arabian Journal of Geosciences*, 15(6). <https://doi.org/10.1007/s12517-022-09767-z>
- [11] Yukselen-Aksoy, Y. (2010). Characterization of two natural zeolites for geotechnical and geo-environmental applications. *Applied Clay Science*, 50(1), 130–136. <https://doi.org/10.1016/j.clay.2010.07.015>
- [12] Vogiatzis, D., Kantiranis, N., Filippidis, A., Tzamos, E., & Sikalidis, C. (2012). Hellenic natural zeolite as a replacement of sand in mortar: Mineralogy monitoring and evaluation of its influence on mechanical properties. *Geosciences (Switzerland)*, 2(4), 298–307.
- [13] Mola-Abasi, H., Kordtabar, B., & Kordnaeij, A. (2016). Parameters controlling strength of zeolite-cement-sand mixture. *International Journal of Geotechnical Engineering*, 11(1), 72–79. <https://doi.org/10.1080/19386362.2016.1186412>
- [14] Villalobos, F. A., Leiva, E. A., Jerez, Ó., & Poblete, M. E. (2018). Experimental study of the fine particles effect on the shear strength of tuff zeolites. *Revista de La Construcción*, 17(1), 23–37. <https://doi.org/10.7764/RDLC.17.1.23>
- [15] Murray, H. H. (2006). *Bentonite Applications*. *Developments in Clay Science*, 2(C), 111–130.
- [16] Sun, Y., Fan, W., Zheng, H., Zhang, Y., Li, F., & Chen, W. (2015) Evaluation of Dewatering Performance and Fractal Characteristics of Alum Sludge, *PLoS ONE*, Vol. 10(6),1-16.

- [17] Komine, H., & Ogata, N. (1999). Experimental study on swelling characteristics of sand-bentonite mixture for nuclear waste disposal. *Soils Found.* 39 (2): 83–97. Komine, H. 2004. "Simplified evaluation on hydraulic conductivities of sand-bentonite mixture backfill." *Appl. Clay Sci.* 26 (1–4): 13–19. <https://doi.org/10.1016/j.clay.2003.09.006>.
- [18] Jobmann, M., & Buntebarth, G. (2009). Influence of graphite and quartz addition on the thermo-physical properties of bentonite for sealing heat-generating radioactive waste. *Applied Clay Science*, 44(3–4), 206–210. <https://doi.org/10.1016/j.clay.2009.01.016>
- [19] Chen, T., Sedighi, M., Jivkov, A. P., & Seetharam, S. C. (2021). A model for hydraulic conductivity of compacted bentonite - Inclusion of microstructure effects under confined wetting. *Geotechnique*, 71(12), 1071–1084. <https://doi.org/10.1680/jgeot.19.P088>
- [20] Sivapullaiah, P. V., Sridharan, A., & Stalin, V. K. (2000). Hydraulic conductivity of bentonite-sand mixtures. *Canadian Geotechnical Journal*, 37(2), 406–413. <https://doi.org/10.1139/t99-120>
- [21] Proia, R., Croce, P., & Modoni, G. (2016). Experimental Investigation of Compacted Sand-bentonite Mixtures. *Procedia Engineering*, 158, 51–56.
- [22] Chalermyanont, T., & S. Arrykul. (2005). Compacted sand-bentonite mixtures for hydraulic containment liners. *Songklanakarin J. Sci. Technol.* 27 (2): 313–323.
- [23] Muntohar, A.S. (1999). Swelling and compressibility characteristics of compacted sand-bentonite mixtures. *Geotechnical Engineering*, 30(1), 1–12.
- [24] Alkaya, D., & Bariş Esener, A. (2011). Usability of sand-bentonite-cement mixture in the construction of unpermeable layer. *Scientific Research and Essays*, 6(21), 4492–4503. <https://doi.org/10.5897/sre10.1189>
- [25] Durukan, S., Pulat, H. F., & Yukselen-Aksoy, Y. (2014). Suction characteristics of compacted zeolite-bentonite and sand-bentonite mixtures. *Waste Management and Research*, 32(2), 149–156. <https://doi.org/10.1177/0734242X13518958>
- [26] ÇŞB, (2011). Malatya Province Environment Status Report. Ministry of Environment and Urbanization, Malatya.
- [27] Dussan, A., Calderón, J. A., & Quiroz, H.P. (2020). Zeolites derived from natural minerals: Solid and volcanic ash., pp. 148-149. DOI:10.1016/j.mattod.2020.03.006
- [28] ASTM D422-63, 2003. Standard Test Method for Particle-Size Analysis of Soils, In *Annual Book of ASTM Standards*, Volume 04.08, Philadelphia, PA, pp. 93-99.
- [29] ASTM D-698, "Standard Test Methods for Laboratory Compaction Characteristics of Soil Using Standard Effort," American Society for Testing and Materials, USA
- [30] ASTM D4318-17e1. Standard Test Methods for Liquid Limit, Plastic Limit, and Plasticity Index of Soils; ASTM International: West Conshohocken, PA, USA, 2017.
- [31] ASTM D 2434-94. Standard test method for permeability of granular soils (constant head). *Annual Book of ASTM Standards*, American Society For Testing and Materials, West Conshohocken, PA (2000).
- [32] ASTM D 3080-98, 2003. Standard Test Method for Direct Shear of Soils Under Consolidated Drained Conditions, In: *Annual Book of ASTM Standards*, Volume 04.08, Philadelphia, PA, pp. 417-422.
- [33] Tiwari, B., & Marui, H. (2003). Estimation of residual shear strength for bentonite-kaolin-Toyouura sand mixture. *Journal of the Japan Landslide Society*, 40(2), 124–133. <https://doi.org/10.3313/jls.40.124>
- [34] Ören, A. H., Kaya, A., & Kayalar, A. Ş. (2011). Hydraulic conductivity of zeolite-bentonite mixtures in comparison with sand-bentonite mixtures. *Canadian Geotechnical Journal*, 48(9), 1343–1353. <https://doi.org/10.1139/t11-042>
- [35] Shang, H. (2015). Geotechnical laboratory characterization of sand- zeolite mixtures, MSc. Thesis, University of Louisville.
- [36] Vadlamudi, S., & Mishra, A. K. (2018). Consolidation characteristics of sand-bentonite mixtures and the influence of sand particle size. *Journal of Hazardous, Toxic, and Radioactive Waste*, 22(4), 06018001.
- [37] Ghadr, S., & Assadi-Langroudi, A. (2018). Structure-based hydro-mechanical properties of sand-bentonite composites. *Engineering Geology*, 235, 53-63. doi.org/10.1016/j.enggeo.2018.02.002
- [38] Mukherjee, K., & Mishra, A. K. (2019). Hydraulic and mechanical characteristics of compacted sand-bentonite: Tyre chips mix for its landfill application. *Environment, Development and Sustainability*, 21(3), 1411-1428.
- [39] Chen, Y., & Meehan, C. L. (2011). Undrained strength characteristics of compacted bentonite/sand mixtures. In *Geo-Frontiers 2011: Advances in Geotechnical Engineering* (pp. 2699-2708).
- [40] Fattah, M. Y., Salim, N. M., & Irshayyid, E. J. (2022). Influence of soil suction on swelling pressure of bentonite-sand mixtures. *European Journal of Environmental and Civil Engineering*, 26(7), 2554-2568. DOI: 10.1080/19648189.2017.1320236
- [41] Komine, H. (2004). Simplified evaluation on

- hydraulic conductivities of sand–bentonite mixture backfill. *Applied clay science*, 26(1-4), 13-19.
- [42] Kwan, P.S., Shahrokhi, R., Park, J., Kim, H., (2019). Zeolite mixtures as adsorptive fill material with sustainable bearing capacity. *Waste Management and Environment IX, WIT Transactions on Ecology and the Environment*, 231, 91-100.
- [43] Aftabi, S., Fathi, S., & Aminfar, M. H. (2020). The Effect of Zeolite on Sandy-Silt Soil Mechanical Properties. *International Journal of Geotechnical and Geological Engineering*, 14(10), 269-278.
- [44] ASTM D5758-01 Test Method for Determination of Relative Crystallinity of Zeolite ZSM-5 by X-Ray Diffraction
- [45] Elsbury, B. R., D. E. Daniel, G. A. Sraders, & D. C. Anderson. (1990). Lessons learned from compacted clay liner." *J. Geotech. Eng.* 116 (11): 1641–1660. [https://doi.org/10.1061/\(ASCE\)0733-9410\(1990\)\(1641\)](https://doi.org/10.1061/(ASCE)0733-9410(1990)(1641))
- [46] Bolt, G. H. (1956). Physico-chemical analysis of the compressibility of pure clays." *Géotechnique* 6 (2): 86–93. <https://doi.org/10.1680/geot.1956.6.2.86>.
- [47] Sridharan, A., & G. V. Rao. (1973). Mechanisms controlling volume change of saturated clays and the role of the effective stress concept. *Geotechnique* 23 (3): 359–382.
- [48] Mitchell, J. K., & Soga, K. (2005). *Fundamentals of soil behavior*. 3rd ed. Hoboken, NJ: Wiley.
- [49] Dutta, J., & A. K. Mishra. (2016). Consolidation behaviour of bentonites in the presence of salt solutions. *Appl. Clay Sci.* 120: 61–69. <https://doi.org/10.1016/j.clay.2015.12.001>.
- [50] Boutwell, G. (1961). Effects of variation of fill construction on the material properties and the subsequent fill performance, Independent study Rep., School of Civ. Engrg., Georgia Institute of Technology, Atlanta, Georgia, USA.
- [51] Blotez, L., Benson, C. & Boutwell, G. (1998). Estimating Optimum Water Content and Maximum Dry Unit Weight for Compacted Clays, *J Geotech. Engrg., ACSE*, 124(9), 907- 912.
- [52] Jesmani, M., Manesh, A. N., & Hoseini, S. M. R. (2008). Optimum water content and maximum dry unit weight of clayey gravels at different compactive efforts. *Electronic Journal of Geotechnical Engineering*, 13 L(June).
- [53] Srikanth, V., & Mishra, A. K. (2016). A Laboratory Study on the Geotechnical Characteristics of Sand–Bentonite Mixtures and the Role of Particle Size of Sand. *International Journal of Geosynthetics and Ground Engineering*, 2(1), 1–10. <https://doi.org/10.1007/s40891-015-0043-1>
- [54] Bowles, J.E. (1998). *Engineering Properties of Soil and Their Measurement*, McGraw-Hill Book Company, Singapore.
- [55] Turkoz, M., & Vural, P. (2013). The effects of cement and natural zeolite additives on problematic clay soils. *Science and Engineering of Composite Materials*, 20(4), 395–405.
- [56] Sivapullaiah, P.V., & Sridharan, A. (1985). Liquid limit of soil mixtures. *Geotech Test J* 8(3):111–116.
- [57] Harianto, T. (2022). Performance of Subbase Layer with Geogrid Reinforcement and Zeolite-Waterglass Stabilization. *Civil Engineering Journal (Iran)*, 8(2), 251–262. <https://doi.org/10.28991/CEJ-2022-08-02-05>
- [58] Sinha, A. N. (1998). Shear Strength of Bentonite-Kaolinite Mix in GCLs. pp. 889–896.
- [59] Xiang, Gs., Ye, Wm. & Jalal, F.E. (2021). Shear strength of bentonite–sand mixture saturated with saline solution. *Environ Earth Sci* 80, 770.
- [60] Cabalar, A. F., & Demir, S. (2022). Geotechnical properties of a bentonite treated with waste glass grains. *Arabian Journal of Geosciences*, 15(9). <https://doi.org/10.1007/s12517-022-10169-4>
- [61] Goh, A. T. C. (1994). Nonlinear modelling in geotechnical engineering using neural networks. *Australian Civil Engineering Transactions*, CE36(4), 293-297.
- [62] Goh, A. T. C. (1995). Empirical design in geotechnics using neural networks. *Geotechnique*, 45(4), 709-714.
- [63] Cabalar, A. F., Cevik, A., & Gokceoglu, C. (2012). Some applications of adaptive neuro-fuzzy inference system (ANFIS) in geotechnical engineering. *Comput Geotech* 40:14–33
- [64] Yıldız, Ö., & Berilgen, M. M. (2020). Artificial Neural Network Model to Predict Anchored-Pile-Wall Displacements on Istanbul Greywackes, *Teknik Dergi*, 31 (4), 10147-10166. <https://doi.org/10.18400/tekderg.492280>
- [65] Yıldız, Ö. (2021). Correlation Between Spt and Pmt Results For Sandy And Clayey Soils. *Eskişehir Technical University Journal of Science and Technology A - Applied Sciences and Engineering*, 22 (2) , 175-188. <https://doi.org/10.18038/estubtda.896491>
- [66] Cabalar, A. F., Karabas, B., Mahmutluoglu, B., & Yıldız, Ö. (2021). An IDW-based GIS application for assesment of geotechnical characterization in Erzincan Turkey. *Arab J Geosci* 14:2129. <https://doi.org/10.1007/s12517-021-08481-6>
- [67] Shahin, M.A., Jaksa, M.B., & Maier, H.R. (2001). Artificial Neural Network applications in geotechnical engineering. *Australian Geomechanics Journal* 36(1): 49–62

SPT-BASED SOIL-LIQUEFACTION MODELS USING NONLINEAR REGRESSION ANALYSIS AND ARTIFICIAL INTELLIGENCE TECHNIQUES

MODELI UTEKOČINJENJA ZEMLJIN NA OSNOVI SPT Z UPORABO REGRESIJSKE ANALIZE IN TEHNIK UMETNE INTELLIGENCE

Mehmet Cemal Acar (*corresponding author*)

Vocational College of Kayseri University,
Department of Construction
Kayseri, Turkey
E-mail: acarc@kayseri.edu.tr

Tülay Hakan

Civil Engineer (Geotechnic) DSİ 12. Bölge Müdürlüğü
Kayseri, Turkey

DOI <https://doi.org/10.18690/actageotechslov.19.2.33-45.2022>

Keywords

liquefaction, standard penetration test (SPT), ANN, ANFIS, NMRA

Ključne besede

utekočinjenje, standardni penetracijski preizkus (SPT), ANN, ANFIS, NMRA

Abstract

Saturated, cohesionless soils can temporarily lose their shear strength due to increased pore-water pressure under the effect of repetitive dynamic loads such as earthquakes. This event is defined as soil liquefaction and causes significant damage to structures. The liquefaction potential of soils depends on many soil parameters obtained in the field and from laboratory tests. In this study new models have been developed to estimate the liquefaction potential of cohesionless soils. For this purpose, 837 soil data sets were collected to calculate the liquefaction potential with nonlinear multiple regression and artificial intelligence in the cities of Kayseri and Erzincan. The models based on Nonlinear Multiple Regression Analysis, Artificial Neural Networks, and Adaptive Neuro-Fuzzy-Inference System techniques were compared with the results of the simplified method. Determination coefficients (R^2) and various error rates were calculated for the performance-evaluation criteria of the models. The proposed ANN model effectively found the complex relationship between the soil and the input parameters and predicts the liquefaction potential more accurately than other methods. It has an overall success rate of 90 percent and the lowest mean absolute error rate of 0.024. With the improvement of existing methods, new models have been introduced to estimate the liquefaction probability of soils.

Izvleček

Zasičene nekoherentne zemljine lahko zaradi povečanega pritiska vode v porah pod vplivom ponavljajočih se dinamičnih obremenitev, kot so potresi, začasno izgubijo svojo strižno trdnost. Ta primer je opredeljen kot utekočinjenje zemljine in povzroči znatno škodo na konstrukcijah. Potencial utekočinjanja zemljin je odvisen od številnih parametrov zemljin, pridobljenih s terenskimi in laboratorijskimi preiskavami. V pričujoči študiji so bili razviti novi modeli za oceno potenciala utekočinjenja nekoherentnih zemljin. V mestih Kayseri in Erzincan je bilo zbranih 837 nizov podatkov o zemljinah za izračun potenciala utekočinjenja z nelinearno multiplo regresijo in umetno inteligenco. Modele, ki temeljijo na tehnikah nelinearne multiple regresijske analize (NMRA), umetnih nevronske mreže (ANN) in sistema prilagodljivega nevro-mehkega sklepanja (ANFIS), smo primerjali z rezultati poenostavljene metode. Za kriterije ocenjevanja uspešnosti modelov so bili izračunani determinacijski koeficienti (R^2) in različne stopnje napak. S predlaganim modelom ANN smo našli kompleksno razmerje med zemljino in vhodnimi parametri ter napovedali potencial utekočinjenja natančneje kot z drugimi metodami. Model ANN ima skupno stopnjo uspešnosti 90 odstotkov in najnižjo srednjo absolutno stopnjo napake 0,024. Z izboljšanjem obstoječih metod so bili uvedeni novi modeli za oceno verjetnosti utekočinjenja zemljin.

1 INTRODUCTION

When natural disasters are evaluated in terms of loss of life and property, earthquakes come first. An earthquake has negative effects on building structures. In particular, when the saturated sandy and silty soils are liquefied, they cannot bear the weight of the structures standing on them, which causes the structures to sink and tilt [1].

The liquefaction of soils can be expressed as the liquid-like behaviors of saturated, cohesionless or low-cohesive soils that lose their shear strength because of the vibrations of cyclic, earthquake shock waves. Liquefaction is the increase of the pressure of the water in the soil void spaces (pores) and the deterioration of the soil's structure under repeated loads from the effect of the earthquake. The increase in pore-water pressure reduces the effective stress in the soil and then leads to a loss of shear strength and the soil starts to act like a liquid.

When earthquakes with a moment magnitude (M_w) greater than 5 are examined, liquefaction occurs most frequently on loose, saturated sandy and silty soils. These deformations caused buildings to collapse or be severely damaged. For example, in the Niigata, Japan earthquake with a moment magnitude of 7.5 occurred in 1964, concrete buildings sank and tilted laterally. In 1995, in the 7.2 magnitude earthquake in Kobe, Japan, bridges, buried pipelines, port facilities, the retaining walls on the coasts were damaged by tilting and the buildings sank due to liquefaction. Similarly, a 7.5 magnitude earthquake occurred in Gölçük-Marmara, Turkey in 1999. Many structures sank into the soil or tilted to one side [1-3]. Assessments of liquefaction risk started with the 1964 Niagata earthquake and became much more important for the 1971 San Fernando, 1985 Mexico City, 1989 Loma Prieta, 1995 Kobe and 1999 Marmara earthquakes.

Laboratory and field tests are used in the liquefaction assessment based on the simplified method. Competent people should prepare the samples representing the field conditions to obtain the correct results from laboratory experiments. It is a challenging and laborious job in practice. Damage often occurs during the collection of the samples from the field and the transportation and preparation for the experiment. Therefore, a determination of the liquefaction potential according to just the results of a laboratory experiment causes errors. Instead, the results of the Standard Penetration Test (SPT) carried out in the field are often used to estimate a soil's liquefaction resistance [4].

Some factors affecting liquefaction include ground water, earthquake moment size, soil type, corrected soil SPT penetration resistance (N_{60}) value, relative density (D_r),

depth of the obtaining SPT N_{60} value (d), fines content (FC), which is defined as the ratio of soils passing a No. 200 (75 μm) sieve, average grain diameter (D_{50}), unit weight (UW), groundwater level (GWL), effective stress (σ'_{vo}), total stress (σ_{vo}), peak ground acceleration (a_{max}) and depth of the earthquake from the surface [1, 2, 5-10]. Seed and Idriss [4] carried out the first studies on liquefaction based on SPT data. They suggested that liquefaction could be estimated with graphs and equations, depending on SPT. A liquefaction assessment using SPT data, which was developed by Seed and Idriss, is referred to as the "simplified method" [4]. Versions of this method improved by other authors are used worldwide [11],[12],[13]. The Turkish Building Earthquake Code (TBEC-2018) accepts the "simplified method", which consists of the empirical equations dependent on the SPT published by Seed and Idriss [4] as the standard method for soil-liquefaction analyses.

The cyclic stress approach is used to evaluate the liquefaction potential. In this approach, the Cyclic Stress Ratio (CSR) represents the earthquake load, i.e., the earthquake's soil liquefaction effect or demand. Depending on the results of the SPT test in the field, the resistance of the soil to liquefaction is represented by the Cyclic Resistance Ratio (CRR). The fact that the liquefaction factor of safety, i.e., the CRR over CSR ratio, is less than 1.10 usually means that soil will liquefy according to TBEC-2018 [38]. The cyclic-stress approach in assessing the liquefaction potential expresses both the earthquake effect (CSR) and the soil-liquefaction resistance (CRR) in cyclical stresses. The cycle number for the CSR, which is a function of the duration of the earthquake movement, is proportional to the magnitude of the earthquake. The cyclic liquefaction resistance (CRR) is obtained in the laboratory by cyclic triaxial and simple shear tests or most often in the field by the SPT. The CRR is expressed in terms of the number of cycles required for the occurrence of collapsing in a soil exposed to cyclic shear stress at a certain level. However, the CRR is affected by the stress and unit deformation history, age, and soil texture, which are disturbed during sampling and are very difficult to simulate in the laboratory. Therefore, field tests are preferred for a liquefaction assessment. The SPT is a widely used field test used to calculate the CRR of the soil.

In recent years the number of scientific studies using numerical methods based on statistical and artificial intelligence techniques for estimating the liquefaction of soils has increased [9, 10, 14-23]. Finn, Dowling and Ventura [22] developed methods that estimate the liquefaction potential and lateral expansion displacements. Boulanger and Idriss [13] studied the probability of triggering liquefaction based on SPT. In their study,

they obtained the maximum probability approach and the liquefaction trigger correlation related to SPT. Keramatikerman, Chegenizadeh, and Nikraz [24] conducted a series of repeated triaxial experiments to determine the effect of fly ash on the liquefaction resistance of sands, and they observed that the resistance to liquefaction increases with the increasing ash ratio and time.

Yang et al. developed an SPT-based empirical equation to assess sand liquefaction [19]. Rahman and Siddiqua [21] estimated the liquefaction resistance of soils using the standard penetration test, cone penetration test, and shear wave velocity data for the cities of Dhaka, Chittagong and Sylhet in Bangladesh. The effects of FC on the liquefaction of soils were also investigated [25]. Anwar et al. obtained a model to find the CRR for MRA-based soil-liquefaction analysis using SPSS and the MATLAB program [26]. Fei-hong [27] investigated the statistical relationship between the liquefaction index and the depth using SPT data to assess soil liquefaction in the port area of Tianjin city, and they showed a significant relationship between the liquefaction index, the depth, and the SPT N-value. Another study claimed that liquefaction is a complex ground-degradation problem involving soil and earthquake parameters, and ground deformations caused by liquefaction should be investigated by nonlinear methods [28]. In a study investigating fuzzy neural network models for the prediction of liquefaction, integrated fuzzy neural network models were developed to evaluate the liquefaction potential [5]. Muduli and Das developed an empirical model using multi-gene genetic programming (MGGP), which is an SPT-based artificial intelligence technique, to determine the CRR of the soil [23]. In a study estimating the safety coefficient against liquefaction with artificial neural networks, the liquefaction potential of the soils in the adjacent area of Gümüşler-Denizli province was evaluated, and the safety coefficient against liquefaction was estimated with the help of ANN [29].

In this study, standard penetration tests were carried out in 63 drill holes in Erzincan and 60 drill holes in Kayseri. Seed and Idriss's simplified liquefaction analysis [4] was used to determine the liquefaction safety coefficient and the effects of various soil parameters on calculating the CRR were investigated.

A data set containing these parameters and the liquefaction safety coefficients was prepared. First, a quadratic nonlinear multiple regression model (NMRA) that predicts the soil liquefaction and reflects the nonlinear behavior of the soil was developed with this data set. Consequently, models that predict the liquefaction of the soils were created with Artificial Neural Networks (ANN) and then with the Adaptive Neuro-Fuzzy Infer-

ence System (ANFIS) using the same training and test data. Randomly selected training and test data were used in the development of the NMRA, ANN, and ANFIS models. To develop the best model, CRR_{act} values obtained as a result of a simplified liquefaction analysis were compared with the predicted CRR_{pred} values using the NMRA, ANN, and ANFIS models. This study examines the estimation methods against the liquefaction hazard that an earthquake can cause. By determining the liquefaction potentials and comparing the estimation methods, the soil improvements and geotechnical designs will be more secure. They can help to prevent the devastating consequences of earthquake-induced liquefaction.

2 METHOD OF MODELLING

The standard penetration test is widely used in the calculation of liquefaction analysis. SPT is a simple and relatively low-cost field test for the evaluation of liquefaction potential due to easy data acquisition, the presence of a database prepared from the data obtained in previous earthquakes, and revealing a good correlation of these data with new earthquakes. Ref [4] proposed equation (1) for the liquefaction analysis.

$$CSR = \left(\frac{\tau_{av}}{\sigma'_{vo}} \right) = 0.65 \left(\frac{a_{max}}{g} \right) \left(\frac{\sigma_{vo}}{\sigma'_{vo}} \right) r_d \quad (1)$$

where

a_{max} = peak horizontal ground acceleration on the soil surface (m/s^2)

g = acceleration due to gravity (m/s^2)

σ_{vo} = total vertical soil stress (kPa)

σ'_{vo} = effective vertical soil stress (kPa)

r_d = stress-reduction coefficient from equations (2) and (3)

The largest (CSR) in the formula is the ratio of the mean shear stress ($\tau_{av} = 0.65 * \tau_{max}$) to the effective vertical stress. The effective stress-reduction coefficient r_d is a value that considers the flexibility of the soil column (e.g., $r_d = 1$ corresponds to rigid mass behavior).

$$\begin{aligned} r_d &= 1.0 - 0.00765z & z \leq 9.15 \text{ m}; \\ r_d &= 1.174 - 0.0267z & 9.15 \text{ m} < z \leq 23 \text{ m} \end{aligned} \quad (2)$$

$$\begin{aligned} r_d &= 0.744 - 0.008z & 23 \text{ m} < z \leq 30 \text{ m}; \\ r_d &= 0.5 & z > 30 \text{ m} \end{aligned} \quad (3)$$

Ref [12] proposed equation (4) for calculating the recurrent resistance ratio ($CRR_{M7.5}$) for clean sands with an FC of less than 5 % and earthquakes with a magnitude of $M_w = 7.5$. The next step is to find the dynamic cyclic resistance ratio (CRR) for the ground, based on the calculated clean sand equivalent.

$$CRR_{M7.5} = \frac{1}{34 - (N_1)_{60cs}} + \frac{(N_1)_{60}}{135} + \frac{1}{50} - \frac{1}{(10(N_1)_{60} + 45)^2} - \frac{1}{200} \quad (4)$$

$CRR_{M7.5}$ = cyclic resistance ratio to soil liquefaction for $M_w = 7.5$ earthquake

Considering the effect of the FC on the liquefaction resistance, the corrected SPT-N values used in the liquefaction analysis are suggested to be corrected as follows. Ref [12] proposed using the $(N_1)_{60}$ value after converting to the clean-sand equivalent $(N_1)_{60cs}$. They wanted to reduce the impact of FC on the soil on the CRR . Equation (5) is given as follows.

$$(N_1)_{60cs} = \alpha + \beta(N_1)_{60} \quad (5)$$

Where α and β are the fines-content correction coefficients.

The $(N_1)_{60cs}$ value is calculated using equations (6), (7) and (8) according to the FC ratio.

$$\text{for } FC \leq 5 \% \quad \alpha = 0 \text{ and } \beta = 1.0 \quad (6)$$

$$\begin{aligned} \text{for } 5 \% < FC < 35 \% \quad \alpha &= \exp \left[1.76 - \left(\frac{190}{FC^2} \right) \right] \\ \text{and } \beta &= \left[0.99 + \left(\frac{FC^{1.5}}{1000} \right) \right] \end{aligned} \quad (7)$$

$$\text{for } FC \geq 35 \% \quad \alpha = 5 \text{ and } \beta = 1.2 \quad (8)$$

where $SPT-N_{field}$ is the value adjusted to 60 % of the energy ratio and $(N_1)_{60cs}$ is the number of SPT blow-count values with the fines-content correction. Liquefaction occurs when the CRR , which shows the soil's resistance to liquefaction, exceeds the liquefaction resistance (CSR) caused by earthquakes. If this situation is explained in terms of safety factor, the Safety Coefficient (F_S) is given by equation (9).

$$F_S = \frac{CRR}{CSR} \quad (9)$$

$F_S \leq 1.1$ is considered as there being a liquefaction potential and $F_S \geq 1.1$ is considered as there being no liquefaction potential [38]. The equations and curves given for the calculation of CRR are valid for an earthquake with a moment magnitude $M = 7.5$. The

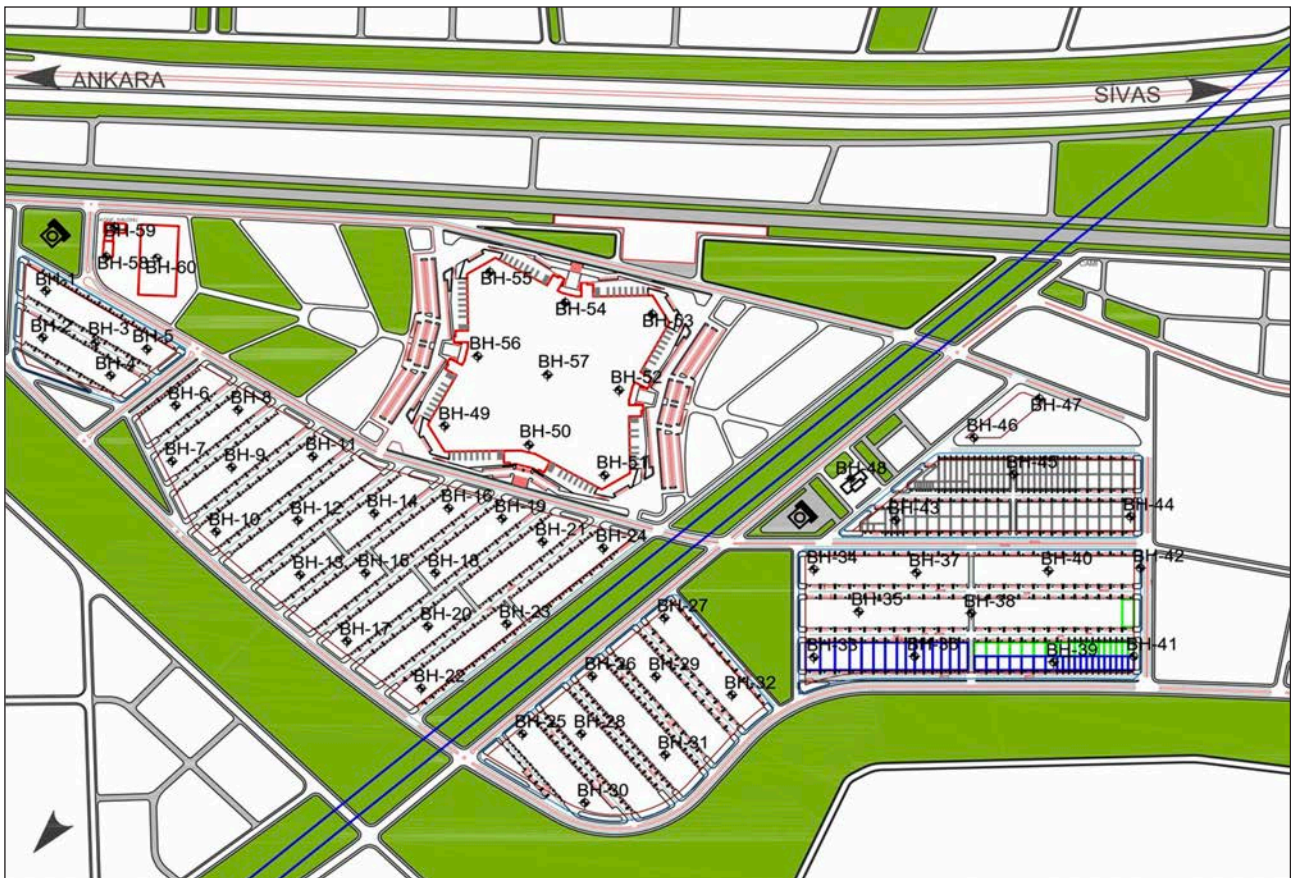


Figure 1. Site layout and borehole location plan in Kayseri province.

earthquake-magnitude correction factor specified in equations (10) and (11) is proposed to use in different earthquake magnitudes.

$$F_s = \frac{CRR}{CSR} * MDF \quad (10)$$

MDF = earthquakmagnitude correction factor

$$MDF = \frac{10^{2.24}}{M^{2.56}} \quad (11)$$

M = earthquake moment magnitude

2.1 Study Area Description

The analysis was performed using data from two different cities (Kayseri and Erzincan). In Kayseri, there are generally sand and silt soil layers in the area under investigation (approximately 1.5 million square

meters) (Figure 1). However, the soil properties of the region have variable soil conditions, and it is silty sand in some places and silty clay with sand inter bands at some other sites. The 60 borehole drillings, shown in Figure 1, were performed in the study area, and SPT was achieved every 1.5 m in drillings between SK1-SK48 and SK49-SK60. The peak horizontal ground acceleration at the ground surface (a_{max}) value can be expressed in gravitational acceleration (g). In the study area of Kayseri, the a_{max} value changes between 0.190 g and 0.200 g (TBEC-2018). The earthquake that is thought to affect Kayseri Province and its surroundings is the movement that might occur in the Ecemiş fault, which is a strike slip fault. The second study area is in the Erzincan plain in the city center of Erzincan. The soil types in Erzincan are generally non-plastic, silty sand and clayey sand. The peak ground acceleration, a_{max} value changes between 0.600 g and 0.615 g in the

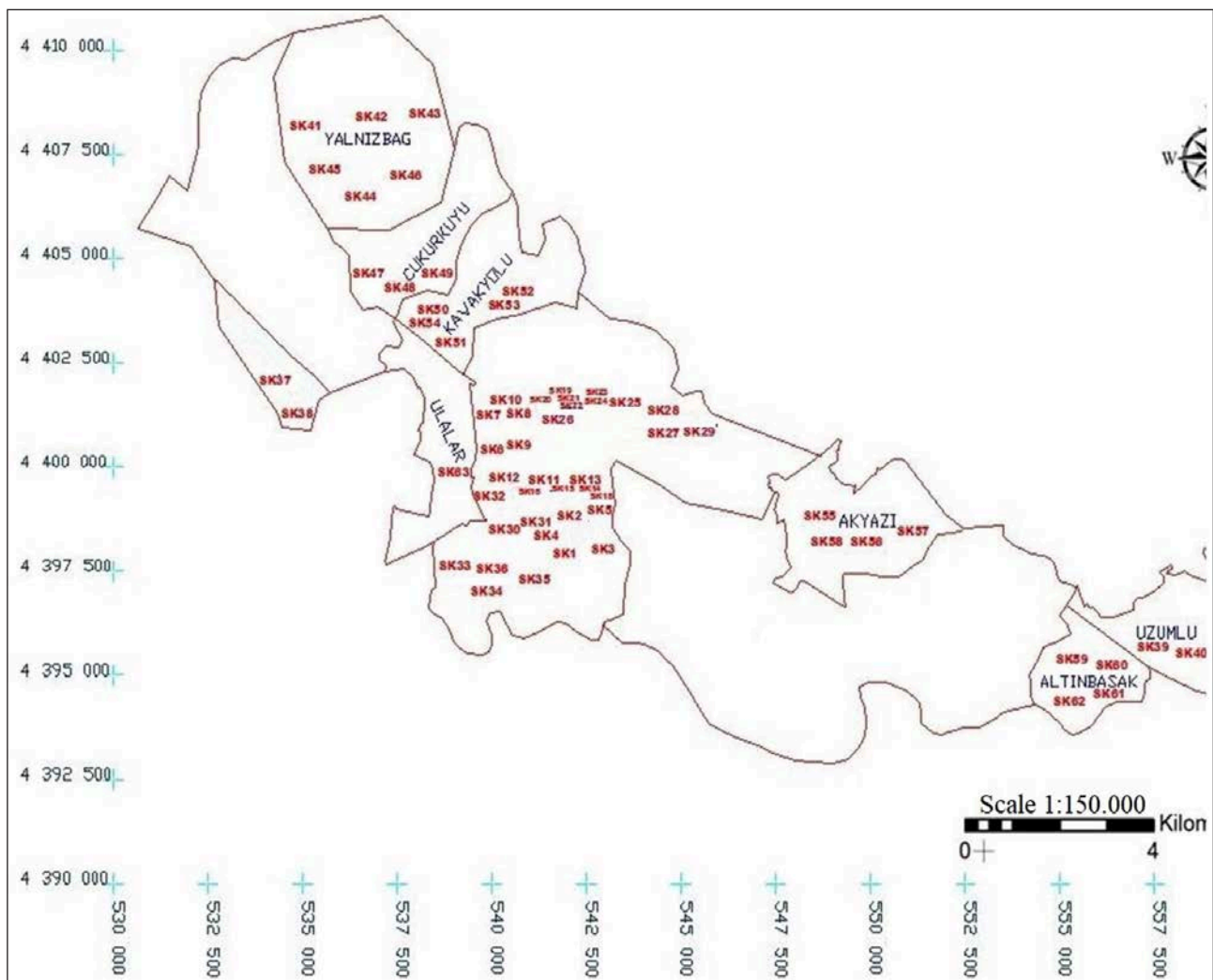


Figure 2. Bore holes in the study area in Erzincan province[33]. Note: SK = Borehole

study area in Erzincan. This region is located on the KAFZ (North Anatolian Fault Zone), which is the most effective fault zone of Turkey.

The earthquake parameters were calculated separately using the geographical location data entry for Erzincan and Kayseri with the interactive web application (<https://depem.afad.gov.tr>). According to the soil class in the study areas, the earthquake ground-motion level with a probability of exceeding 10 % in 50 years (recurrence period of 475 years) was taken into account (this is called DD-2, TBEC-2018). According to the earthquake ground-motion level, the peak acceleration values varied between 0.600 g and 0.615 g and 0.190 g and 0.200 g in the study area of Erzincan and Kayseri, respectively (TBEC-2018). According to these acceleration values, it was estimated as M_w 7.5 for Erzincan and M_w 6 for Kayseri. In the estimation of these moment-magnitude values, the approaches given in the literature were used [39].

In the city of Erzincan, 63 borehole drillings with depths of 1.5 m to 20 m, shown in Figure 2, were made. The soil parameters and SPT data were collected, and soil profiles were created for these drillings.

3 PROCESSING AND ANALYSIS OF DATA

This study explains the CRR values obtained from Simplified Liquefaction Analysis [4], NMRA, ANFIS, and ANN methods for Kayseri and Erzincan. Groundwater levels varied between 1.7 and 2.8 m in the study area in Kayseri. The Unit Weight Test to determine the mass properties of the soil, the Water Content Test to determine the amount of water in the unit volume of the ground, the Liquid Limit and Plastic Limit Tests to determine the consistency characteristics, the Sieve Analysis Test to determine the grain diameter and distribution of the soil and Hydrometer test to determine the FC were carried out in the samples taken from the investigated area. As the result of the tests, it was observed that the unit-weight values varied between 15 and 20 kN/m^3 , the FC ranged from 12 to 45 %, and the water contents ranged between 13 % and 47 %. The soils' liquid limit (LL) values varied between 30 % and 47 %, and the plastic limit (PL) values ranged from 20 % to 27 %.

In Erzincan, 63 boreholes were drilled in 16 different locations with depths ranging from 1.5 to 20 m. The soil types are SM (silty sands), SC (clayey sands), and CL (inorganic clay of low plasticity), which are characterized as primarily coarse-grained soils. Therefore, tests were made on the samples and the following results were obtained; the unit-weight values varied between 16.93 and 19.96 kN/m^3 , FC ranged from 12 to 77 %,

and the water-content (w) value varied between 10 and 30 %. The soil types in the study area were generally non-plastic (NP) according to the PL and LL test results. According to the results of the SPT obtained from both regions and the laboratory experiments, 837 data sets were obtained. The reason for choosing these data is that the groundwater table is close to the ground surface and the soil properties also show the liquefaction potential in both regions. These data were randomly divided into two groups: a training group composed of 70 % (586) and a test group consisting of 30 % (251) of the data. Data of the parameters used in CRR calculation were the earthquake magnitude (M_w), depth (d), corrected soil SPT penetration resistance (N_{60}), saturated Unit Weight (UW), peak ground acceleration (a_{max}), fines content (FC), cyclic stress ratio (CSR), groundwater level (GWL), total stress (σ_{vo}) and average grain diameter (D_{50}). There are the effects of 9 different independent variables on the calculation of CRR .

In liquefaction, the groundwater level is generally crucial up to the first 3 m from the surface. Although liquefaction rarely occurs in environments where the groundwater level is deeper than 10 m from the surface, liquefaction is not expected in environments where the groundwater level is deeper than 20 m, in general [36]. In a complex hydrogeological environment, the groundwater level is variable due to hydraulic transitions that affect the hydraulic properties of the soil. Moss et al. (2017) investigated the effect of the groundwater level on the liquefaction potential and the effect of changing the depth of the water table on the liquefaction according to seasonal variations. The water level rises to its maximum during the rainy season due to rain. The study highlights the need for seasonal liquefaction-sensitivity studies [37].

The groundwater levels varied between 1 and 2.7 m and 1.7 and 2.8 m in the study area of Erzincan and Kayseri, respectively. The groundwater table is assumed to be at the surface for the worst-possible scenario for both regions in determining the liquefaction hazard by considering seasonal and global climate change. Besides, since the groundwater-depth values measured in the field show minor local variations according to the regions, these parameters did not make a significant difference in the training of the prediction models compared to the effect of other parameters. For this reason, it was not preferable to use the groundwater-level depth parameters as variables in the models.

In estimating the CRR , N_{60} , d , FC , D_{50} , UW , GWL , effective stress (σ'_{vo}), and total stress (σ_{vo}) parameters were considered. The soils are completely saturated below the water table since the groundwater layer is assumed to be at the surface. Saturated unit weights were used

for a point below the groundwater table to calculate the effective unit weight. However, since the soil depth and UW are used to calculate the total stress values, only the depth and saturated unit weight represent the total stress to avoid over-learning in the estimation methods.

In addition, a Variance Influence Factor (VIF) analysis was performed to see the effect of independent variables on CRR . All the estimation models used in this study are based on the five most influential variables for the saturated condition of the soils as a result of a VIF analysis. These are, namely, the SPT value (N_{60}), fines content (FC), saturated unit weight (UW), depth from which SPT is obtained (d), and average grain diameter (D_{50}) parameters.

Regression analysis coefficients, T-test values, and VIF values, which were obtained with the analysis performed to determine the relationship between the dependent and independent variables, are given in Table 1. In Table 1, the N_{60} , UW , D_{50} , d , and FC parameters are preferred as independent variables, since the VIF values were less than 5. It is clear that the t values obtained were not within the range $-1.645 < t < 1.645$, which were determined for $t_{critical} = 1.645$. Thus, the N_{60} , UW , D_{50} , d , and FC parameters were significant in the CRR estimation and were used in the analysis.

Table 1. Results of regression analysis according to t test and VIF analysis.

Independent variables	Regression coefficients	t	VIF
Constant	2.7806	6.88	
N_{60}	0.0212426	26.39	1.581
FC	0.17645	2.03	1.268
UW	-0.16398	-7.08	1.795
d	0.0018631	2.24	1.112
D_{50}	0.6052	2.78	1.257
$t_{critical} = 1.645$			

Table 2. Data statistics.

Parameters	n	Min	Max	Mean	Standard deviation
N_{60}	837	2	53	16.86	9.873
FC	837	0.12	0.77	0.36	0.076015
UW	837	16.93	19.96	18.16	0.36116
d	837	1.50	40.50	11.23	7.86592
D_{50}	837	0.01	0.334	0.042	0.023233
CRR	837	0.084	1.24	0.30	0.1426768

It was reported that the test performance of fuzzy logic-based models such as ANFIS decreases with an increase in the number of independent variables [5]. Therefore, the number of independent variables was limited to 5 in this study. Table 2 shows the statistical data of this dependent (CRR) and the independent variables.

3.1 Performance Criteria

In estimating the CRR value, MAE, MSE, RMSE, MARE, and R^2 are taken into account to compare the performance of the models. The model error rate occurs because it does not fully represent a proper relationship between the predicted and the actual parameters. As a result of this incomplete relationship, different error-rate indices can be expressed. The mean absolute error (MAE) is the measured difference between two variables. The MAE is also the average horizontal distance between each data point and the best-fit line. Since the MAE value is easily interpretable, it is frequently used in regression and artificial intelligence techniques. The MAE value can vary from zero to infinity. The mean square error (MSE) measures the performance of the model, the estimator, telling how close the prediction curve is to a set of points. When the MSE value is zero, the model has the best-possible performance. The RMSE (root-mean-square error) is the standard deviation of the estimation errors. The RMSE is a measure of the distribution of residues. The RMSE value can range from zero to infinity. A zero RMSE value means that the model made no errors. The MARE expresses the difference between the estimated value and the observed value. The MARE is a non-negative error rate that can take a value from zero to infinity. When the MARE value is zero, the considered model has the best-possible performance. The performance criteria used for model evaluation in this study are given in Table 3. These are (R^2), MAE, MARE, MSE and RMSE. Here, the value of R^2 indicates the closeness of our model (as a percentage) to the real values. In Table 3, CRR_{act} , \overline{CRR}_{act} , CRR_{pred} , \overline{CRR}_{pred} are the real values of CRR_{act} , calculated by simplified liquefaction analysis, the calculated real mean \overline{CRR}_{act} , the predicted CRR_{pred} , and the predicted mean \overline{CRR}_{pred} , respectively.

Equation (12) is used to normalize the data to transfer to the MATLAB program.

$$X_n = \frac{(X_0 - X_{min})}{(X_{max} - X_{min})} \quad (12)$$

Here, X_n is normalized data, X_0 is original data, X_{min} is minimum data and X_{max} is maximum data. All data were scaled between 0 and 1.

Table 3. Performance-evaluation criteria.

Evaluation criteria	Definition
Coefficient of determination (R^2)	$R^2 = \left[\frac{\sum_{i=1}^n (CRR_{act} - \overline{CRR}_{act})(CRR_{pred} - \overline{CRR}_{pred})}{\sqrt{\sum_{i=1}^n (CRR_{act} - \overline{CRR}_{act})^2} \sqrt{\sum_{i=1}^n (CRR_{pred} - \overline{CRR}_{pred})^2}} \right]^2$
Mean absolute error (MAE)	$MAE = \frac{1}{n} CRR_{pred} - CRR_{act} $
Mean absolute relative error (MARE)	$MARE = \frac{1}{n} 100 \times \frac{CRR_{act} - CRR_{pred}}{CRR_{pred}} $
Mean square error (MSE)	$MSE = \frac{1}{n} \sum_{i=1}^n (CRR_{act} - CRR_{pred})^2$
Root mean square error (RMSE)	$RMSE = \sqrt{\frac{\sum_{i=1}^n (CRR_{act} - CRR_{pred})^2}{n}}$

3.2 Nonlinear Multiple Regression Analysis (NMRA) model

Nonlinear multiple regression analysis (NMRA) is used to detect two or more correlations. NMRA is a statistical method that can reveal the relationship between more than one independent variable and a single dependent

variable, make predictions, and create a mathematical model. In this study, quadratic regression was used to estimate the CRR value. The basic equation of the regression model is relatively simple, as given by Equation 13. CRR represents the dependent variable; N_{60} , FC , UW , d , and D_{50} are the independent variables. The ability of the estimations to give reliable results depends on the coefficient of determination (R^2) being the largest value and the error rates being the smallest value.

Then, with the help of the SPSS program, various functions were tested with these independent variables, and the best fit for the distribution is the nonlinear quadratic equation. The quadratic NMRA equation was chosen, which gave the highest R^2 and the lowest RMSE values. The nonlinear regression equation obtained from the NMRA analysis is shown in Equation 13.

Thus, the R^2 was 0.718 for the training data and 0.681 for the test data. Other error statistics of the NMRA model are shown in Table 6. As shown in Figure 3, the CRR_{act} and CRR_{pred} values were close to each other. However, as shown in Figure 3, the CRR values diverged from the calculated CRR values after 0.80, which results in a reduction of the determination coefficient.

$$CRR_{pred} = 0.233 + 0.022 \cdot N_{60} - 0.322 \cdot FC + 0.622 \cdot FC^2 + 0.267 \cdot UW - 0.016 \cdot UW^2 - 0.035 \cdot d + 0.001 \cdot d^2 + 1.633 \cdot D_{50} - 0.614 \cdot D_{50}^2 \quad (13)$$

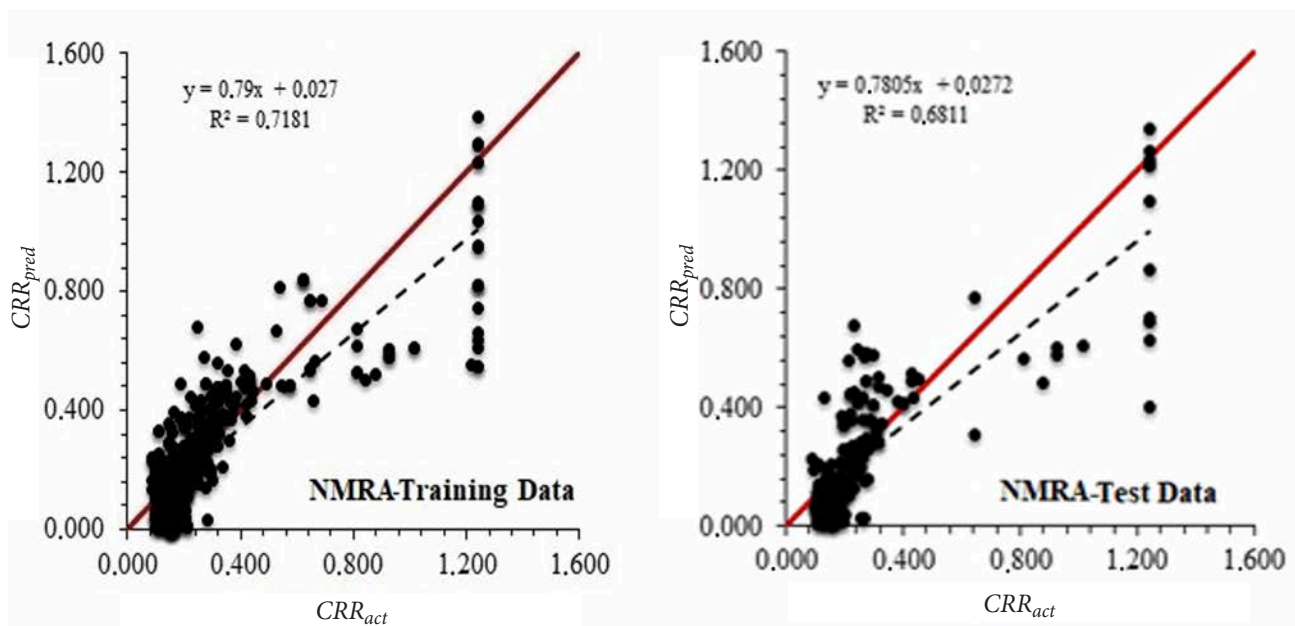


Figure 3. Comparison of predicted and actual CRR values for NMRA model in training and test data (Nonlinear Multiple Regression Analysis).

3.3 Artificial Neural Network (ANN) model

The estimation method, called ANN (Artificial Neural Networks), is the most well-known and widely used method among the artificial intelligence techniques. This method estimates the dependent variable by finding linear or nonlinear relationships between the parameters that represent many independent variables. In this technique, the working system imitates the human brain. ANN makes routing with multi-layer sensor networks and can learn and generalize between the input and output layers. The ANN structure consists of an input layer, an output layer, many hidden layers, and a large number of neurons corresponding to each independent variable. An ANN is very successful in finding nonlinear relationships between independent variables about the dependent variable. The output layer also corresponds to the predicted dependent variable. The system updates the weight values, moving from the output layer to the input layer, and the error value is minimized [5,10]. The CRR was estimated with the ANN model. In the prediction model, the input parameters are N_{60} , FC , UW , d , D_{50} , and the output parameter is the CRR (Figure 4).

The feed-forward ANN model inputs with five variables consisting of N_{60} , FC , UW , d and D_{50} , and a single output system CRR was obtained, as shown in the diagram in Figure 4. In the training of the models, a random selection of 586 parameters was used, and 251 parameters were used to test the prediction model's performance. First, the most appropriate and widely used tansig, logsig and purelin functions from 11 member functions were used in the multi-layered ANN method in MATLAB [34]. The input data were trained with the

Levenberg-Marquardt algorithm, due to its ease of use, convergence rate and predictive success in linear and nonlinear models. The numbers of neurons in a hidden layer ranged from 2 to 10, and the numbers of iterations ranged from 1 to 100. Using a trial-and-error method, a model was determined from the network structures obtained. In this model, the input membership function was logsig, which gives the lowest all error statistic values and the highest Determination Coefficient (R^2) value, and its output membership function was purelin.

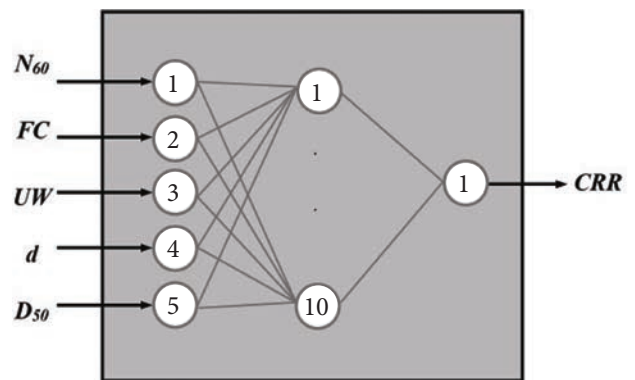


Figure 4. ANN block diagram for the designed system.

Table 4. Best ANN model for predicting CRR.

Membership function		Membership function number	Iteration number
Input	Output		
Logsig	Purelin	10	95

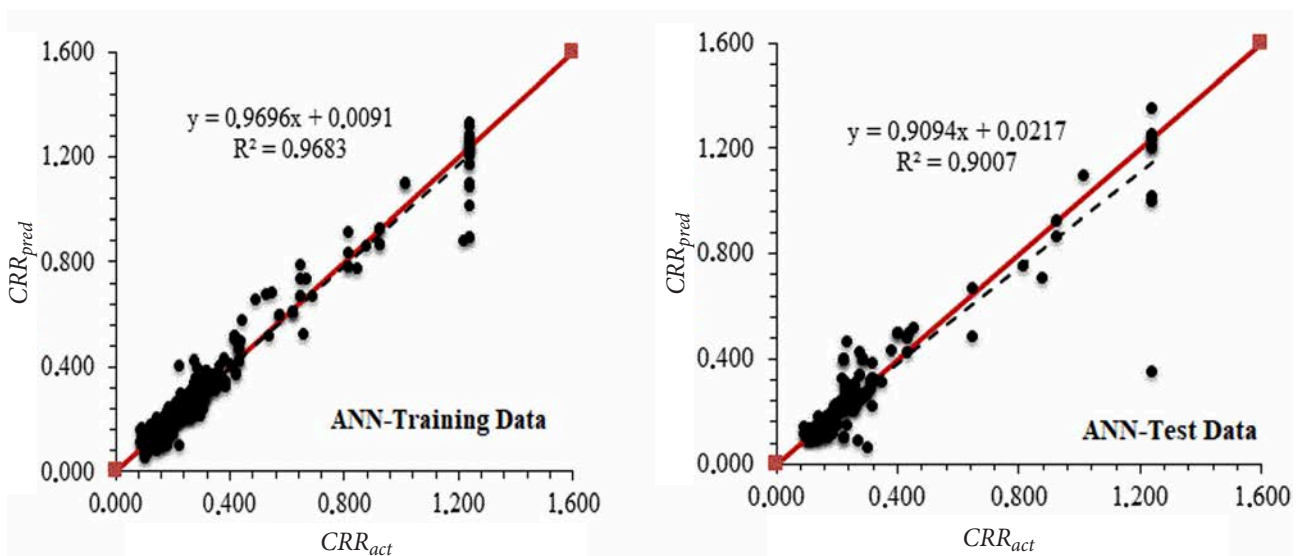


Figure 5. Comparison of predicted CRR and actual CRR values for ANN model.

ANN characteristics of the best ANN model obtained after various trial-and-error attempts are given in Table 4. All the statistical error values of the best ANN model are given in Table 6. According to Table 6, the error statistic values were within acceptable values. As can be seen in Table 6, and Figure 5, the ANN model revealed successful results. However, it can be seen in Figure 5 that the predictive CRR values diverged between 1.0 and 1.5 from the calculated CRR values.

3.4 Adaptive neuro-fuzzy inference system (ANFIS) model

The adaptive ANN-based fuzzy inference system (ANFIS) is one of the essential artificial intelligence techniques that can optimize parameters with an inference system. ANFIS provides for the optimization of rule-base and membership function values to model systems with known input and output values with fuzzy logic. The optimization process involves the learning methods of ANN. In this way, fuzzy systems, which normally cannot learn, gain a learning ability for the data sets to be modeled. ANFIS uses the backpropagation method, as a learning method, or a combination of the backpropagation method and the least-squares estimation method. The ANFIS architecture consists of six layers. The first layer (input layer) transmits the incoming input signals to the other layers. The second layer is called the fuzzy layer, the third layer is the rule layer, and the fourth layer is the normalization layer. The fifth layer is the annotation layer, and finally, in the sixth layer, the values from the annotation layer are aggregated

within this layer to obtain the actual output value of the ANFIS system [5]

In the ANFIS model, since the increase in the membership function numbers, as mentioned above, decreased the performance of the ANFIS model, the input membership function numbers 2 and 3 were taken. After determining the Gaussian membership function (gaussmf) and the triangular (trimf) membership function as the input membership functions and the constant and linear functions as the output functions, the best ANFIS model was determined by trial and error in iteration numbers ranging from 1 to 5. Depending on the type of input and output functions, Gaussmf-constant, Gaussmf-linear, trimf-constant and trimf-linear combinations were determined. The lowest errors criteria and the highest R^2 are used to select the best model among the four different ANFIS combinations. The ANFIS features of the best ANFIS model obtained from various trial-and-error attempts are given in Table 5. The input membership function is Trimf, and the output membership function is linear. All the error-statistics values of the best ANN model and successful results of the ANFIS model are given in Table 5, Figure 6 and Table 6.

Table 5. Best ANFIS model for CRR prediction.

Membership function		Membership function number	Iteration number
Input	Output		
Trimf	Linear	2	4

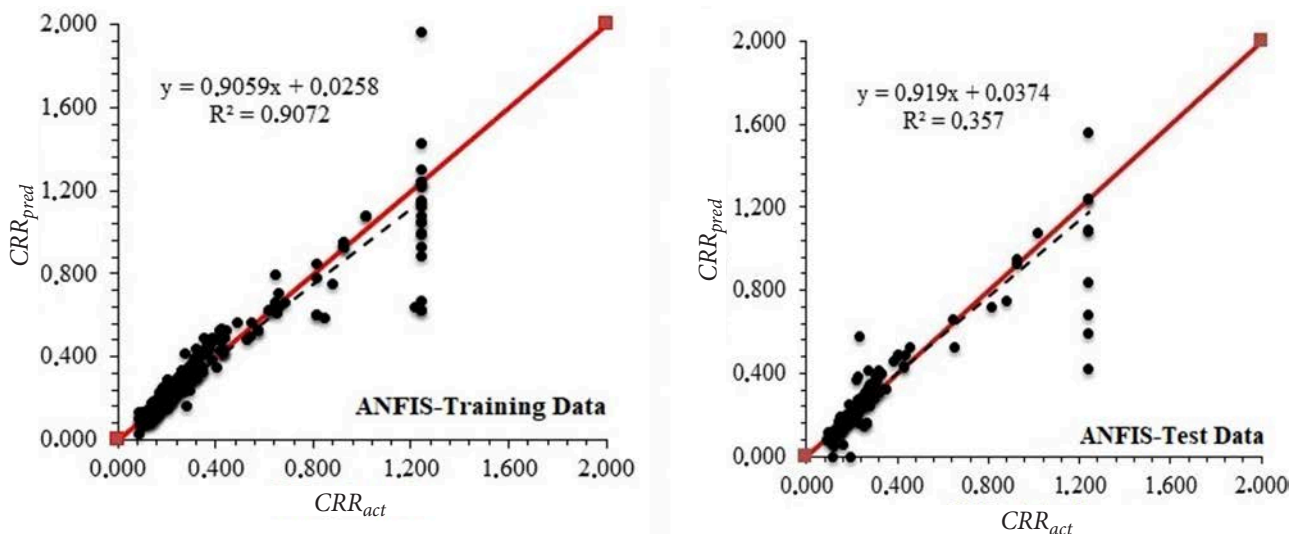


Figure 6. Comparison of predicted CRR and actual CRR values for the ANFIS model.

However, as can be seen in the scatter chart (Figure 6), the CRR_{pred} values between 1.0 and 1.5 diverged from the CRR_{act} values. This situation, which decreases the R^2 coefficient value, indicated that the model failed between 1.0 and 1.5 values.

4 RESULTS AND DISCUSSION

As shown in Table 6, the accuracy of the model's results was accepted as satisfactory, with a determination coefficient greater than 70 % obtained for all the methods. However, considering all the error statistics, the ANN model seems the best among these three methods in terms of R^2 value and the lowest MAE, highest MARE, and MSE ratios. (Table 6).

The results of the models based on the Nonlinear Multiple Regression Analysis (NMRA), Artificial Neural Networks (ANN), and Adaptive Neural Fuzzy Inference System (ANFIS) were compared with simplified analysis results in order to develop the best model for estimating the liquefaction of soils. In all models developed using statistical and artificial intelligence techniques, N_{60} , FC , UW , d , D_{50} were used as the input parameters, and the CRR value was estimated as the output parameter.

Table 6. Performance statistics of all models.

		ANN	ANFIS	NMRA
Training	MAE	0.024	0.0350	0.095
	MARE	95.214	11.0330	41.900
	MSE	0.0019	0.0068	0.018
	RMSE	0.0432	0.0822	0.134
	R^2	0.968	0.885	0.718
Test	MAE	0.034	0.036	0.098
	MARE	12.675	10.798	0.441
	MSE	0.006	0.010	0.021
	RMSE	0.0777	0.1002	0.145
	R^2	0.901	0.838	0.681

The R^2 and various error ratios were calculated by comparing the performance of the models created with the training data. It was concluded that the most suitable model is the ANN model based on the success rates and consistency of the models. Liquefaction analysis was carried out for different drilling depths and soil properties. The liquefaction status was calculated by loading data into the Excel spreadsheet. The VIF analysis was performed to see which parameters influence the CRR

calculation. The numerical studies in the CRR calculation showed that the N_{60} , FC , UW , d , and D_{50} parameters affect the CRR estimation after the VIF analysis. Thus, new models with higher accuracy were produced using these most influential parameters. The determination coefficients were 0.681, 0.838, and 0.901 in the NMRA, the ANFIS, and the ANN methods, respectively. These values show that a desired level of estimation is achieved. When the error criteria in the NMRA, ANN, and ANFIS methods were evaluated, it was observed that the ANN method was superior to the other methods, with an overall success rate of 90 % and the lowest mean absolute error rate of 0.024.

5 CONCLUSIONS

In this study, a nonlinear multiple regression analysis was performed between the CRR value and the other soil parameters. Then, the CRR estimation was made with fuzzy logic and artificial neural networks for the N_{60} , FC , UW , d and D_{50} variables, which gave high correlation coefficients. The most sensitive parameters to the soil's liquefaction are d , FC , and N_{60} , while the least sensitive ones are the UW and D_{50} soil parameters. The ANN model used in the CRR estimation has more successful performance criteria when the comparing R^2 and errors. The ANN model has lower error values and a higher correlation than the NMRA and ANFIS models. Improving the existing methods for predicting the liquefaction of soils and estimating the probability of liquefaction with the new models to be developed will enable civil engineers to take precautions against liquefaction. In addition, this study has demonstrated the successful and rapid use of artificial intelligence techniques in solving geotechnical problems, especially in modeling nonlinear complex soil behavior, such as liquefaction. This study is the basis for further studies on liquefaction. In future studies that can be performed to obtain better results in the calculation of the CRR , the number of model data can be increased by adding new data. Also, new models and higher accuracy results can be obtained using different artificial intelligence techniques.

REFERENCES

- [1] Yoshida, N., Tokimatsu, K., Yasuda, S., Kokusho, T., and Okimura, T. (2001). Geotechnical aspects of damage in Adapazari city during 1999 Kocaeli, Turkey earthquake. *Soils and foundations*, 41(4), 25-45.

- [2] Youd, T. L. (1993). Liquefaction-induced damage to bridges. *Transportation Research Record*, 1411, 35-41.
- [3] Finn, W. L., Byrne, P. M., Evans, S., and Law, T. (1996). Some geotechnical aspects of the Hyogoken Nanbu (Kobe) earthquake of January 17, 1995. *Canadian Journal of Civil Engineering*, 23(3), 778-796.
- [4] Seed, H. B. and Idriss, I. M. Simplified procedure for evaluating soil liquefaction potential. *Journal of Soil Mechanics Foundations Div*, 97, No SM9, PROC PAPER 8371, (1971) 1249-1273.
- [5] Rahman, M. S. and Wang, J. Fuzzy neural network models for liquefaction prediction. *Soil Dynamics and Earthquake Engineering*, 22, 8, (2002) 685-694.
- [6] Boulanger, R. W. and Idriss, I. M. Probabilistic Standard Penetration Test-Based Liquefaction-Triggering Procedure. *Journal of Geotechnical and Geoenvironmental Engineering*, 138, 10, (2012) 1185-1195.
- [7] Anwar, A., Jamal, Y., Ahmad, S. and Z Khan, M. Assessment of liquefaction potential of soil using multi-linear regression modeling. *International Journal of Civil Engineering & Technology (IJCIET)*, 7, (2016) 373-415.
- [8] Muduli, P. and Das, S. "Evaluation of liquefaction potential of soil based on standard penetration test using multi-gene genetic programming model". In *Proceedings of the Indian Geotechnical Conference IGC2016 (Chennai, India, (2016))*.
- [9] Kurnaz, T. F. and Kaya, Y. SPT-based liquefaction assessment with a novel ensemble model based on GMDH-type neural network. *Arabian Journal of Geosciences*, 12, 15, (2019) 456.
- [10] Sabbar, A. S., Chegenizadeh, A. and Nikraz, H. Prediction of Liquefaction Susceptibility of Clean Sandy Soils Using Artificial Intelligence Techniques. *Indian Geotechnical Journal*, 49, 1, (2019) 58-69.
- [11] Seed, H. and Idriss, I. *Ground motions and soil liquefaction during earthquakes: engineering monographs on earthquake criteria, structural design, and strong motion records. MNO-5. Earthquake Engineering Research Institute, Oakland, CA, (1982)*.
- [12] Youd, T. L. and Idriss, I. M. Liquefaction resistance of soils: summary report from the 1996 NCEER and 1998 NCEER/NSF workshops on evaluation of liquefaction resistance of soils. *Journal of geotechnical geoenvironmental engineering*, 127, 4, (2001) 297-313.
- [13] Boulanger, R. W. and Idriss, I. Probabilistic standard penetration test-based liquefaction-triggering procedure. *Journal of Geotechnical Geoenvironmental Engineering*, 138, 10, (2012) 1185-1195.
- [14] Geyin, M., Baird, A. J. and Maurer, B. W. Field assessment of liquefaction prediction models based on geotechnical versus geospatial data, with lessons for each. *Earthquake Spectra*, (2020) 1-26.
- [15] Farrokhi, F., Firoozfar, A. and Maghsoudi, M. S. Evaluation of liquefaction-induced lateral displacement using a GMDH-type neural network optimized by genetic algorithm. *Arabian Journal of Geosciences*, 13, 1, (2020) 4.
- [16] Moayedi, H., Mosallanezhad, M., Rashid, A. S. A., Jusoh, W. A. W. and Muazu, M. A. A systematic review and meta-analysis of artificial neural network application in geotechnical engineering: theory and applications. *Neural Computing Applications*, (2018) 1-24.
- [17] Kırbaş, İ. Short-term multi-step wind speed prediction using statistical methods and artificial neural networks. *Sakarya University Journal of Science*, 22, (2018) 24-38.
- [18] Asvar, F., Shirmohammadi Faradonbeh, A. and Barkhordari, K. Predicting potential of controlled blasting-induced liquefaction using neural networks and neuro-fuzzy system. *Scientia Iranica* 25, 2, (2018) 617-631.
- [19] Yang, Y., Chen, L., Sun, R., Chen, Y. and Wang, W. A depth-consistent SPT-based empirical equation for evaluating sand liquefaction. *Engineering Geology*, 221, (2017) 41-49.
- [20] Şenol, Ü. and Musayev, Z. Estimating wind energy potential by artificial neural networks method. *Bilge International Journal of Science and Technology Research*, 1, 1, (2017) 23-31.
- [21] Rahman, M. Z. and Siddiqua, S. Evaluation of liquefaction-resistance of soils using standard penetration test, cone penetration test, and shear-wave velocity data for Dhaka, Chittagong, and Sylhet cities in Bangladesh. *Environmental Earth Sciences*, 76, 5, (2017) 207.
- [22] Finn, W. D. L., Dowling, J. and Ventura, C. E. Evaluating liquefaction potential and lateral spreading in a probabilistic ground motion environment. *Soil Dynamics and Earthquake Engineering*, 91, (2016) 202-208.
- [23] Muduli, P. K. and Das, S. K. Model uncertainty of SPT-based method for evaluation of seismic soil liquefaction potential using multi-gene genetic programming. *Soils and Foundations*, 55, 2, (2015) 258-275.
- [24] Keramatikerman, M., Chegenizadeh, A. and Nikraz, H. Experimental study on effect of fly ash on liquefaction resistance of sand. *Soil Dynamics and Earthquake Engineering*, 93, (2017) 1-6.
- [25] Maurer, B. W., Green, R. A., Cubrinovski, M. and Bradley, B. A. Fines-content effects on liquefaction

- hazard evaluation for infrastructure in Christchurch, New Zealand. *Soil Dynamics and Earthquake Engineering*, 76, (2015) 58-68.
- [26] Anwar, A., Jamal, Y., Ahmad, S., Z Khan, M. and Publication, I. Assessment of liquefaction potential of soil using multi-linear regression modeling. *International Journal of Civil Engineering & Technology (IJCIET)*, 7,(2016) 373-415.
- [27] Fei-hong, G. Evaluation of Soil Liquefaction in Harbor District in Tianjin City. *The Open Civil Engineering Journal*, 10, (2016) 293-300.
- [28] Siyahi, B., Akbas, B. and Dogan Onder, N. "Evaluation Of Liquefaction-Induced Lateral Spreading By A Neural Network (Nn) Model". In *Proceedings of the 14th World Conference on Earthquake Engineering (Beijing, China, 2008)*.
- [29] Şen, G., Akyol, E. and Fırat, M. Sıvılaşmaya Karşı Güvenlik Katsayısının Yapay Sinir Ağları İle Tahmin Edilmesi: Denizli-Gümüşler Örneği. *Selçuk Üniversitesi Mühendislik, Bilim Ve Teknoloji Dergisi*, 22, (2007) 177-184.
- [30] Kramer, S. L. *Geotechnical Earthquake Engineering*. (United States of America. Prentice Hall) 1996.
- [31] Sönmezer, Y. B., Çeliker, M. and Kılınç, M. Y. Kırıkkale İli Bahçelievler ve Fabrikalar Mahallelerinin Sıvılaşma Potansiyelinin Coğrafi Bilgi Sistemlerinde Analizi. *International Journal of Engineering Research and Development*, 4, 1, (2012) 33-40.
- [32] Seed, H. B. and Idriss, I. M. *Ground motions and soil liquefaction during earthquakes*. (Berkeley. Earthquake Engineering Research Institute) 1982.
- [33] Duman, E. S. Erzincan il merkezi ve çevresindeki zeminlerin standart penetrasyon deneyi verileri kullanılarak sıvılaşma potansiyelinin belirlenmesi. (Determination of the liquefaction potential of soils in and around the centre of the city of Erzincan using standard penetration-test data) *Karadeniz Teknik Üniversitesi/Fen Bilimleri Enstitüsü*, 2013.
- [34] Beale, M. H., Hagan, M. T. and Demuth, H. B. J. T. *M. Neural network toolbox™ user's guide*,(2010).
- [35] Subaşı Duman, E. Erzincan il merkezi ve çevresindeki zeminlerin standart penetrasyon deneyi verileri kullanılarak sıvılaşma potansiyelinin belirlenmesi (Determination of the liquefaction potential of soils in and around the centre of the city of Erzincan using standard penetration-test data). MSc. Thesis, Karadeniz Technical University Science Institute, Trabzon, Turkey, 2013.
- [36] Youd, T. L. 1984. Geological effects-liquefaction and associated ground failure. *Geological and Hydrogeological Hazards Training Program*, United States Geological Survey Open-File Report 87-76, 210-232.
- [37] Moss RES, Baise LG, Zhu J, Kadkha D (2017) Examining the discrepancy between forecast and observed liquefaction from the 2015 Gorkha, Nepal, earthquakes. *Earthq Spectra* 33(S1): S73–S83. <https://doi.org/10.1193/120316EQS220M>
- [38] General Directorate for Foundations, Turkish Building Earthquake Code, TBEC-2018, Ankara, Turkey, (2018).
- [39] Wang, B. (2020). Geotechnical investigations of an earthquake that triggered disastrous landslides in eastern Canada about 1020 Cal BP. *Geoenvironmental Disasters*, 7(1), 1-13.

NAVODILA AVTORJEM

Vsebina članka

Članek naj bo napisan v naslednji obliki:

- Naslov, ki primerno opisuje vsebino članka in ne presega 80 znakov.
- Izvleček, ki naj bo skrajšana oblika članka in naj ne presega 250 besed. Izvleček mora vsebovati osnove, jedro in cilje raziskave, uporabljeno metodologijo dela, povzetek izidov in osnovne sklepe.
- Največ 6 ključnih besed, ki bi morale biti napisane takoj po izvlečku.
- Uvod, v katerem naj bo pregled novejšega stanja in zadostne informacije za razumevanje ter pregled izidov dela, predstavljenih v članku.
- Teorija.
- Eksperimentalni del, ki naj vsebuje podatke o postavitvi preiskusa in metode, uporabljene pri pridobitvi izidov.
- Izidi, ki naj bodo jasno prikazani, po potrebi v obliki slik in preglednic.
- Razprava, v kateri naj bodo prikazane povezave in posplošitve, uporabljene za pridobitev izidov. Prikazana naj bo tudi pomembnost izidov in primerjava s poprej objavljenimi deli.
- Sklepi, v katerih naj bo prikazan en ali več sklepov, ki izhajajo iz izidov in razprave.
- Vse navedbe v besedilu morajo biti na koncu zbrane v seznamu literature, in obratno.

Dodatne zahteve

- Vrstice morajo biti zaporedno oštevilčene.
- Predložen članek ne sme imeti več kot 18 strani (brez tabel, legend in literature); velikost črk 12, dvojni razmik med vrsticami. V članek je lahko vključenih največ 10 slik. Isti rezultati so lahko prikazani v tabelah ali na slikah, ne pa na oba načina.
- Potrebno je priložiti imena, naslove in elektronske naslove štirih potencialnih recenzentov članka. Urednik ima izključno pravico do odločitve, ali bo te predloge upošteval.

Enote in okrajšave

V besedilu, preglednicah in slikah uporabljajte le standardne označbe in okrajšave SI. Simbole fizikalnih veličin v besedilu pišite poševno (npr. v , T itn.). Simbole enot, ki so sestavljene iz črk, pa pokončno (npr. Pa, m itn.). Vse okrajšave naj bodo, ko se prvič pojavijo, izpisane v celoti.

Slike

Slike morajo biti zaporedno oštevilčene in označene, v besedilu in podnaslovu, kot sl. 1, sl. 2 itn. Posnete naj bodo v katerem koli od razširjenih formatov, npr. BMP, JPG, GIF. Za pripravo diagramov in risb priporočamo CDR format (CorelDraw), saj so slike v njem vektorske in jih lahko pri končni obdelavi preprosto povečujemo ali pomanjšujemo.

Pri označevanju osi v diagramih, kadar je le mogoče, uporabite označbe veličin (npr. v , T itn.). V diagramih z več krivuljami mora biti vsaka krivulja označena. Pomen oznake mora biti razložen v podnapisu slike.

Za vse slike po fotografskih posnetkih je treba priložiti izvirne fotografije ali kakovostno narejen posnetek.

Preglednice

Preglednice morajo biti zaporedno oštevilčene in označene, v besedilu in podnaslovu, kot preglednica 1, preglednica 2 itn. V preglednicah ne uporabljajte izpisanih imen veličin, ampak samo ustrezne simbole. K fizikalnim količinam, npr. t (pisano poševno), pripišite enote (pisano pokončno) v novo vrsto brez oklepajev. Vse opombe naj bodo označene z uporabo dvignjene številke¹.

Seznam literature

Navedba v besedilu

Vsaka navedba, na katero se sklicujete v besedilu, mora biti v seznamu literature (in obratno). Neobjavljeni rezultati in osebne komunikacije se ne priporočajo v seznamu literature, navedejo pa se lahko v besedilu, če je nujno potrebno.

Oblika navajanja literature

V besedilu: Navedite reference zaporedno po številkah v oglatih oklepajih v skladu z besedilom. Dejanski avtorji so lahko navedeni, vendar mora obvezno biti podana referenčna številka.

Primer: »..... kot je razvidno [1,2]. Brandl and Blovsky [4], sta pridobila drugačen rezultat...«

V seznamu: Literaturni viri so oštevilčeni po vrstnem redu, kakor se pojavijo v članku. Označimo jih s številkami v oglatih oklepajih.

Sklicevanje na objave v revijah:

- [1] Jelušič, P., Žlender, B. 2013. Soil-nail wall stability analysis using ANFIS. Acta Geotechnica Slovenica 10(1), 61-73.

Sklicevanje na knjigo:

- [2] Šuklje, L. 1969. Rheological aspects of soil mechanics. Wiley-Interscience, London

Sklicevanje na poglavje v monografiji:

- [3] Mitchel, J.K. 1992. Characteristics and mechanisms of clay creep and creep rupture, in N. Guven, R.M. Pollastro (eds.), Clay-Water Interface and Its Rheological Implications, CMS Workshop Lectures, Vol. 4, The clay minerals Society, USA, pp. 212-244..

Sklicevanje na objave v zbornikih konferenc:

- [4] Brandl, H., Blovsky, S. 2005. Slope stabilization with socket walls using the observational method. Proc. Int. conf. on Soil Mechanics and Geotechnical Engineering, Bratislava, pp. 2485-2488.

Sklicevanje na spletne objave:

- [5] Kot najmanj, je potrebno podati celoten URL. Če so poznani drugi podatki (DOI, imena avtorjev, datumi, sklicevanje na izvorno literaturo), se naj prav tako dodajo.

INSTRUCTIONS FOR AUTHORS

Format of the paper

The paper should have the following structure:

- A Title, which adequately describes the content of the paper and should not exceed 80 characters;
- An Abstract, which should be viewed as a mini version of the paper and should not exceed 250 words. The Abstract should state the principal objectives and the scope of the investigation and the methodology employed; it should also summarise the results and state the principal conclusions;
- Immediately after the abstract, provide a maximum of 6 keywords;
- An Introduction, which should provide a review of recent literature and sufficient background information to allow the results of the paper to be understood and evaluated;
- A Theoretical section;
- An Experimental section, which should provide details of the experimental set-up and the methods used to obtain the results;
- A Results section, which should clearly and concisely present the data, using figures and tables where appropriate;
- A Discussion section, which should describe the relationships shown and the generalisations made possible by the results and discuss the significance

Podatki o avtorjih

Članku priložite tudi podatke o avtorjih: imena, nazive, popolne poštne naslove, številke telefona in faksa, naslove elektronske pošte. Navedite kontaktno osebo.

Sprejem člankov in avtorske pravice

Uredništvo si pridržuje pravico do odločanja o sprejemu članka za objavo, strokovno oceno mednarodnih recenzentov in morebitnem predlogu za krajšanje ali izpopolnitev ter terminološke in jezikovne korekture. Z objavo preidejo avtorske pravice na revijo ACTA GEOTECHNICA SLOVENICA. Pri morebitnih kasnejših objavah mora biti AGS navedena kot vir.

Vsa nadaljnja pojasnila daje:

Uredništvo
ACTA GEOTECHNICA SLOVENICA
Univerza v Mariboru,
Fakulteta za gradbeništvo, prometno inženirstvo in arhitekturo
Smetanova ulica 17, 2000 Maribor, Slovenija
E-pošta: ags@um.si

- of the results, making comparisons with previously published work;
- Conclusions, which should present one or more conclusions that have been drawn from the results and subsequent discussion;
- A list of References, which comprises all the references cited in the text, and vice versa.

Additional Requirements for Manuscripts

- Use double line-spacing.
- Insert continuous line numbering.
- The submitted text of Research Papers should cover no more than 18 pages (without Tables, Legends, and References, style: font size 12, double line spacing). The number of illustrations should not exceed 10. Results may be shown in tables or figures, but not in both of them.
- Please submit, with the manuscript, the names, addresses and e-mail addresses of four potential referees. Note that the editor retains the sole right to decide whether or not the suggested reviewers are used.

Units and abbreviations

Only standard SI symbols and abbreviations should be used in the text, tables and figures. Symbols for physical quantities in the text should be written in Italics (e.g. *v*, *T*, etc.). Symbols for units that consist of letters should

be in plain text (e.g. Pa, m, etc.).

All abbreviations should be spelt out in full on first appearance.

Figures

Figures must be cited in consecutive numerical order in the text and referred to in both the text and the caption as Fig. 1, Fig. 2, etc. Figures may be saved in any common format, e.g. BMP, JPG, GIF. However, the use of CDR format (CorelDraw) is recommended for graphs and line drawings, since vector images can be easily reduced or enlarged during final processing of the paper.

When labelling axes, physical quantities (e.g. v , T , etc.) should be used whenever possible. Multi-curve graphs should have individual curves marked with a symbol; the meaning of the symbol should be explained in the figure caption. Good quality black-and-white photographs or scanned images should be supplied for the illustrations.

Tables

Tables must be cited in consecutive numerical order in the text and referred to in both the text and the caption as Table 1, Table 2, etc. The use of names for quantities in tables should be avoided if possible: corresponding symbols are preferred. In addition to the physical quantity, e.g. t (in Italics), units (normal text), should be added on a new line without brackets.

Any footnotes should be indicated by the use of the superscript¹.

LIST OF references

Citation in text

Please ensure that every reference cited in the text is also present in the reference list (and vice versa). Any references cited in the abstract must be given in full. Unpublished results and personal communications are not recommended in the reference list, but may be mentioned in the text, if necessary.

Reference style

Text: Indicate references by number(s) in square brackets consecutively in line with the text. The actual authors can be referred to, but the reference number(s) must always be given:

Example: "... as demonstrated [1,2]. Brandl and Blovsky [4] obtained a different result ..."

List: Number the references (numbers in square brackets) in the list in the order in which they appear in the text.

Reference to a journal publication:

- [1] Jelušič, P., Žlender, B. 2013. Soil-nail wall stability analysis using ANFIS. *Acta Geotechnica Slovenica* 10(1), 61-73.

Reference to a book:

- [2] Šuklje, L. 1969. Rheological aspects of soil mechanics. Wiley-Interscience, London

Reference to a chapter in an edited book:

- [3] Mitchel, J.K. 1992. Characteristics and mechanisms of clay creep and creep rupture, in N. Guven, R.M. Pollastro (eds.), *Clay-Water Interface and Its Rheological Implications*, CMS Workshop Lectures, Vol. 4, The clay minerals Society, USA, pp. 212-244.

Conference proceedings:

- [4] Brandl, H., Blovsky, S. 2005. Slope stabilization with socket walls using the observational method. *Proc. Int. conf. on Soil Mechanics and Geotechnical Engineering*, Bratislava, pp. 2485-2488.

Web references:

- [5] As a minimum, the full URL should be given and the date when the reference was last accessed. Any further information, if known (DOI, author names, dates, reference to a source publication, etc.), should also be given.

Author information

The following information about the authors should be enclosed with the paper: names, complete postal addresses, telephone and fax numbers and E-mail addresses. Indicate the name of the corresponding author.

Acceptance of papers and copyright

The Editorial Committee of the Slovenian Geotechnical Review reserves the right to decide whether a paper is acceptable for publication, to obtain peer reviews for the submitted papers, and if necessary, to require changes in the content, length or language.

On publication, copyright for the paper shall pass to the ACTA GEOTECHNICA SLOVENICA. The AGS must be stated as a source in all later publication.

For further information contact:

Editorial Board
 ACTA GEOTECHNICA SLOVENICA
 University of Maribor,
 Faculty of Civil Engineering, Transportation Engineering and Architecture
 Smetanova ulica 17, 2000 Maribor, Slovenia
 E-mail: ags@um.si

NAMEN REVIJE

Namen revije ACTA GEOTECHNICA SLOVENICA je objavljane kakovostnih teoretičnih člankov z novih pomembnih področij geomehanike in geotehnike, ki bodo dolgoročno vplivali na temeljne in praktične vidike teh področij.

ACTA GEOTECHNICA SLOVENICA objavlja članke s področij: mehanika zemljin in kamnin, inženirska geologija, okoljska geotehnika, geosintetika, geotehnične konstrukcije, numerične in analitične metode, računalniško modeliranje, optimizacija geotehničnih konstrukcij, terenske in laboratorijske preiskave.

Revija redno izhaja dvakrat letno.

AVTORSKE PRAVICE

Ko uredništvo prejme članek v objavo, prosi avtorja(je), da prenese(jo) avtorske pravice za članek na izdajatelja, da bi zagotovili kar se da obsežno razširjanje informacij. Naša revija in posamezni prispevki so zaščiteni z avtorskimi pravicami izdajatelja in zanje veljajo naslednji pogoji:

Fotokopiranje

V skladu z našimi zakoni o zaščiti avtorskih pravic je dovoljeno narediti eno kopijo posameznega članka za osebno uporabo. Za naslednje fotokopije, vključno z večkratnim fotokopiranjem, sistematičnim fotokopiranjem, kopiranjem za reklamne ali predstavitvene namene, nadaljnjo prodajo in vsemi oblikami nedobičkonosne uporabe je treba pridobiti dovoljenje izdajatelja in plačati določen znesek.

Naročniki revije smejo kopirati kazalo z vsebino revije ali pripraviti seznam člankov z izvlečki za rabo v svojih ustanovah.

Elektronsko shranjevanje

Za elektronsko shranjevanje vsakršnega gradiva iz revije, vključno z vsemi članki ali deli članka, je potrebno dovoljenje izdajatelja.

ODGOVORNOST

Revija ne prevzame nobene odgovornosti za poškodbe in/ali škodo na osebah in na lastnini na podlagi odgovornosti za izdelke, zaradi malomarnosti ali drugače, ali zaradi uporabe kakršnekoli metode, izdelka, navodil ali zamisli, ki so opisani v njej.

AIMS AND SCOPE

ACTA GEOTECHNICA SLOVENICA aims to play an important role in publishing high-quality, theoretical papers from important and emerging areas that will have a lasting impact on fundamental and practical aspects of geomechanics and geotechnical engineering.

ACTA GEOTECHNICA SLOVENICA publishes papers from the following areas: soil and rock mechanics, engineering geology, environmental geotechnics, geosynthetic, geotechnical structures, numerical and analytical methods, computer modelling, optimization of geotechnical structures, field and laboratory testing.

The journal is published twice a year.

COPYRIGHT

Upon acceptance of an article by the Editorial Board, the author(s) will be asked to transfer copyright for the article to the publisher. This transfer will ensure the widest possible dissemination of information. This review and the individual contributions contained in it are protected by publisher's copyright, and the following terms and conditions apply to their use:

Photocopying

Single photocopies of single articles may be made for personal use, as allowed by national copyright laws. Permission of the publisher and payment of a fee are required for all other photocopying, including multiple or systematic copying, copying for advertising or promotional purposes, resale, and all forms of document delivery.

Subscribers may reproduce tables of contents or prepare lists of papers, including abstracts for internal circulation, within their institutions.

Electronic Storage

Permission of the publisher is required to store electronically any material contained in this review, including any paper or part of the paper.

RESPONSIBILITY

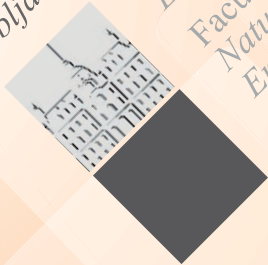
No responsibility is assumed by the publisher for any injury and/or damage to persons or property as a matter of product liability, negligence or otherwise, or from any use or operation of any methods, products, instructions or ideas contained in the material herein.



University of Maribor
Faculty of Civil Engineering,
Transportation Engineering
and Architecture

www.fgpa.um.si

University
of Ljubljana



Faculty of
Civil and Geodetic
Engineering
Faculty of
Natural Sciences and
Engineering

www.fgg.uni-lj.si
www.ntf.uni-lj.si



www.sloged.si



SLOVENSKO DRUŠTVO ZA
PODZEMNE GRADNJE
SLOVENIAN SOCIETY FOR
UNDERGROUND STRUCTURES

www.ita-slovenia.si